Development of rotating tube reactor for biodiesel production
from palm oil

Miss Narita Chanthon

A Dissertation Submitted in Partial Fulfillment of the Requirements
for the Degree of Doctor of Engineering in Chemical Engineering
Department of Chemical Engineering
FACULTY OF ENGINEERING
Chulalongkorn University
Academic Year 2021
Copyright of Chulalongkorn University

การพัฒนาเครื่องปฏิกรณ์แบบท่อหมุนสำหรับการผลิตไบโอดีเซลจากน้ำมันปาล์ม

น.ส.นริตา จันทร์ทนต์

Thesis Title   Development of rotating tube reactor for biodiesel
                        production from palm oil
By   Miss Narita Chanthon
Field of Study   Chemical Engineering
Thesis Advisor   Professor SUTTICHAI ASSABUMRUNGRAT
Thesis Co Advisor   Assistant Professor Kanokwan Ngaosuwan

     Accepted by the FACULTY OF ENGINEERING, Chulalongkorn University
in Partial Fulfillment of the Requirement for the Doctor of Engineering

                                   Dean of the FACULTY OF
                                   ENGINEERING
       (Professor SUPOT TEACHAVORASINSKUN, D.Eng.)

DISSERTATION COMMITTEE
                                   Chairman
      (Assistant Professor Worapon Kiatkittipong)
                                   Thesis Advisor
      (Professor SUTTICHAI ASSABUMRUNGRAT)
                                   Thesis Co-Advisor
      (Assistant Professor Kanokwan Ngaosuwan)
                                   Examiner
      (Akawat Sirisuk, Ph.D.)
                                   Examiner
      (Pattaraporn Kim, Ph.D.)
                                   Examiner
      (Pongtorn Charoensuppanimit, Ph.D.)

นิรตา จันทร์ทนต์ : การพัฒนาเครื่องปฏิกรณ์แบบท่อหมุนสำหรับการผลิตไบโอดีเซลจากน้ำมัน
ปาล์ม. (Development of rotating tube reactor for biodiesel
production from palm oil) อ.ที่ปรึกษาหลัก : ศ. ดร.สุทธิชัย อัสสะบำรุงรัตน์, อ.ที่
ปรึกษาร่วม : ผศ. ดร.กนกวรรณ ง้าวสุวรรณ

เครื่องปฏิกรณ์แบบท่อหมุนเป็นเทคโนโลยีการรวมกระบวนการที่สามารถเพิ่มสมรรถนะการผสม
และสร้างความร้อนที่เพียงพอสำหรับการผลิตไบโอดีเซล โดยงานวิจัยนี้ได้ศึกษาภาวะที่เหมาะสม รูปแบบการ
ไหลของของไหล และกระจายเวลาของสารที่อยู่ในเครื่องปฏิกรณ์แบบท่อหมุน (RTR) เพื่อเพิ่มอัตราการ
ผลิตไบโอดีเซลผ่านปฏิกิริยาทรานส์เอสเทอริฟิเคชันโดยใช้เบสเป็นตัวเร่งปฏิกิริยา โดยพบว่าภาวะการ
ดำเนินงานของเครื่องปฏิกรณ์แบบท่อหมุน โดยใช้อัตราส่วนเมทานอลต่อน้ำมัน 6:1 อัตราการไหลรวม 30
มิลลิลิตรต่อนาที ความเร็วรอบในการหมุน 1,000 รอบต่อนาที โดยทำปฏิกิริยาที่อุณหภูมิห้อง จะให้
ผลได้ไบโอดีเซลสูงที่สุดถึง 97.5% มีประสิทธิภาพผลผลิต 3.75×10^{-3} กรัมต่อจูล และได้ผลได้ไบ
โอดีเซลที่มีคุณภาพตรงตามมาตรฐาน ASTM จากการหาค่าของตัวแปรไร้หน่วย 2 ตัวแปร ประกอบด้วย
เรย์โนลด์นัมเบอร์แบบหมุน (Re_r) เทย์เลอร์นัมเบอร์ (Ta) ร่วมกับผลของแรงบิดเพื่อหาความสัมพันธ์ของ
รูปแบบการไหลในเครื่องปฏิกรณ์แบบท่อหมุนกับผลได้ของไบโอดีเซล พบว่ารูปแบบการไหลแบบมอดูเลท
เวฟวีวอร์เทค (MWVF) จะช่วยส่งเสริมให้ผลได้ไบโอดีเซลในเครื่องปฏิกรณ์แบบท่อหมุนเพิ่มสูงขึ้น
ในขณะที่การเพิ่มขึ้นของค่า Re_r, Ta และแรงบิดจะทำให้เกิดรูปการไหลแบบปั่นป่วนเพิ่มขึ้น ทำให้เกิด
ความร้อนที่มากเกิน ส่งผลให้อัตราการระเหยของเมทานอลเพิ่ม ทำให้ผลได้ไบโอดีเซลลดลง การกระจายเวลา
ของสารที่อยู่ในเครื่องปฏิกรณ์แบบท่อหมุนพบว่าไม่เป็นไปตามการไหลในอุดมคติด้วยเช่นกัน โดยรูปแบบ
การกระจายตัวของปริมาณสารต่อเวลามีลักษณะเป็นยอดสูงและแหลม ระยะเวลาเฉลี่ยที่สารอยู่ในเครื่อง
ปฏิกรณ์ และค่าการกระจายของอนุภาคสามารถแสดงถึงความปั่นป่วนของการผสม ซึ่งเกิดขึ้นอย่างชัดเจนใน
ภาวะที่อัตราการไหลสูงและมีความเร็วรอบการหมุนสูง แต่อย่างไรก็ตามอัตราการไหลที่สูงเกินไปทำให้การ
ผสมตามแนวแกนมีอิทธิพลมากกว่าการผสมในแนวรัศมีอย่างมีนัยสำคัญ ส่งผลให้การไหลมีความปั่นป่วน
ลดลง นอกจากนี้ยังมีการพัฒนาเครื่องปฏิกรณ์แบบท่อหมุนร่วมกับระบบสร้างพลังงานจากแสงอาทิตย์-
จักรยานเพื่อแสดงให้เห็นถึงความเป็นไปได้ในการใช้พลังงานทางเลือกสำหรับการผลิตไบโอดีเซลที่ยั่งยืนและ
คุ้มค่าทางเศรษฐศาสตร

สาขาวิชา	วิศวกรรมเคมี	ลายมือชื่อนิสิต
		....
ปีการศึกษา	2564	ลายมือชื่อ อ.ที่ปรึกษาหลัก
		....
		ลายมือชื่อ อ.ที่ปรึกษาร่วม
		....

5971464421 : MAJOR CHEMICAL ENGINEERING

Narita Chanthon : Development of rotating tube reactor for biodiesel production from palm oil. Advisor: Prof. SUTTICHAI ASSABUMRUNGRAT Co-advisor: Asst. Prof. Kanokwan Ngaosuwan

Rotating tube reactor (RTR), one of process intensification technologies, could highly increase the mixing performance and generate sufficient heat for biodiesel production. This research explored the optimum condition, essential characteristics of hydrodynamic regime and residence time distribution inside the rotating tube reactor (RTR) to enhance the biodiesel production rate using alkali-catalyzed transesterification. The operating condition of this RTR was 6:1 methanol-to-oil molar ratio, total flowrate of 30 mL/min and rotational speed of 1,000 rpm at room temperature, giving the highest biodiesel yield of 97.5% with yield efficiency of 3.75×10^{-3} g/J and the quality of biodiesel achieving the ASTM specification. Two dimensionless numbers, including rotating Reynolds number (Re_r) and Taylor number (Ta), as well as torque, were used to determine the hydrodynamic regime in this RTR which can be related to biodiesel yield. This indicates that the modulated wavy vortex flow (MWVF) is required to promote biodiesel yield in the RTR. Whereas the increment values of Re_r, Ta and torque associated with the turbulent Taylor vortex flow regime produced more extra heat to enhance methanol vaporization rate, leading to reduced biodiesel yield. The residence time distribution (RTD) of RTR was also found in the nonideal flow pattern. The peak of RTD, mean residence time and dispersion number could reveal turbulent mixing degree in the RTR. High turbulent mixing obviously appears at a higher flowrate and higher rotational speed. However, at excessive flowrate, the role of axial mixing was more significant than that of the radial mixing, resulting in the reduction of turbulent flow. Moreover, the RTR combined with a solar-bicycle generator system was developed to demonstrate the possible use of alternative energy for economical and sustainable production of biodiesel.

Field of Study:	Chemical Engineering	Student's Signature	....
Academic Year:	2021	Advisor's Signature	....
		Co-advisor's Signature	....

ACKNOWLEDGEMENTS

TABLE OF CONTENTS

LIST OF TABLES

Page

LIST OF FIGURES

LIST OF ACRONYMS AND ABBREVIATIONS

Acronyms/Abbreviations	Definition
A_{IS}	Area of methyl heptadecanoate (internal standard)
$\sum A$	Total area of fatty acid methyl ester
C_{IS}	Concentration of methyl heptadecanoate (mg/mL)
C_i	Measured tracer concentration (mmol/L)
CSTRs	Continuous stirred tank reactors
d	Gap width (m)
D/uL	Dispersion number (-)
$E(t)$	Exit-age distribution curve (-)
$E(\theta)$	Dimensionless exit-age distribution curve (-)
FAME	Fatty acid methyl ester
FFAs	Free fatty acids
m_S	Mass of biodiesel sample (mg)
MWVF	Modulated wavy vortex flow
PFRs	Plug flow reactors
R_i	Radius of the inner cylinder (m)
Re_r	Rotating Reynolds number (-)

$Re_{r,cr}$	Critical rotating Reynolds number (-)
Re_{x}	Axial Reynolds number (-)
RPO	Refined palm oil
RTD	Residence time distribution
RTR	Rotating tube reactor
t_i	Time (min)
Δt_i	Different time of two measurements (min)
Ta	Taylor number (-)
Ta_{cr}	Critical Taylor number (-)
TGs	Triglycerides
TVF	Taylor vortex flow
TTVF	Turbulent Taylor vortex flow
V_{IS}	Volume of methyl heptadecanoate (mL)
V_{m}	Mean axial velocity (m/s)
WVF	Wavy vortex flow

Greek symbols

η	Radius ratio (-)
Ω	Angular velocity (rad/s)

Ω_i Inner cylinder velocity (rad/s)

ν Kinematic viscosity (m^2/s)

τ Mean residence time (min)

θ Dimensionless time parameter

σ_t^2 Variance of the residence time distribution

σ_θ^2 Normalized variance the residence time distribution

CHAPTER 1
INTRODUCTION

This chapter presents introduction of this research, research objectives, scope of work, and expected outputs.

1.1 Introduction

In 20th century, the extremely increase in population and in modernization lead to an increase in the world's total primary energy consumption (TPEC). In many countries, most of energy is consumed by expansion of large industries, communication and transportation, and household use. Figure 1.1 shows the percentage growth of global gross domestic product (GDP), population, TPEC, and carbon dioxide (CO_2) emissions during 2010 and 2050 [1, 2]. It appears that the dramatic growth of total primary energy consumption brings to greenhouse gas (GHG) emissions and environmental problems.
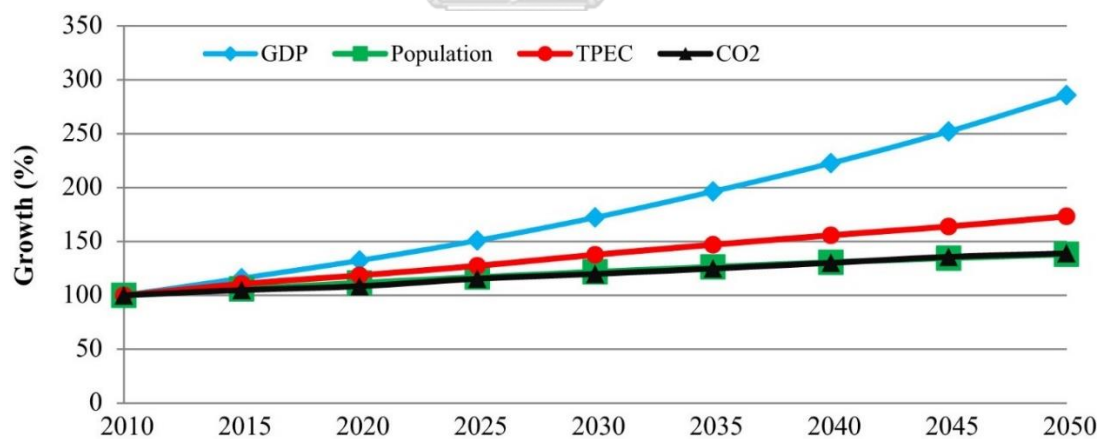
Figure 1.1 Trends in global gross domestic product (GDP), population, TPEC, and carbon [2].

Communication and transportation are the main sectors that require fuel to operate several engines. Currently, around 80% of the total energy used in the world is provided by fossil fuel [3, 4]. The usage of renewable energy instead of conventional energy, such as fossil fuel, become more reasonable in these days since renewable energy is produced from a renewable resource such as biomass, solar, wind, etc. In

addition, the cultivation of plants which is employed as biomass consumes CO_2 for producing plant food. Therefore, occurrence of CO_2 emissions can be reduced. To restrain CO_2 emission growth, renewable energy as biodiesel, bioethanol, etc. are used instead of the conventional energy from fossil fuel.

Biodiesel as a renewable energy resource is produced from triglycerides (TGs) and methanol in presence of an acid, base or enzyme catalyst to produce fatty acid methyl ester (FAME) and glycerol as a byproduct [5]. Vegetable oils, especially palm oil, are favored feedstocks for a biodiesel production process in Southeast Asia due to the suitable climate related to land efficiency, productivity and utilization [6]. High efficiency of biodiesel production is achieved by various methodologies including supercritical process, esterification, and transesterification. Advantage and disadvantage of each process are different from another. Supercritical process focusses on using extremely high temperature and pressure in producing process. The advantage of supercritical process is that catalyst is needless, which probably to reduce the production cost. However, this process requires the higher cost to design and construct reactor which could be higher than the cost of the catalyst [7]. The addition of esterification process focusses on using an acid catalyst to produce biodiesel. Esterification is a suitable process for feedstocks which have high free fatty acids (FFAs) because this process converts FFAs to ester. Mild condition around $50 - 65$ $^{\circ}$C at atmospheric pressure is sufficient for esterification as a pretreatment of high FFA feedstocks, resulting to lower instrument cost than supercritical process. However, using acid catalyst especially homogeneous acid catalyst causes the corrosion on the instrument's surface resulting in increasing the cost of maintenance [8]. In transesterification, can be operated at the mild condition as well as the esterification, but catalyst is needed to change to be the base catalyst, to provide the faster reaction rate of transesterification than esterification around 1,000 times [9]. Moreover, corrosion on the surface of the instrument is more like less occur. Accordingly, alkali catalyzed transesterification is the most commonly process for biodiesel production.

The main limitation of biodiesel production is the presence of mass transfer resistance which depends on the immiscibility of vegetable oil and the alcohol leading to slow reaction rate. To decrease heat and mass transfer resistance, several researches

study proposed the improvement of the biodiesel production using process intensification technology, including ultrasonic irradiation (US) [10], microwave (MW) [11], supercritical conditions [12], oscillatory flow reactor (OFR) [13], microchannel reactor [14], laminar flow reactor-separator [15], liquid-liquid flow reactor [16], zigzag micro-channel reactor [17], slit channel reactor [18], centrifugal contractor separator [19], spiral reactor [20], spinning disc reactor (SDR) [21], and rotating tube reactor (RTR) [22].

Rotating tube reactor (RTR) is one of the process intensification technologies. It could highly increase the mixing performance and generate sufficient heat for biodiesel production. Thin film of substances occur in the gap between rotor and stator while the rotor is rotated at high rotational speed, leading to increased interfacial area of substances and generation of heating by shear force [23]. In the previous studies, the Taylor-Couette reactor which is similar to the RTR consists of two concentric cylinders to generate a unique flow regime in the gap between the two concentric cylinders driven by the rotational speed of the inner cylinder with a static outer cylinder or a counterrotating cylinder [24]. The shear force derived from the rotational speed of the inner cylinder is slowly increased from zero and becomes unstable, resulting in the classification of hydrodynamic regime into 5 types based on increasing rotational speed including 1) circular Couette flow (CCF), 2) Taylor vortex flow (TVF), 3) wavy vortex flow (WVF), 4) modulated wavy vortex flow (MWVF) and 5) turbulent Taylor vortex flow (TTVF) [25], respectively. The rotating Reynold number (Re_r), Taylor number (Ta) and axial Reynold number (Re_x) are the dimensionless which is applied to classify the hydrodynamic regimes in the RTR. The increase of the rotational speed induces a high torque generation and turbulence inside the RTR, indicating the transition of hydrodynamic regimes from CCF to TTVF [25]. Because of the important ability to efficiently transfer of heat and mass of RTR, it can be applied in various processes such as emulsion polymerization [26], photocatalytic reaction [27], crystallization [28, 29] particle generation/classification [24] and phase transformation [30, 31]. Most of the previous studies required the TTVF regime to achieve their applications [26, 27, 30]. However, none of the above studies revealed the effect of the hydrodynamic regime on

biodiesel production efficiency in the RTR as described by the correlation of (Re_r, Ta, Re_x and torque).

The flow pattern inside the RTR reactor as an actual reactor should not exactly follow ideal flow pattern of plug flow or back-mixed flow. The information of hydrodynamic regime cannot fully explain the flow behavior of each particle movement inside the reactor. As the theoretical flow regime is characterized by Re_r, the ripple on film surface can change the film hydrodynamic and velocity distribution which affects the residence time distribution (RTD) on the RTR [32]. The RTD and mean residence time (τ) as the important parameters of chemical reactor can provide more information of the mixing and flow behavior inside the RTR [33]. Moreover, the calculation of variance of the RTD can be used to determine the dispersion number resulting in the extent of axial dispersion in the vessel.

Additionally, biodiesel production using RTR consumes less energy during operation [34], the biodiesel process can be more sustainable using the other power generation source such as solar cell [35], wind or even the human power. Mechtenberg et al. [36] reported the used of human power to generate the electricity which able to provide 100-150 per person using bicycle.

The purpose of this research is first to design and construct the RTR prototype for biodiesel production through alkali-catalyzed transesterification under mild reaction conditions. The performance of the reactor can be enhanced by modifying various operational parameters such as methanol-to-oil molar ratio, the NaOH loading, rotational speed, total flowrate and temperature. Dimensionless groups of Re_r, Ta and Re_x as characterized by the hydrodynamic regimes were emerged together with biodiesel yield in the RTR. The correlations between the discontinuities of linear fitted in Torque-$\sqrt{Ta}$ and the range of biodiesel yields were originally proposed to classify the category of the hydrodynamic regimes and explore the high-efficiency condition for biodiesel production in the RTR. Moreover, the study of RTD, τ and dispersion number are investigated to gain more understanding on the fluid movement behavior related to the actual hydrodynamic regime inside the RTR. Additionally, the solar-

bicycle generator is developed to generate electricity instead of electrical power from households to reduce the operating cost and being a sustainable process.

1.2 Research and objectives

    1.2.1 To design, construct, and optimize the rotating tube reactor for biodiesel production from palm oil with the option of solar-bicycle generator as electricity source.

    1.2.2 To investigate the hydrodynamic regime and residence time distribution inside the rotating tube reactor related to biodiesel production.

1.3 Scope of work

    1.3.1 To design and construct the RTR prototype for biodiesel production from palm oil using homogeneous catalyst to produce biodiesel according to EN standard.

    1.3.2 To investigate the optimum condition of biodiesel production using the RTR including operating parameters:

        - methanol-to-oil molar ratio (3:1, 4.5:1, 6:1 and 9:1)

        - rotational speed (900, 1,000, 1,100 and 1,200 rpm)

        - catalyst loading (0.5, 1.0 and 1.5 wt.%)

        - total flowrate (30, 45, 60 and 75 mL/min)

    1.3.3 To investigate the effect of the hydrodynamic regime on biodiesel production in the RTR as described by the correlation of (Re_r, Ta, Re_x and torque)

    1.3.4 To calculate the RTD, τ and dispersion number related to the hydrodynamic behavior of viscous fluid (50 wt.% of water/glycerol) inside the RTR using operating conditions including:

        - rotational speed (0, 300, 600, 900 and 1,200 rpm)

- flowrate (30, 45, 60 and 75 mL/min)

1.3.5 To propose solar-bicycle generator as an electricity source option for biodiesel production in the RTR

1.4 Expected outputs

1.4.1 The RTR prototype and the combined process of the RTR in bench scale with the option of solar-bicycle generator as electricity source is achieved.

1.4.2 The optimum condition, optimum FAME purity and yield efficiency of the individual RTR of biodiesel production through homogeneous alkali-catalyzed transesterification is provided.

1.4.3 The correlation between Re_r, Ta, Re_x and torque to classify the category of hydrodynamic regime can explore the high-efficiency biodiesel production in the RTR.

1.4.4 The fluid movement behavior of the RTR is described in terms of the actual τ and dispersion number.

จุฬาลงกรณ์มหาวิทยาลัย

CHULALONGKORN UNIVERSITY

CHAPTER 2
THEORY AND BASIC KNOWLEDGE

This chapter refers to the theory and basic knowledge in the field of biodiesel production and process intensification technology including a situation of world energy consumption and the statistics of fuel energy consumption of Thailand, overview of biodiesel production, basic principle of shear force assisting biodiesel production, flow behaviors inside RTR and residence time distribution (RTD) for continuous reactor.

2.1 Energy consumption statistics

This topic explains the situation of world energy consumption in OECD countries and non-OECD countries from 1990 to 2040. Moreover, the statistics of fuel energy consumption of Thailand in 2017 is exposed.

2.1.1 World energy consumption statistics

Energy is the basic requirement of human in daily life. Because the growth of human population increase, total energy which is increase employment in transportation session, industrial application session, and power generation session. According to the International Energy Outlook 2017 [37] reported by U.S. energy information administration, the world energy consumption increases from around 400 Btu in 2010 to 575 Btu in 2015. Moreover, the world energy consumption is predicted to be 736 Btu in 2040. During 2010 and 2040 (Figure 2.1), the economic and population growth of the non-organization for economic co-operation and development (non-OECD) countries extremely rise the world energy consumption to around 41%. In contrast, the growth of organization for economic co-operation and development (OECD) countries simply increases by 9%. Thus, to reduce world energy consumption, energy consumption should be concerned and renewable energy consumption should be encouraged in non-OECD countries.
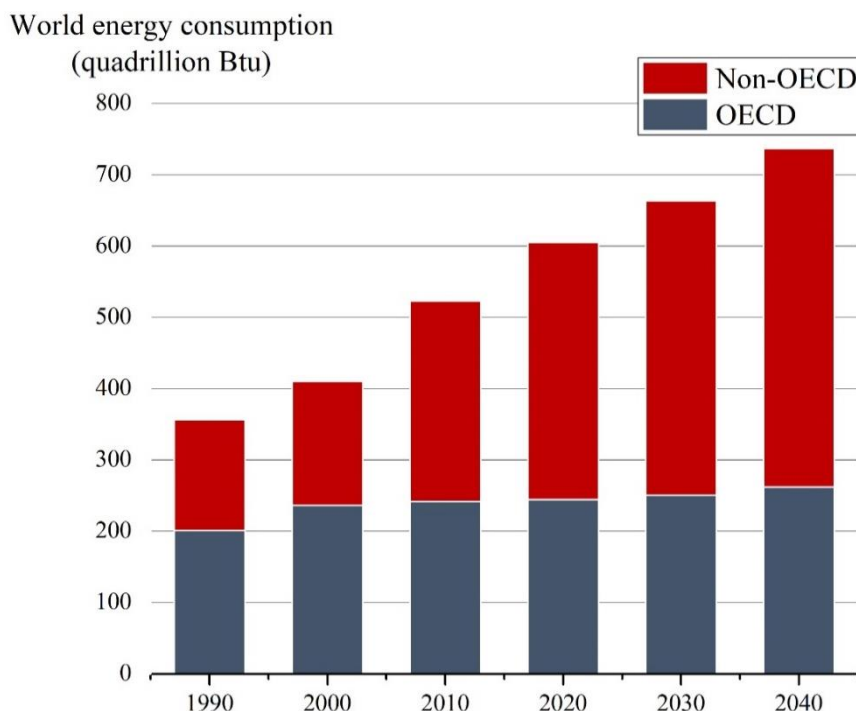
Figure 2.1 World total energy consumption; history and projection [37].

2.1.2 Fuel energy consumption statistics of Thailand

Since Thailand is one of the non-OECD country, the trend of energy consumption also continuously increases. According to energy balance of Thailand 2017 [37] that set by the department of alternative energy development and efficiency (DEDE), Ministry of Energy. Thailand's fuel final energy consumption increases by 1.0% to 80,752 kilotonne of oil equivalent (ktoe) from 2016 to 2017. The total value of fuel energy consumption was 1,072 billion baht. The petroleum products, electricity, coal and its products, natural gas, renewable energy consumption (including solar, fuel wood, paddy husk, bagasse, agricultural waste, municipal solid waste, and biogas), and traditional renewable energy consumption (including fuel wood, charcoal, paddy husk and agricultural waste) totaled 40,501, 16,519, 5,327, 5,767, 7,322 and 5,316 ktoe, respectively, as shown in Figure 2.2. Hence, the petroleum products were the highest proportion of the final energy consumption (50.10%) in 2017.
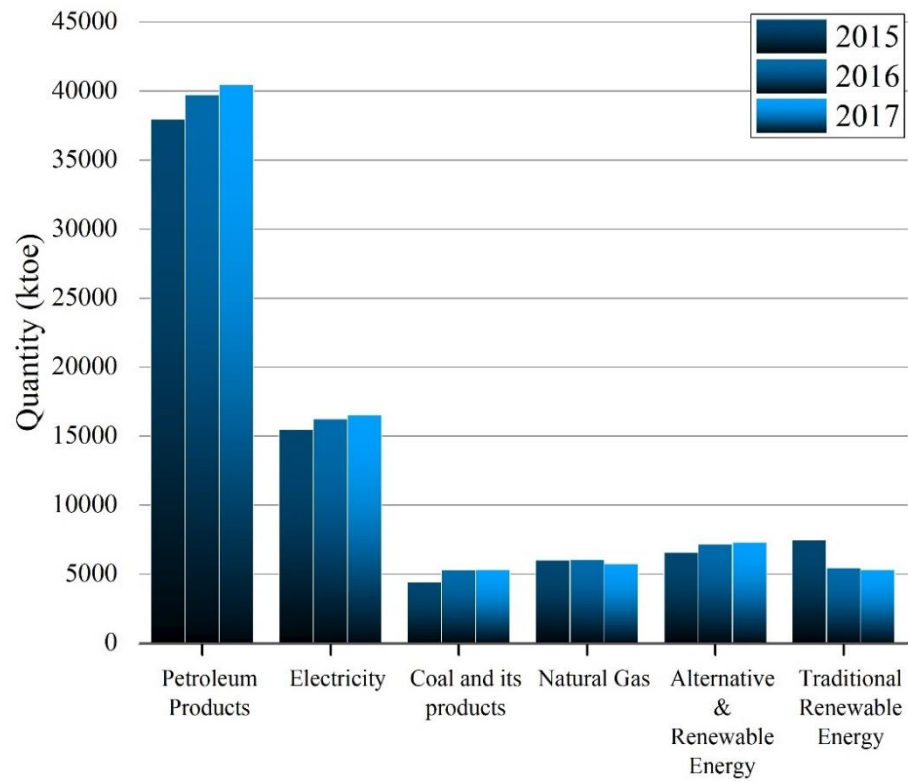
Figure 2.2 Final Energy Consumption by fuel type in 2017 [37].

Figure 2.3 describes the statistics of energy consumption by economic sectors in 2017. The transportation sector is the greatest proportion which is shared 40.0% of the energy consumption and followed by industrial and residential, respectively.
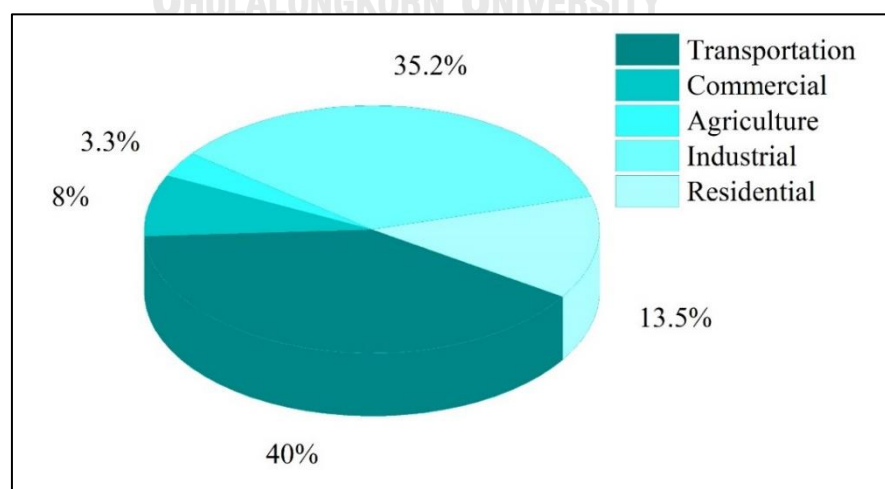
Figure 2.3 Final Energy Consumption by Economic Sectors in 2017 [37].

Since the direction of Thailand's energy consumption is continuously enlargement especially the energy consumption in transportation sector, the study and development of the sustainable alternative energy for transportation is remarkable. Biodiesel is the most advisable alternative energy which is suitable for Thailand because of the available and localized feedstocks. Moreover, the proportion of diesel consumption to fuel energy consumption in Thailand is found to be around 29 – 30% per year. The intensification of biodiesel production process should be valuable for human existence in the world especially in Thailand.

2.2 Biodiesel: An overview

This topic mentions to the classification of biodiesel feedstocks, composition of feedstocks for biodiesel production, reactions of biodiesel production, and catalysts for transesterification.

Since diesel is mainly employed in the transportation, economic, agriculture, and industrial sector, using alternative fuel to substitute the petroleum could be the positive impact for economy and environment. Biodiesel, one of the alternative fuels, has physical and chemical properties which closely resemble of petroleum diesel fuel. Combustion of biodiesel in diesel engine can reduce CO_2 emission around 78% compared with petroleum diesel fuel [38]. Besides reducing CO_2 emission, particle matter (PM) from biodiesel combustion is over 90% less than petroleum diesel fuel combustion [39]. Moreover, the content of sulfur and aromatic which generate from the combustion of fuel are also low and toxic gas is insufficiently emitted [40]. Although the use of biodiesel can reduce CO_2, PM, sulfur, and aromatic emission but oxide of nitrogen is highly generated. Because nitrogen content in biodiesel is higher than diesel fuel, the combustion of biodiesel leads to higher emissions of oxide of nitrogen (NOx) [41]. The problem of NOx can be solved by using biodiesel fuel in low temperature combustion or by providing selective catalytic reduction [42-44].

According to the American society for testing and materials (ASTM) [45], biodiesel is determined as mono-alkyl esters of long chain fatty acids derived from vegetable oils and animal fats. The main component of vegetable oil and animal fat are

triglyceride (TGs) which is ester of fatty acids connected with glycerol. TGs consists of three different fatty acids which affect to physical and chemical properties of vegetable oil and animal fat.

The United States of America (US) and European (EU) biodiesel specifications are shown in Table 2.1.

Table 2.1 US and EU biodiesel specifications [46, 47].

Property	ASTM D975-08a	ASTM D6751-12 2-B	1-B	Test	EN 590:2004		EN 14214:2012	
Flash point, min	No 1D 38°C, No 2D 52°C		93°C	D93	55°C	EN 22719	101°C	EN ISO 2719
Water & sediment, max	0.05 vol.%	0.050 vol.%		D2709				
Water, max					200 mg/kg	EN ISO 12937	500 mg/kg	EN ISO 12937
Total contamination, max					24 mg/kg	EN 12662	24 mg/kg	EN 12662
Distillation temperature (vol.% recovered)	90%, 1D 288°C max, 2D 282-338°C	90%: 360°C max		D1160, D86	65%: 250°C min, 85%: 350°C max	EN ISO 3405		
Kinematic viscosity	1D 1.3 - 2.4 mm^2/s, 2D 1.9-4.1 mm^2/s	1.9 - 6.0 mm^2/s		D445	2.0-4.5 mm^2/s	EN ISO 3104	3.5-5.0 mm^2/s	EN ISO 3104

Table 2.1 US and EU biodiesel specifications [46, 47]. *cont.*

Property	ASTM D975-08a	ASTM D6751-12 2-B	1-B	Test	EN 590:2004	EN 14214:2012
Density at 15 °C					820-845 kg/m³ EN ISO 3675 / EN ISO 12185	860-900 kg/m³ EN ISO 3675 / EN ISO 12185
Ester content	5 vol.% max EN 14078				5 vol.% max FAME EN 14078	96.5% min EN 14103
Ash, max	0.01 wt. % D482				0.01 wt.% EN ISO 6245	
Sulfated Ash, max		0.020% mass		D874		0.02% mass ISO 3987
	1D and 2D: D5453 D2622 D129²	Two grades:		D5453	Two grades: EN ISO 14596	10.0 mg/kg EN ISO 20846
Sulfur, max (by mass)	S15 15 mg/kg	S15 15ppm			50 mg/kg EN ISO 8754	EN ISO 20884
	S500 0.05%	S500 0.05%			10 mg/kg EN ISO 24269	EN ISO 13032
	S5000 0.50%					
Copper strip corrosion, max	No 3 D130	No 3		D130	class 1 EN ISO 2160	class 1 EN ISO 2160

Table 2.1 US and EU biodiesel specifications [46, 47]. *cont.*

Property	ASTM D975-08a		ASTM D6751-12 2-B	1-B	Test	EN 590:2004		EN 14214:2012	
Cetane number, min	40	D613		47	D613	51.0	EN ISO 5165	51	EN ISO 5165
Cetane index, min						46.0	EN ISO 4264		
One of[a]:									
- cetane index	40 min	D976-80							
- aromaticity	35 vol.% max	D1319							
PAH, max						11 wt.%	EN 12916		IP 391
Operability, one of:									
- cloud point	Report	D2500							
- LTFT/CFPP		D4539 D6371							
Cloud point					Report D2500	Location & season dependent	EN 23015	Location & season dependent	EN 23015

Table 2.1 US and EU biodiesel specifications [46, 47]. *cont.*

Property	ASTM D975-08a	ASTM D6751-12 2-B	1-B	Test	EN 590:2004	EN 14214:2012
CFPP					Location & season dependent EN 116	Location & season dependent EN 116
Carbon residue on 10% distillation residue, max	1D: 0.15 wt.% 2D: 0.35 wt.% D524			0.050 wt.% D4530	0.30 wt.% EN ISO 10370	
Acid number, max				0.50 mg KOH/g D664		0.50 mg KOH/g EN 14104
Oxidation stability				3 h min EN 14112	25 g/m^3 max EN ISO 12205	8 h min EN 14112
Iodine value, max						120 g Iod/100g EN 14111 EN 16300
Linolenic acid methyl ester, max						12.0 wt.% EN 14103

Table 2.1 US and EU biodiesel specifications [46, 47]. *cont.*

Property	ASTM D975-08a	ASTM D6751-12			EN 590:2004	EN 14214:2012
		2-B	1-B	Test		
Polyunsaturated methyl esters, max						1.00 wt.% EN 15779
Alcohol control		0.2 wt.% methanol max, or 130°C flash point min		EN141 10 D93		0.20 wt.% methanol max EN 14110
Monoglycerides, diglycerides & triglycerides, max		MG 0.40 wt.%		D6584		MG 0.70 wt.% EN 14105 DG 0.20 wt.% TG 0.20 wt.%
Group I metals (Na + K), max		5 mg/kg		EN 14538		5.0 mg/kg EN 14108 EN 14109 EN 14538
Group II metals (Ca + Mg), max		5 mg/kg		EN 14538		5.0 mg/kg EN 14538

Table 2.1 US and EU biodiesel specifications [46, 47]. *cont.*

Property	ASTM D975-08a		ASTM D6751-12			EN 590:2004	EN 14214:2012	
			2-B	1-B	Test			
Free glycerin, max				0.020 wt.%	D6584		0.02 wt.%	EN 14105
								EN 14106
Total glycerin, max				0.240 wt.%	D6584		0.25 wt.%	EN 14105
Phosphorous, max				0.001 wt.%	D4951		4.0 mg/kg	EN 14107
								prEN 16294
Lubricity, max	520 μm	D6079				460 μm	ISO 12156-1	
Conductivity, min	25 pS/m	D2624 D4308						
Cold soak filtration time (CSFT), max			360 s	200 s	D7501			

2.2.1 Classification of biodiesel feedstocks

Currently, biodiesel is classified based on the sustainability issue into five generations [1] as shown in Figure 2.4. The first generation uses edible crops as a feedstock such as corn, soybean, and sunflower oil etc. Because the main composition of edible oil crops is easy to be transformed into biodiesel. In addition, using edible oil crops can unlimited produce biodiesel compared diesel fuel due their renewable feedstocks. The limitation of the first-generation feedstocks is the high requirement of abundant fertile lands and water resources to cultivate edible oil crops which contributes to the large on-going land use change (LUC). Moreover, using edible crops for biodiesel production contribute to food competition, food shortage, and food price elevation. Therefore, the fuel and food/feed competition over crops, limitation of arable land, and limitation of fresh water are the main issues from the first generation which should be improved.

Non-edible crops feedstocks including non-edible crops (such as jatropha seed oil, and cottonseed oil, etc.), animal fat and grease are used for the second generation. Although the consumption of non-edible crops is not direct competition over food crops, LUC and water resource problem still occurred. Moreover, GHG emissions is contributed by fertilizers, irrigation, harvesting, and transferring result in increasing their carbon footprints. As a result, using waste products is remarkable for improving in the next generation.

The third-generation feedstocks is sustained using the waste-based biofuel including lignocellulosic feedstocks and non-edible waste oil such as waste cooking oil (WCO) and wastes from animal or vegetable residues. The application of waste-based biofuel for biodiesel production could handle various limitation such as reducing the cost of feedstock, decreasing the environmental emission (carbon footprint), and eliminating the competition over food, land, and water. Moreover, biomass and waste resources are available and diversity. Accordingly, biomass and waste resources are sustainable feedstocks for biodiesel production.

The fourth and fifth generations are derived from the microalgae and genetically engineered crops and algae, respectively. Currently, two generations are the recent

concepts for biodiesel production in the lab or pilot scale because the capital of production when using these feedstocks is higher than the capital of diesel fuel production. Therefore, both fourth and fifth generation are in the research and development steps for biodiesel production.
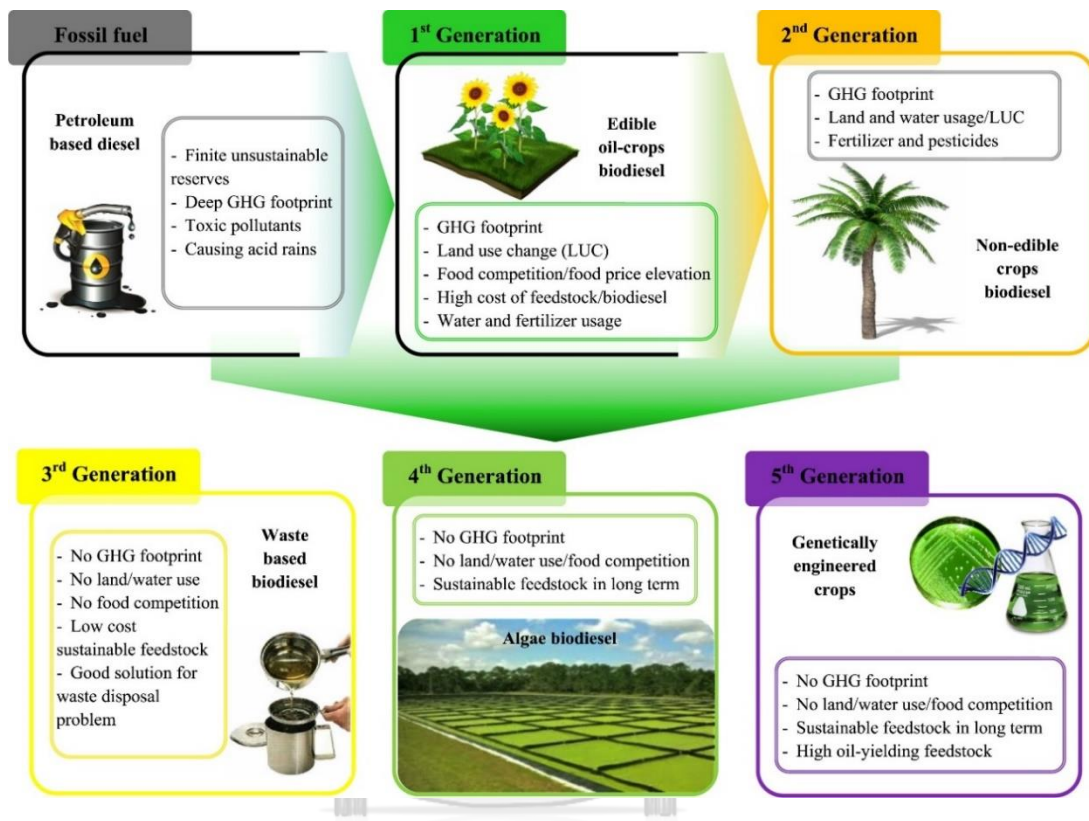
Figure 2.4 New classification of biodiesel feedstocks based on sustainability issue [1].

2.2.2 Composition of feedstocks for biodiesel production

Vegetable oils or edible oil crops consist of both saturated fatty acids and unsaturated fatty acids. Because oil content and proportion of fatty acids in each type of vegetable oil are different, their physical and chemical properties of oil are also different. The oil content and the fatty acid composition of the vegetable oil are shown in Table 2.2 and Table 2.3, respectively.

Table 2.2 Oil content of different sources of oil for biodiesel production [48]

Type of oils	Oil content (%)
Corn oil	45 - 50
Olive oil	45 - 70
Palm oil	30 - 60
Sesame oil	40 - 42
Soybean oil	15 - 20
Sunflower oil	25 - 35
Rapeseed oil	38 - 46
Peanut oil	45 - 55
Canola oil	40 - 45
Coconut oil	63 - 65

According to Table 2.2, the highest and lowest oil content of edible oil are coconut oil (63 – 65%) and soybean oil, respectively. Generally, oil content of edible oils is between 15 and 70% (depend on type of edible oil). Although the oil content of palm oil is lower than various plants, widely palm oil cultivation and cheaper palm oil price are two supporting reasons for selection of palm oil as a feedstock for biodiesel production especially in Thailand and Southeast Asia. Fatty acid in palm oil is mainly composes of palmitic acid (16:0) 36.70 wt.%, stearic acid (18:0) 6.60 wt.%, oleic acid (18:1) 41.82 wt.% and linoleic acid (18:2), and other fatty acids 8.60 wt.% [45].

Table 2.3 Fatty acid composition of different sources of oil for biodiesel production [45].

Type of fatty acid		Fatty acid composition (wt.%)						
Common name	Formula	Corn oil	Olive oil	Palm oil	Sesame oil	Soybean oil	Sunflower oil
Lauric acid (12:0)	$C_{12}H_{24}O_2$	-	-	0.10	-	-	0.53
Myristic acid (14:0)	$C_{14}H_{28}O_2$	-	-	0.70	-	-	-
Palmitic acid (16:0)	$C_{16}H_{32}O_2$	-	11.60	36.70	9.80	16.29	6.14
Palmitoleic acid (16:1)	$C_{16}H_{30}O_2$	11.67	1.00	0.10	-	-	0.09
Stearic acid (18:0)	$C_{18}H_{36}O_2$	1.85	3.10	6.60	6.30	6.66	4.11
Oleic acid (18:1)	$C_{18}H_{34}O_2$	25.16	75.00	46.10	41.82	22.70	34.30
Linoleic acid (18:2)	$C_{18}H_{32}O_2$	60.60	7.80	8.60	40.50	44.13	51.17
Linolenic acid (18:3)	$C_{18}H_{30}O_2$	0.48	0.60	0.30	0.32	8.97	2.23
Arachidic acid (20:0)	$C_{20}H_{40}O_2$	0.24	0.30	0.40	0.67	0.62	0.17
Gadoleic acid (20:1)	$C_{20}H_{38}O_2$	-	-	0.20	-	-	-

Table 2.3 Fatty acid composition of different sources of oil for biodiesel production [45]. *cont.*

Type of fatty acid		Fatty acid composition (wt.%)					
Common name	Formula	Corn oil	Olive oil	Palm oil	Sesame oil	Soybean oil	Sunflower oil
Eicosenoic acid (20:1)	$C_{20}H_{38}O_2$	-	-	-	-	-	-
Behenic acid (22:0)	$C_{22}H_{44}O_2$	-	0.10	0.10	-	0.63	0.41
Erucic acid (22:1)	$C_{22}H_{42}O_2$	-	-	-	-	-	0.53
Lignoceric acid (24:0)	$C_{24}H_{48}O_2$	-	0.50	0.10	-	-	-
Nervonic acid (24:1)	$C_{24}H_{46}O_2$	-	-	-	-	-	-
Others	-	-	-	-	-	-	Margaric 0.09 Margaroleic 0.06 Eicosenic 0.17

2.2.3 Reactions of biodiesel production

The reactions of biodiesel production are divided into 2 groups including main reaction and side reaction. Transesterification and esterification are the main reactions for producing biodiesel while hydrolysis and saponification are being as the side reactions.

Transesterification

In the transesterification of vegetable oil, a triglyceride in vegetable oil reacts with alcohol in presence of acid or alkaline catalyst to produce fatty acid alkyl esters and glycerol as shown in Figure 2.5. From stoichiometry, three moles of alcohol completely react with one mole of triglyceride. Since the transesterification is reversible reactions, the excess reactant is required for increasing yield by shifting equilibrium to the right side of the reaction equation.
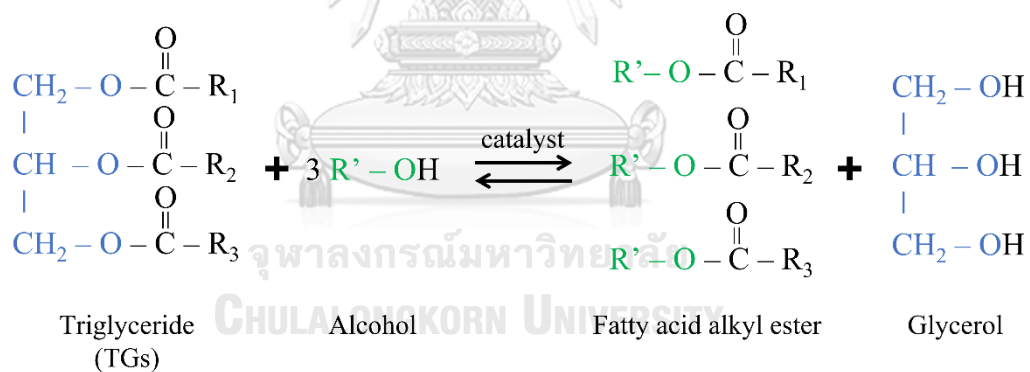
Figure 2.5 Overall transesterification of vegetable oil.

The mechanism of transesterification depends on the different types of catalyst. For alkali-catalyzed transesterification as shown in Figure 2.6, the mixture of alcohol reacts with alkali catalyst to produce an alkoxide and the protonated catalyst in the first step. After that, the nucleophilic of alkoxide ion attacks the carbonyl group of the triglyceride molecule to generate a tetrahedral intermediate in the second step. Then, the alkyl ester and anion of the diglyceride are formed in the third step. Finally, the

catalyst is deprotonated to the active species which can reuse in the next catalytic cycle. Both diglycerides and monoglycerides are also converted by the same mechanism to produce alkyl esters and glycerol [49, 50].
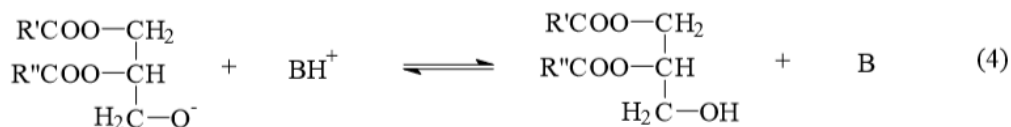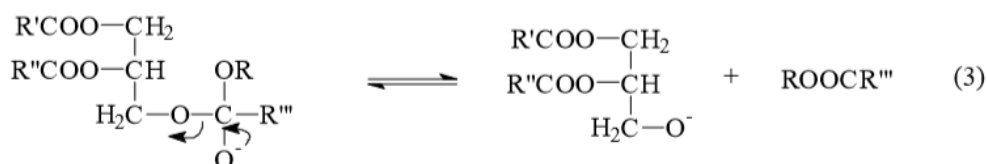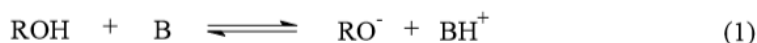
Figure 2.6 Mechanism of the alkali-catalyzed transesterification of vegetable oils [49].
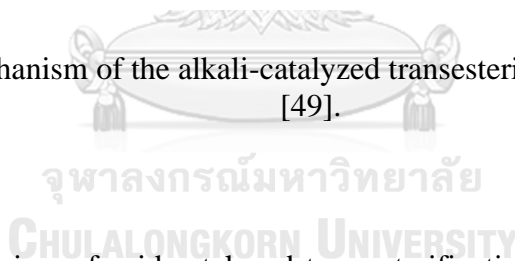
The mechanism of acid-catalyzed transesterification is shown in Figure 2.7. The protonation of the carbonyl group produces carbocation. After that, a nucleophilic reacts with alcohol to produce the tetrahedral intermediate. Lately, alkyl ester is generated by eliminating glycerol and regenerating the H^+ catalyst. According to this mechanism, the carbocation can react with water to form carboxylic acid which is a side reaction of transesterification. The absence of water in the acid-catalyzed transesterification is the significant suggestion of this process to avoid catalyst deactivation [48-50].
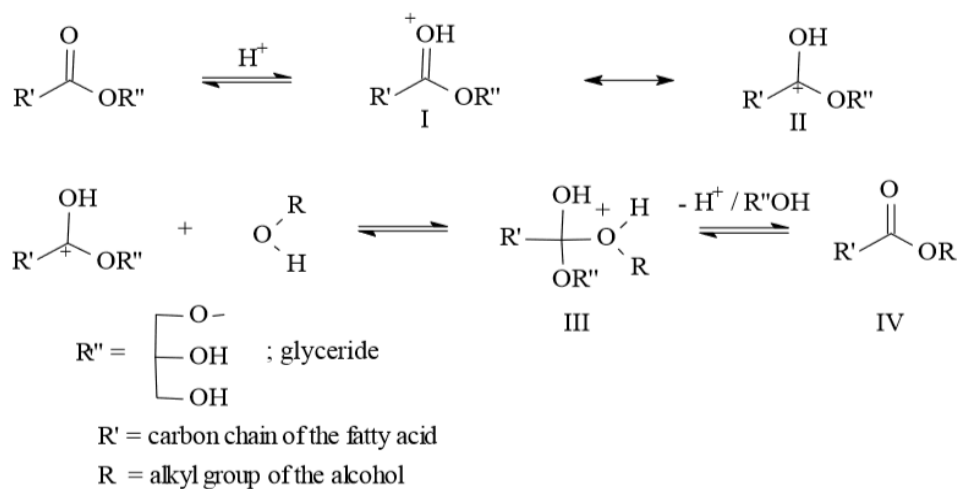
Figure 2.7 Mechanism of the acid-catalyzed transesterification of vegetable oils [49].

Esterification

For esterification, fatty acid reacts with alcohol in presence acid catalyst to produce fatty acid alkyl ester and water. Currently, the major application of esterification is a pretreatment of oil containing high FFAs because of reducing FFAs content and increasing high yield of biodiesel. Figure 2.8 shows the esterification of FFAs.
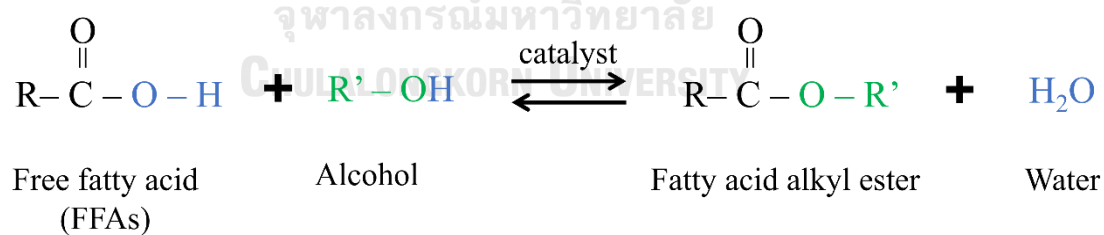
Figure 2.8 Esterification of FFA.

Hydrolysis
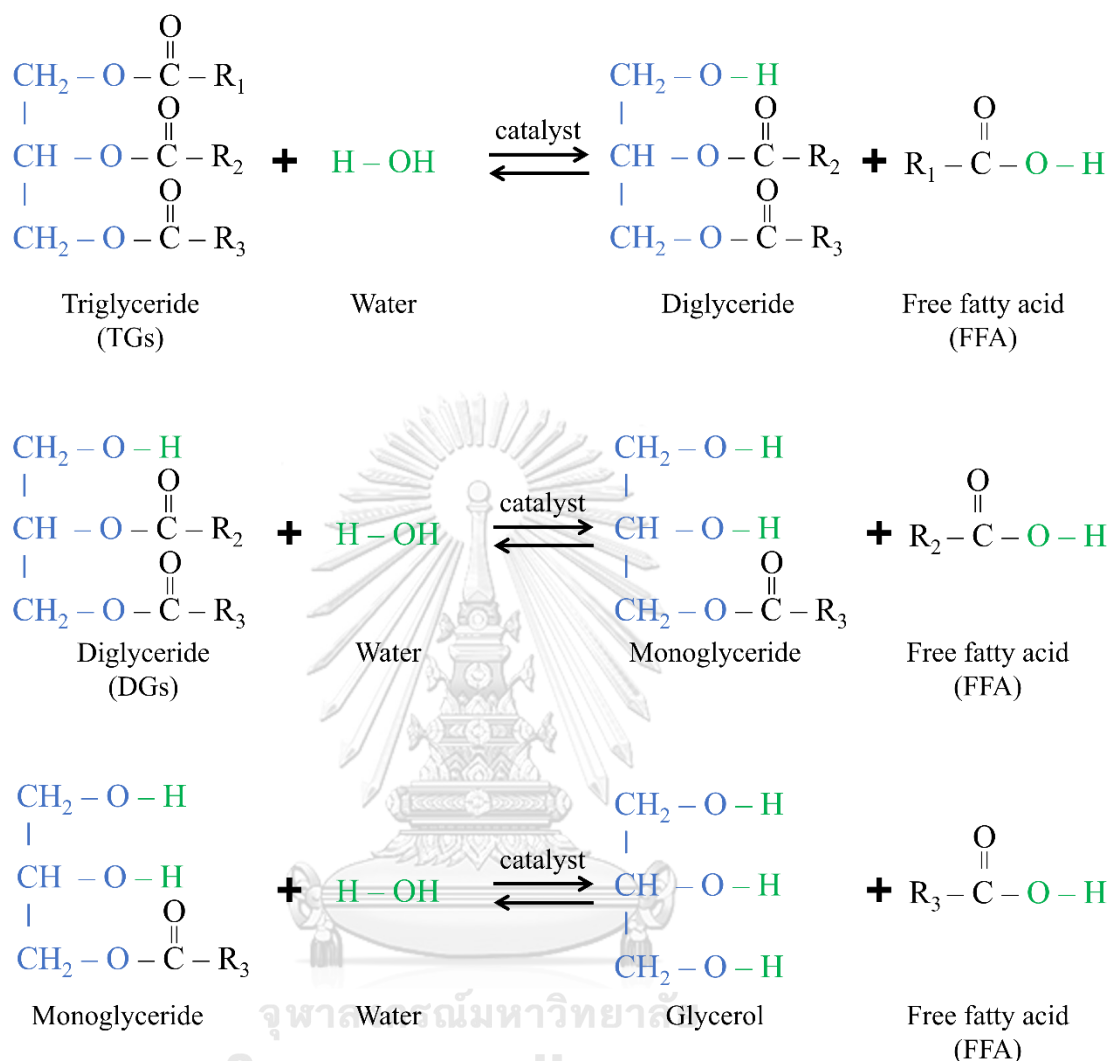
Figure 2.9 Hydrolysis reaction of triglyceride.

Figure 2.9 shows a reversible reaction of triglyceride hydrolysis. Water encourages the transformation of triglyceride to FFAs by the hydrolysis. Although the hydrolysis and the transesterification similarly consume the main feedstocks, the competition of both reactions may be possible. However, the hydrolysis requires the harsh conditions which opposite to the condition of transesterification. Hence, the competition reaction of hydrolysis and transesterification is very difficult especially using alkali as a catalyst.

Saponification

Saponification or soap formation reaction is the seriously undesirable reaction of biodiesel production which satisfies to high water and FFA content. Because reactants of saponification are similar to reactants of transesterification, the formation of soap results in the reduction of biodiesel yield. Moreover, glycerol as a byproduct of saponification influences on the formation of emulsification which causes the separation and purification problem. Figure 2.10 shows the saponification of triglyceride in the presence of alkali catalyst [49].
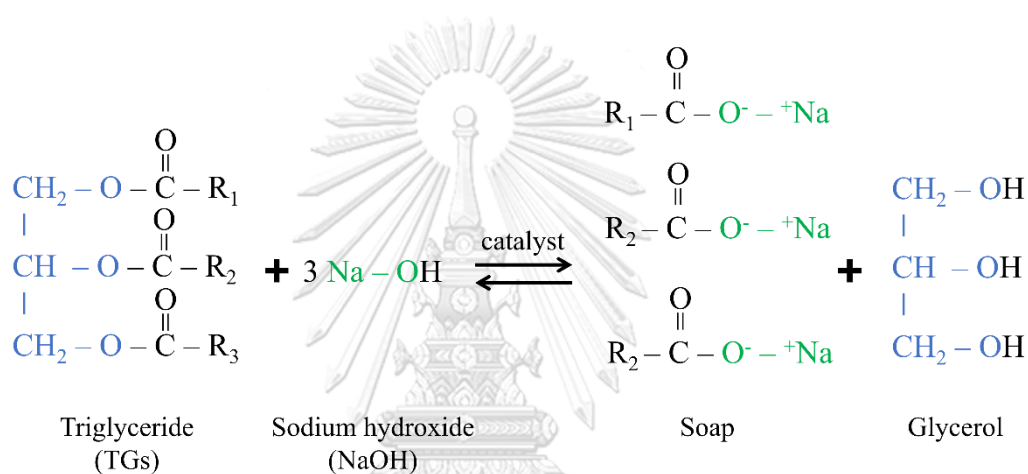
Figure 2.10 Saponification reaction of triglyceride.

2.2.4 Catalysts for transesterification

Catalysts for transesterification are mainly divided into 4 types including acid catalysts, alkali catalysts, enzymes and bifunctional catalyst as shown in Figure 2.11.
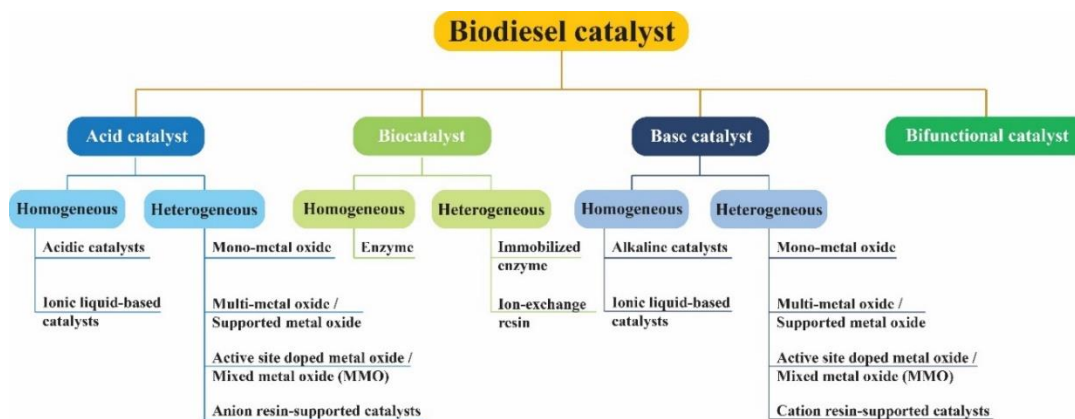
Figure 2.11 Classification of the catalysts for biodiesel production [51]

Acid catalysts

Acid catalysts are suitable for feedstock with high FFA and water content because of the avoidable soap formation. Significantly, the acid catalysts can only be used in esterification/transesterification or the simultaneous esterification and transesterification. However, long reaction time has occurred when using acid catalyst because of the weak catalytic activity and slow reaction rate. Moreover, the requirement of temperature, pressure, and alcohol to oil ratio for acid-catalyzed transesterification are higher than that of alkali catalyst. Most of all, the equipment in the process is required the high specific grade material since the effect of acid corrosion. The favor acid catalysts of transesterification are H_2SO_4, HCl, HF, H_3PO_4, ZrO, TiO, ZnO, and zeolite [9, 52].

Ouachab, N. and T. Tsoutsos [53] studied the two-step acid base homogenous catalyzed transesterification of olive pomace oil to produce biodiesel under mild reaction conditions. The optimal production of methyl esters (97.8%) was achieved for the experimental conditions: 20 wt.% of H_2SO_4 with methanol to oil molar ratio of 35:1 at 40∘C for the esterification and same catalyst concentration with methanol to oil molar ratio of 9:1 at 60∘C for the transesterification process.

Zhang, Y. et al. [54] reported that the optimal synthesis condition of $HClSO_3$–ZrO_2 is prepared from the reaction of $Zr(OH)_4$ with 15 mL/g of 0.5 M chlorosulfonic

acid followed by calcination at 600 ºC for 3 h. $Zr(OH)_4$ was prepared by precipitation $ZrOCl_2.8H_2O$ and $NH_3.H_2O$ at pH around 9–10. The result showed that the fatty acid methyl ester yield increased to 100 % continually for 5 cycles even under mild conditions by using methanol to oleic acid ratio of 8:1, 3 wt.% of catalyst, and reaction temperature around 100 ºC for 12 h.

Alkali catalyst

For transesterification, alkali catalyst is better than acid catalyst due to its high catalytic activity and faster reaction time. To compare the activity of acid and alkali catalyst, the result showed that the catalytic activity of alkali catalyst is 1,000 times higher than the acid catalysts [9]. Furthermore, the capital cost including cost of catalyst and operation cost of alkali-catalyzed transesterification is cheaper since alkali catalyst can be practicable and durable in the modest operational conditions. Nevertheless, the usability of alkali catalyst should restrict the FFA and water content which are the cause of side reactions including saponification and hydrolysis. The regularly alkaline catalyst is NaOH, KOH, $NaOCH_3$, CaO, MgO, and SrO [9, 52].

Leung, D.Y.C. and Y. Guo [55] explored that the characteristics and performance of NaOH, KOH, and $NaOCH_3$ was evaluated by using edible canola oil and used frying oil (UFO) as feedstocks. The optimal condition for the transesterification of UFO with an acid value of 2 and viscosity of 35 cSt could be achieved at 60 °C for a reaction time of 20 min, 1.1 wt.% of NaOH and methanol to UFO molar ratio of 7:1. For commercial edible canola oil, the optimal conditions were 40–45 °C for a reaction time of 60 min, 1.0 wt.% of NaOH and methanol to oil molar ratio of 6:1.

Noiroj, K. et al. [56] studied the transesterification of palm oil to methyl esters using KOH loading on Al_2O_3 and NaY zeolite supports as heterogeneous catalysts. The research found the optimal condition of the transesterification of palm oil to methyl esters around 91.07% was achieved for the experimental conditions: 25 wt.% of KOH/Al_2O_3 and 10 wt.% KOH/NY catalysts, palm oil to methanol molar ratio of 1:15, catalyst amount 3 – 6 wt.% at temperature below 70 ºC within 2 – 3 h.

Biocatalyst

The highlight of biocatalyst is the enzyme catalysts which are proper for the transesterification which employs the high FFA and water content feedstocks. This process is eco-friendly because of the absence of soap formation and without pollution. Nonetheless, the low catalytic activity and low reaction rate are the limitation of reaction when using enzyme as a catalyst. Additionally, the higher cost of enzyme catalyst is the drawback of this catalyst.

Watanabe, Y. et al. [57] investigated the conversion of waste edible oil to biodiesel fuel in a fixed-bed bioreactor. This process uses three columns packed with 3 g of immobilized *Candida antarctica* lipase. For the first step reaction, a mixture of waste oil and 1/3 molar equivalent of methanol against total fatty acids in the oil was used as substrate. For the second and the third step reaction, previous step eluates and 1/3 molar equivalent of methanol were used. The conversion of waste oil to methyl esters was 90% by feeding substrate mixtures into the first, second, and third reactors at flow rates of 6, 6, and 4 mL/h, respectively.

Bifunctional catalyst

Bifunctional catalysts derived from the mixed metal oxides are reported to be active for transesterification in terms of the enhancement of the catalytic activity and stability. The bifunctional catalysts are mainly developed for high FFAs and high water content feedstocks. However, the deactivation of catalyst could reduce catalytic activity of catalyst when used for a long-time. Since the characteristics of each catalyst are different, the intensive study of the physical and chemical properties of catalyst should be further intensively investigated [58-61].

Table 2.4 shows the summarization of the advantages and disadvantages of acidic homogeneous, acid heterogeneous, alkaline homogeneous, alkaline heterogeneous, enzyme and bifunctional catalyst for biodiesel production.

Table 2.4 Summary of the advantages and disadvantages of biodiesel catalysts [52].

Type of Catalyst	Example of catalysts	Advantages	Disadvantages
Acidic homogeneous catalysts	H_2SO_4, HCl, HF, H_3PO_4, sulfonic acid	• Insensitive to FFA and water content in oil • Catalyzed simultaneous esterification and transesterification reactions • Avoid soap formation	• Slow reaction rate • Long reaction time • Equipment corrosion • Higher reaction temperature and pressure • High alcohol to oil requirement
Acidic heterogeneous catalysts	ZrO, TiO, ZnO, ion-exchange resin, sulfonic modified mesostructured silica, sulfonated carbon-based catalyst, HPA, and zeolites	• Insensitive to FFA and water content in oil • Catalyzed simultaneous esterification and transesterification reactions • Recyclable, eco-friendly	• Weak catalytic activity • Catalyst is difficult to recycle • Slow reaction rate • Long reaction time • Higher reaction temperature and pressure • High alcohol to oil requirement • Weak catalytic activity • Low acidic site

Table 2.4 Summary of the advantages and disadvantages of biodiesel catalysts [52]. *cont.*

Type of Catalyst	Example of catalysts	Advantages	Disadvantages
Acidic heterogeneous Catalysts *cont.*		• Non-corrosive to reactor and reactor parts	• Low micro porosity • Leaching of active catalyst sites • Diffusion limitation • Complex and expensive synthesis route
Alkali homogeneous catalysts	NaOH, KOH, NaoCH$_3$, KOCH$_3$	• High catalytic activity • Faster reaction time • Low cost • Favorable kinetics • Modest operational conditions	• Low FFA requirement in the feedstock (<1 wt.%) • Highly sensitive to water and FFA • Saponification as side reaction • Soap formation • High volume of wastewater • Catalyst is non-recyclable • Equipment corrosion
Alkali heterogeneous catalysts	CaO, MgO, SrO, mixed oxide and hydrotalcite	• Non corrosive • Environmentally benign	• Slow reaction rate compared to homogeneous • Low FFA requirement in the feedstock

Table 2.4 Summary of the advantages and disadvantages of biodiesel catalysts [52]. *cont.*

Type of Catalyst	Example of catalysts	Advantages	Disadvantages
Alkali heterogeneous Catalysts *cont.*		• Recyclable • Fewer disposal problems • Easy separation • Higher selectivity • Longer catalyst life	(<1 wt.%) • Highly sensitive to water and FFA • Saponification as side reaction • Soap formation • High volume of wastewater • Leaching of active catalyst sites • Diffusion limitation • Complex and expensive synthesis route
Enzyme	Candida antarctica fraction B lipase, Rhizomucor miehei lipase	• Insensitive to FFA and water content in the oil • Avoid soap formation • Non-polluting • Easy purification	• Very slow reaction rate • Highly expensive • Highly sensitive to alcohol • Denaturation of enzyme

Table 2.4 Summary of the advantages and disadvantages of biodiesel catalysts [52]. *cont.*

Type of Catalyst	Example of catalysts	Advantages	Disadvantages
Enzyme *cont.*		• Possible reuse	
Bifunctional	Fe_2O_3-MnO-SO_4^{2-}/ZrO_2,	• Insensitive to FFA and water content in the oil	• Highly expensive
	La_2O_3/CaO,	• Longer catalyst life	• Complex synthesis
	MgO/Al-Ce-MCM-41	• High activity and stability	
		• Non-corrosive	

2.3 Basic principle of shear force assisted biodiesel production

In the continuous biodiesel production, the enhancement of physical processes including heat, mass and momentum transfer is the main objective for increasing efficiency of the intensification reactor. The stimulated wall shear stress by generating cavitation bubbles in a narrow gap is an alternative to develop the mixing characteristic of the reactor. While reaction mixture flows through the narrow gap, thin film system and friction on surface area between the mixture and reactor are created within reactor surface which results to expansion of the interfacial area of reaction mixture and generating sufficient heat for biodiesel production. Two basic principle of shear force used to design the intensification reactor are to generate a thin film system and to create cavitation bubbles inducing the wall shear stress in a narrow gap.

2.3.1 A thin film system

A thin film system is an essential requirement to increase heat transfer and interfacial area of reactant in chemical process. During operation in thin film system, all of reactants on the surface of rotating body are flung out on the axis of the body. Force which is generated by rotation of the body induces a film of the reactant medium on the surface of rotating body leading to provide high mixing efficiency. Since the higher viscous reaction media can use for the thin film system, it is especially advantageous over the conventional processes. Generally, the sufficiency of force for transporting the reactant medium across the surface is estimated. Supposing transportation force for proceeding the chemical reaction is insufficiency, the rotational speed will be increase until the product satisfactorily reaches the discharge zone. Most of all, the rotating of equipment at high speed conducts the spreading, mixing, as well as the reaction in a thin film pattern, without the requirement of additional mechanical member to spread or maintain the thin film [62]. The small thickness can provide a very high surface area per volume ratio (around 1,000) to improve the interaction of reactants film with its surrounding [63]. Lodha, H. et al. [63] reported the effect of lip (weir) thickness on the conversion of canola oil to biodiesel production. The result showed

that the oil conversion was increased with an increase in the lip thickness from 5,000 to 1,100 μm as shown in Figure 2.12 [64].
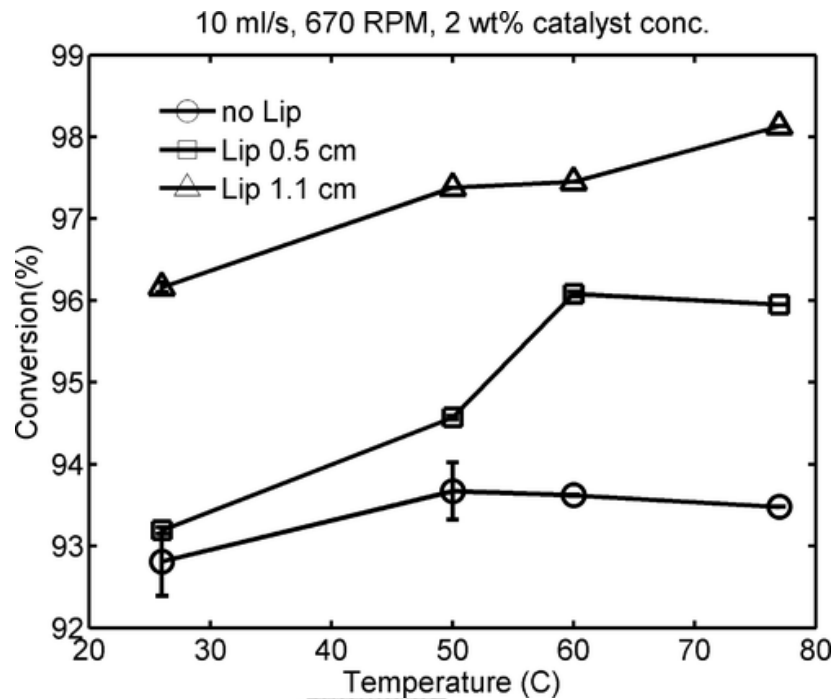
Figure 2.12 Effect of the variation in lip thickness on the oil conversion [64].

2.3.2 Cavitation bubbles and wall shear stress

Cavitation is the formation of largely empty voids in liquid which can be observed on ship propeller, rudders, and turbine blades. When the liquid flow passages a narrow gap of two rigid material, cavitation is also occurred and may result in damaging of contacting surface in the devices. The cavitation bubbles are generated by striking of the liquid flow to the surface result in generating the strong shear forces [64, 65]. Moreover, the unsteady boundary layer flow is created by the oscillating flow near the wall and lead to the occurrence of high shear force [66]. Since high shear force is particularly useful for homogenizing, dispersing and dissolving material, as well as suitable to improve the mass transfer for biodiesel production process.

2.4 Design and operating principle of the RTR[22]

The basic principle of the spinning tube in tube reactor, which is similar to the rotating tube reactor (RTR), is to design uniformity of the radial spacing between the narrow gaps. The symmetrical alignment of reactor is the importance role of design thus the adding of motor bearing and rotor bearing as the support is the method to reduce the effect of the manufacturing tolerances.

The spinning tube in tube reactor consists of (1) the first cylindrical tube which acts as a stator and (2) the second cylindrical tube, which has a smaller diameter, acts as a rotor. The upper and lower ends of second tube are disposed of the smallest tube, then the smallest tube was rotated by motor at the vertical longitudinal axis. The distance between the interior surface of stator and the exterior surface of rotor is the reaction zone in which reactants are passed to react together. While the passage flow through the reaction zone, the relative rotation of the two surfaces provides the shear forces inside the reactor. Since this reactor is designed in a vertical location, two entries of feeding are specified at the lower end. The second entry point has to locate above the first entry point to mix with the first reactant while the exit stays at the upper of the reaction passenger. The motor is connected to the upper of rotor providing axial and angular freedom for the rotation of rotor. When the rotor rotates, the uniformity of the radial spacing of rotor and stator around their circumference is maintained by the hydrodynamic effect in the reactant liquid or liquid mixture which passes the reaction passenger. The apparatus of the rotating tube in tube emphasizes very high rates of uniform micro-mixing resulting in the requirement of shorter axial distance and shorter reaction time, respectively. The typical shear rates are obtained from the radial rotation between 5,000 and 500,000 s^{-1}. The fact that high speed, uniform, forced, molecular inter-diffusion of the reactant fluid performs the rapidly of mixing. Generally, the spinning tube in tube is faster than a conventional stirred tank over 100 to several 1,000 times while it is faster than a micro-reactor around 100 times.

The main claim in the design specification of spinning tube in tube reactor includes:

(1) The radial spacing between the rotor and stator surfaces is from 50 to 500 micrometers

(2) The speed of relative rotation between the rotor and stator is from 5 to 100,000 rpm

(3) The thin film thickness is from 50 to 500 micrometers
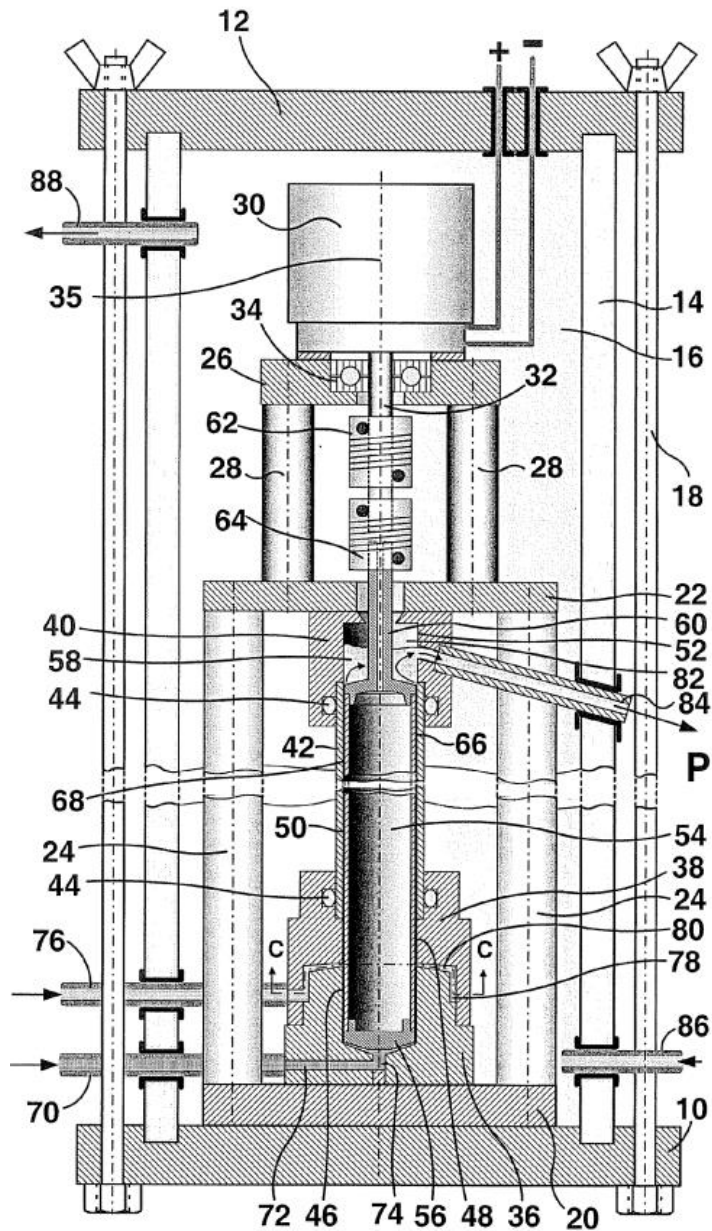
Figure 2.13 Cross section of spinning tube in tube reactor [22].

The cross section of a spinning tube in tube reactor is shown in Figure 2.13. The composition of the spinning tube in tube is:

10. Flat lower base member

12. Flat upper member

14. Elongated cylindrical body

16. Gas-tight enclosure

18. Tie rods connecting 10 and 12

20. Flat bottom base plate

22. Flat intermediate plate

24. Vertical posts between plates 20 and 22

26. Flat motor mounting plate

28. Vertical posts between plates 22 and 26

3O. Electric drive motor

32. Motor drive shaft

34. Thrust bearing

35. Common vertical axis of rotation

36. Cup shaped stator base member

38. Annular stator intermediate member

40. Annular stator upper member

42. Stator cylindrical tube

44. O-rings between tube and members 38 and 40

46. Cylindrical inside surface of base member 36

48. Cylindrical inside surface of intermediate member 38

50. Cylindrical inside surface of tube 42

52. Cylindrical inside surface of upper member 40

54. Rotor cylindrical tube

56. Rotor lower end member

58. Rotor upper end member

60. Rotor upper end drive shaft

62. Upper serially connected flexible connection

64. Lower serially connected flexible connection

66. Rotor external cylindrical operative surface

68. Annular reaction passage between Surfaces 66 and 46-52

70. Entry pipe for first reactant

72. Entry bore from pipe 70 into member 36

74. Inlet into reaction passage 68 from bore 72

76. Entry pipe for second reactant

78. Annular entry plenum between members 36 and 38

80. Bottom surface of ring shaped slit inlet from plenum 78 to reaction passage 68

82. Reception chamber for product at upper end of reaction passage 68

84. Outlet overflow pipe from reception chamber 82

86. Inlet pipe to enclosure 16

88. Outlet pipe from enclosure 16

2.5 Hydrodynamic regimes inside the RTR [67]

The structure and operating of RTR resemble the principal Taylor-Couette flow device which consists of an inner cylinder rotates inside the concentric stationary cylinder. The narrow gap between the inner cylinder and the outer tube generates a thin film flow. Circular Couette flow (CCF) is the fundamental state of fluid flow through the RTR with no disruption. While the rotational speed is slowly increased from the rest, the laminar axisymmetric flow, also called Couette flow becomes unstable to increase degree of mixing. The rotating Reynold number (Re_r) and Taylor number (Ta) are two dimensionless groups which are used to describe the flow behavior inside the RTR.

Based on the literature review [25, 68, 69], dimensionless groups including rotating Reynolds number (Re_r), axial Reynolds number (Re_x) and Taylor number (Ta) have been used to classify the hydrodynamic regimes in the Couette-flow device as well as the RTR reactor [70]. The Taylor-Couette device composes of the rotating inner tube within the concentric stationary outer tube. The effect of entry length on the hydrodynamic regime is assumed to be negligible for this calculation. The correlation of Re_r and Ta is used to classify the type of hydrodynamic regime. Re_r defined in Equation (1).

$$Re_r = \Omega_i R_i d / \nu \qquad (1)$$

Re_r is based on inner cylinder angular velocity (Ω_i), the radius of the inner cylinder (R_i), gap width (d) and kinematic viscosity (ν). Ta is dimensionless which expresses the ratio of centrifugal force to viscous force based on Re_r, gap width (d) and the radius of the inner cylinder (R_i) is defined in Equation (2). [71, 72]

$$Ta = Re_r^2 d / R_i \qquad (2)$$

Since the continuous operating system uses two pumps to feed the substances into the reactor. To minimize disturbance of annular hydrodynamic regime, Re_x is also an important factor which is calculated from the factor of axial flow rates of centrifugal pumps as expressed in Equation (3). [25]

$$Re_x = V_m d/v \qquad (3)$$

The calculation of Re_x is based on the mean axial velocity (V_m), gap width (d) and kinematic viscosity (v).

The circular Couette flow (CCF) is the initial type of flow transition inside the RTR. When the axial flow is fed to the Taylor-Couette flow device, the circular flow stability can increase resulting to delay in the development of CCF to TVF hydrodynamic regime. Only CCF is considered as a stable hydrodynamic regime because of the absence of secondary instability. The CCF can develop to the TVF hydrodynamic regime when the Taylor number (Ta) is higher than the critical Taylor number (Ta_{cr}), as shown in Figure 2.14.
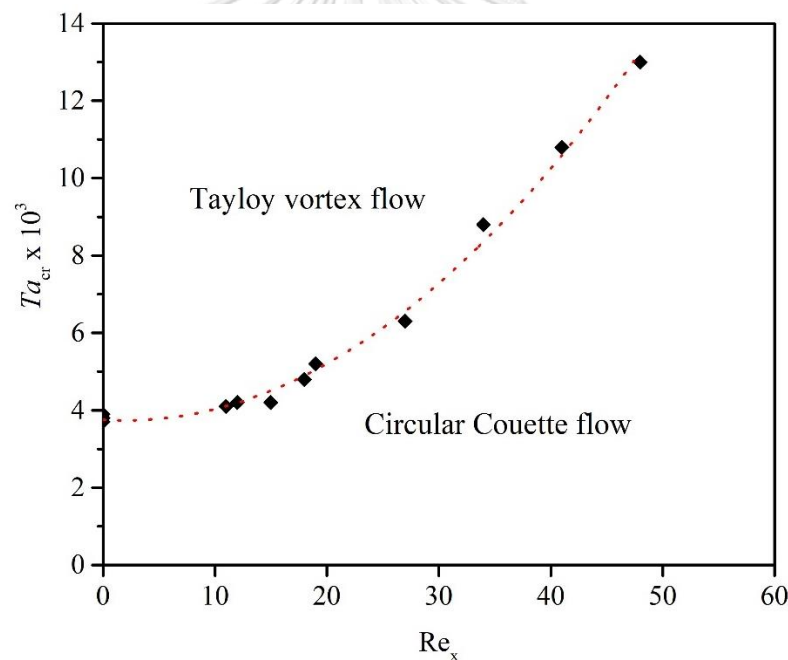
Figure 2.14 The critical Taylor number versus the axial Reynold number [25].

While the inner tube rotates, the Couette flow becomes unstable and generates a secondary instability state resulting in the appearance of axisymmetric toroidal vortices, known as Taylor vortex flow (TVF). Increasing the rotational speed related to the angular velocity, induces the development of flow behavior inside the RTR from

laminar to turbulent flow by generating the secondary vortices, as shown in Figure 2.15.
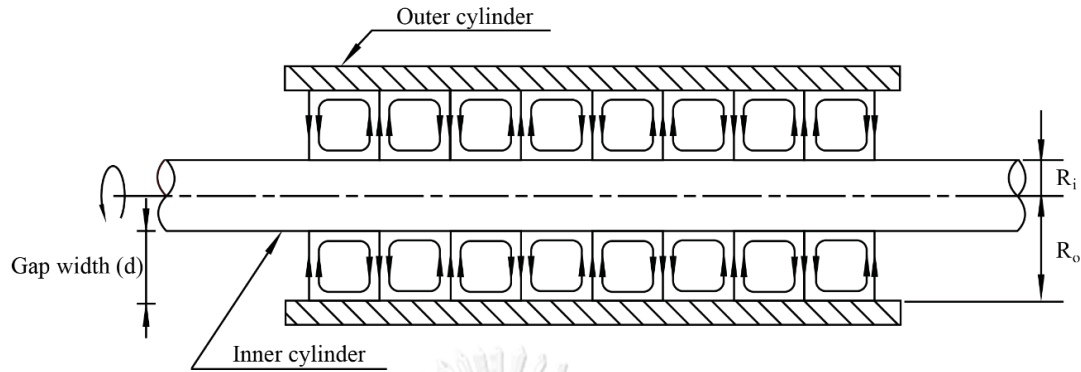
Figure 2.15 The secondary vortices generation in the RTR.

The hydrodynamic regimes of the RTR as an important role in the hydrodynamic behavior inside the reactor can be separated into 5 types including: circular Couette flow (CCF), Taylor vortex flow (TVF), wavy vortex flow (WVF), modulated wavy vortex flow (MWVF) and turbulent Taylor vortex flow (TTVF), respectively.

Figure 2.16 shows the development of hydrodynamic regimes inside the RTR. For TVF regime, the secondary instability is active to provide the generation of secondary vortices. However, the instantaneous velocity fields are insignificant to the secondary boundary, the deformation of each vortex shape is negligible. In the transition to WVF regime, the oscillations of entire vortex disturb the axial velocity of fluid. The instantaneous velocity fields oscillate both axial and radial motion resulting in the loss of rotational symmetry and destroying the surface boundary of stream which enables fluid flow to cross the vortices boundary. For MWVF regime, the amplitude of wave is modulated leading to the appearance perfectly of asymmetry wave and the generation of complex flow. Finally, the turbulent spots or the initially tertiary vortex are occurred when the disorder of flow motion is developed to TTVF regime [70].

	Taylor vortex flow (TVF)	Wavy vortex flow (WVF)	Modulated wavy vortex flow (MWVF)	Turbulent Taylor vortex flow (TTVF)
Type of flow regimes				
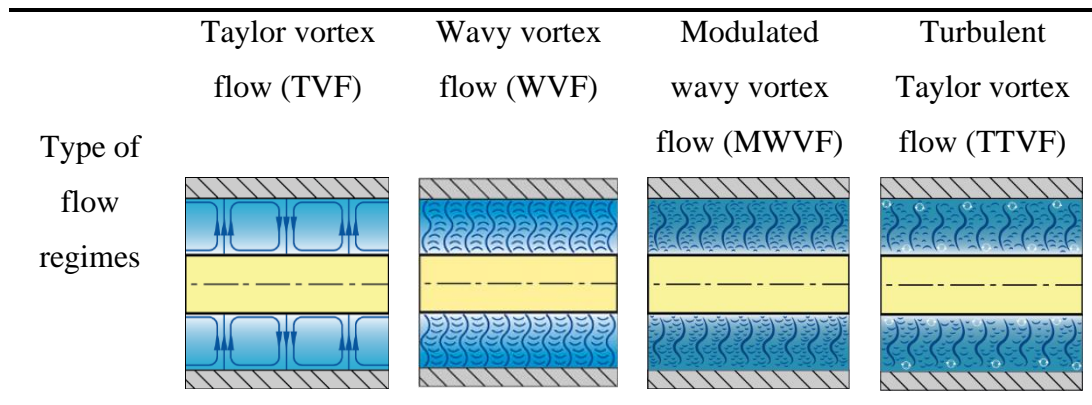
Figure 2.16 Different flow regimes inside Taylor-Couette flow device [73].

2.6 Residence time distribution (RTD) calculation [32, 74]

The residence time distribution (RTD) is important parameter for technical design and operation in the continuous process. The flow pattern of plug flow reactors (PFRs) represents the no mixing of the medium along the long axis (x-axis) or length of the reactor. All fluid travelling inside the PFR with the same time resulting to the narrow RTD and high surface to volume ratio. CSTRs substituted the flow is completely and instantly mixed into the reactor, however, some of the entering fluid in the CSTR is immediately leaving because of the continuously withdrawn from the reactor. The other fluid is left-over in the reactor due to all the fluids cannot withdraw from the reactor at the same time resulting to generate the exponential RTD curve. The nonideal flow reactor is the specific reactor which has the different fluid movement behavior inside the reactor. The study of RTD and τ are the essential parameters to provide the information of the mixing and flow behavior of fluid flow inside the nonideal flow reactor.

The age distribution functions ($E(t)$) demonstrates the quantitative time of fluid spent in the reactor which is expressed in terms of the variation of tracer concentration at the exit, $E(t)$ is defined in Equation (4).

$$E(t) = C(t)/\int_0^\infty C(t)\, dt \tag{4}$$

The dimensionless formulation of the mean residence time (τ), dimensionless time parameter (θ) and residence time distribution density ($E(\theta)$) are expressed in Equations (5) – (7), respectively.

$$\tau = \sum t_i C_i \Delta t_i \,/\, \sum C_i \Delta t_i \tag{5}$$

$$\theta = t_i / \tau \tag{6}$$

$$E(\theta) = \tau E(t) \tag{7}$$

The mean residence time (τ) is a function of the measured tracer concentration (C_i) at the time (t_i) and the different time of two measurements (Δt_i) while the dimensionless time parameter (θ) is represented the ratio of the instantaneous time with the mean residence time (τ).

The variance of the residence time distribution (σ_t^2) and the normalized variance (σ_θ^2) can be estimated as Equations (8) and (9)

$$\sigma_t^2 = \int_0^\infty t^2 \cdot E(t) dt - \tau^2 \tag{8}$$

$$\sigma_\theta^2 = \sigma_t^2 / \tau^2 = 2(D/uL) - [2(D/uL)^2\left(1 - e^{-uL/D}\right) \tag{9}$$

The variance referred to the distribution of the measured concentration of methylene blue is used to explain the flow behavior inside the RTR. The value of $D/uL \to 0$ defined as the dispersion can be negligible which is the ideal plug flow (PFRs) behavior while $D/uL \to \infty$ defined the dispersion is significant which is the characteristic of ideal continuous stirred tank reactor (CSTRs) or ideal mixed flow reactor (MFRs) behavior.

The tracer experiment is the main method to monitor the flow behavior of the nonideal reactor by collecting and analyzing samples over time. The important role of the tracer study is the tracer-fluid should not react or absorb the fluid inside the reactor. Pulse input and step input are two major types of tracer feed injection for the RTD test as presented in Figure 2.17. In the case of pulse injection, a small quantity of tracer-

fluid is injected into the reactor in the shortest time while the step is the injection of a constant concentration over a period of time. The response of the tracer concentration at the outlet of the reactor is collected resulting in the analysis and interpretation in the RTD curve.
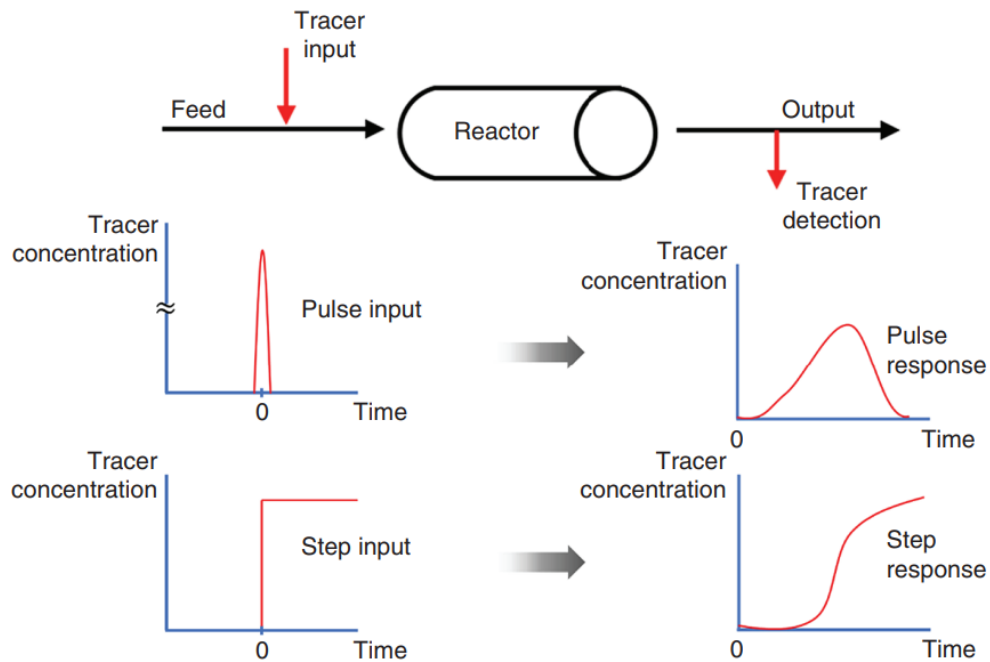
Figure 2.17 Difference of the pulse and step input for the measurement of RTD [75].

The pulse input is a favor measurement of the RTD because of its easy and saving cost of the tracer-fluid. Figure 2.18 represents the characteristic of tracer signal at input and output. The output RTD curve is sharp and narrow because of a simultaneous injection of tracer-fluid from pulse input. The response signal at the outlet expresses in terms of the correlation of relative product or product and time is used to describe the flow behavior. The RTD can analyze by comparing the flow behavior of the reactor based on the ideal PFRs or ideal CSTRs. The narrower and sharp peak implies the ideal PFRs behavior while the exponential broader peak indicates the ideal CTSRs behavior, as showed in Figure 2.18(b).
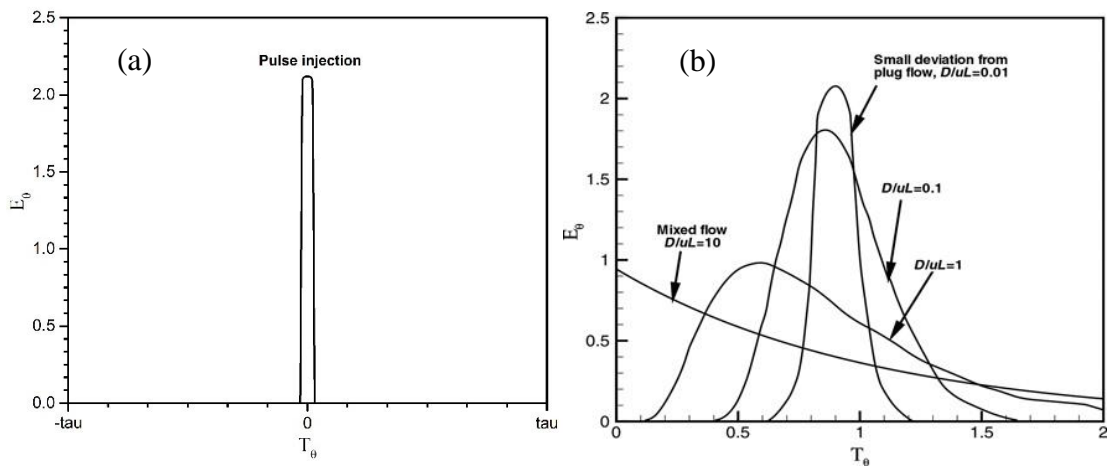
Figure 2.18 Input signal and response signal of the pulse injection [76].

Besides RTD curve and τ, axial dispersion is one of the important parameters which can used to describe the hydrodynamic behavior resulting in the improvement of design and operation of the continuous process. The highlight of the low dispersion is better for minimizing time to complete reaction. In contrast, the high dispersion is better for the process which requires fluctuations or disturbances. Axial dispersion number (D/uL) and mean residence time (τ) can be calculated based on the analytical solution of the axial dispersion model and experimental $E(t)$-curve data. Numerical modeling tools can be used to quantify the disturbances by axial dispersion and reactor configuration.

CHAPTER 3
LITERATURE REVIEWS

This chapter provides the literature reviews related to the conventional process and process intensification of biodiesel production. Moreover, the hydrodynamic regimes and residence time distribution are also reviewed to gain more understanding the flow behavior inside RTR. Lastly, using a human power device as a viable electricity generator for the intensification process is presented in the last topic of this chapter.

3.1 The conventional biodiesel production process

Transesterification is mostly selected to produce fatty acid methyl ester (FAME) since it is faster than esterification around 1,000 times (when using alkali catalyst) [9]. The reaction can be operated under mild condition, instrument cost and operating cost are lower than esterification. Alkali catalyst is a favor catalyst employed in transesterification because the reaction is very fast and the corrosion which does not occur on the instrument surface. However, saponification similarly requires feedstocks as transesterification. Soap formation via saponification can reduce the yield of esters. Moreover, glycerol as a byproduct of this reaction influences the formation of emulsification resulting in the complication of separation and purification [49].

The conventional process of biodiesel production is divided into 2 steps including synthesis and purification as shown in Figure 3.1.

A- Mixer 1
B- Reactor
C- Decanter 1
D- Rotary evaporator
E- Decanter 2
F- Mixer 2
G- Vacuum filtration unit

1- Methanol
2- Catalyst
3- Methanolic solution
4- Oil
5- Products from the reaction
6- Biodiesel + methanol + impurities
7- Glycerol + methanol + impurities
8- Biodiesel + impurities

9- Glycerol + impurities
10- Distilled water
11- HCl 0.2%
12- Biodiesel + water
13- Sodium sulphate anhidrous
14- Biodiesel + hydrated sodium sulphate
15- Biodiesel
16- Hydrated sodium sulphate

Figure 3.1 Diagram of the conventional process for biodiesel production [77].

Synthesis of biodiesel is usually produced via transesterification. A defined amount of methanol is pre-mixed with the different catalysts homogeneously. The reaction starts when the mixture of alcohol and catalyst is added to the reactor for pre-heating step of oil at the reaction temperature (60 ℃). The reactor set consists of a round-bottom flask which immerses in the oil bath for controlling the temperature, a cooled condenser for condensing alcohol, and magnetic stirrer for mixing the mixture. At the end of the reaction, product is left to ensure the separation to oil-rich phase and glycerol-rich phase.

After settlement, the reaction mixture is separated to 3 levels including methanol in the upper phase, biodiesel in the middle phase, and glycerol in a lower phase. Methanol is recovered by using a rotary evaporator under reduced pressure.

The biodiesel phase is washed with 10 – 50 vol.% of distillation water until the pH of washing water is similar to distillation water. To remove residual water, biodiesel is dried over 100 ℃. Then anhydrous sodium sulfate is added (leave overnight). Finally, biodiesel is filtered to obtain the final product.

Table 3.1 Research studies of conventional process for biodiesel production.

Oil source	Catalyst	Methanol-to-oil molar ratio	Temperature (°C)	Reaction time (min)	Ester content (%)	Ref.
Rice bran oil	0.75 wt.% of NaOH	9	55	60	90.18	[78]
Sunflower seed oil	2 wt.% of NaOH	7	60	60	96	[79]
Rapeseed oil	1 wt.% of KOH	6	65	120	95 - 96	[80]
Crude palm oil (CPO)	1 wt.% of KOH	6	60	60	88	[81]
Waste frying oil (WFO)	0.83 wt.% of KOH	9.5	50	20 and 40	98	[82]
Waste frying oil (WFO)	0.5 wt.% of NaOH	7.5	50	30	~97	[83]

Table 3.1 summarizes the study of conventional process for biodiesel production using a mechanical stirrer. The results showed that the requirement of catalyst concentration, methanol to oil molar ratio, temperature, and reaction time of each oil sources are different because of the different composition in oil feedstocks. The range of optimum condition of catalyst concentration, methanol to oil molar ratio, temperature, and reaction time for transesterification were 0.5 – 2.0 wt.%, 6 – 9.5, 50 – 60 °C, and 20 – 60 min, respectively. Although the high purity of ester content was achieved in conventional process, it cannot scale-up for increasing the productivity of biodiesel.

A plug flow reactor (PFR) is type of continuous reactor which is used instead of batch process to increase productivity. Theerayut, L. et al. [84] studied the production performance and necessary parameters for scaling-up the 6 stages continuous reactor (2.272 L) for transesterification of refined, bleached, and deodorized palm oil. The reactor could produce methyl ester at purities ranging from 97.5 to 99.2 wt.% in presence of 1.0 wt.% of NaOH and methanol to oil molar ratio of 6:1 within residence times of 6 to 12 min in which production capacities were in range of 17.3 to 8.5 L/h and power consumptions of stirrer were in range of 0.6 to 0.2 kW/m^3. Since the production performance of this reactor is equivalent to a PRF, it has a potential application for biodiesel production in the industry.

In the commercial process, crude biodiesel must be washed with water to remove impurities and to neutralize contaminants, such as metal ions, catalyst, salts, and free fatty acids. After that, biodiesel is separated from the water phase by using centrifugal and it is washed with water again. Later in the complete washing process, the remaining water is eliminated from biodiesel by drying process. Since the amount of water remaining in biodiesel after drying is low, absorbent materials should be used to remove these traces of water [85].

Although the conventional continuous process of biodiesel production is highly effective, the heat transfer, mass transfer, and mixing performance limitation from immiscible of oil and alcohol are still occurred. In addition, the high amount of washing water which is used in the conventional purification leads to an increase in wastewater generation. Thus, process intensification technology of biodiesel production and purification by modifying reactor and improving purification process are achieved.

3.2 Process intensification of biodiesel production

To intensify the biodiesel production process, modification and development of reactor is investigated. This topic refers to application of intensified reactors and their optimum condition including static mixer reactor (SM), helical static mixers reactor (HSMs), microchannel reactor, micromixer with static elements (MES), advanced flow

reactor (AFR), liquid-liquid film reactor (LLFR), packed tubular reactor, rotating packed bed (RPB) reactor, oscillatory flow reactor (OFR), helical tube reactor, microwave reactor (MW), acoustic cavitation/Ultrasonic reactor (US), hydrodynamic cavitation reactor, high speed homogenizer (HSM), spinning disk reactor (SDR), and rotating/spinning tube reactor (RTR).

3.2.1 Static mixer reactor

Static mixer reactor is the reactor which contains the mixing elements fixed within a pipe for increasing the interfacial area of mixing. The application of static mixers is to enhance the mixing efficiency of insoluble liquids under mild condition. The advantages of static mixer reactor are minimum maintenance requirement, low energy consumption, low operating cost, and low space requirement because the static mixers have no moving parts [86, 87].

Somnuk, K. et al. [88] reported the comparison of methyl ester purities in biodiesel production from refined palm oil (RPO) using plug flow reactor (PF), static mixer reactor (SM), ultrasound clamp on tubular reactor (US), and static mixer combined with ultrasound (SM/US). When using 12 g/L of KOH, methanol content of 20 vol.% with 20 L/h flow rate of RPO at 60 °C, the highest purity of methyl esters was 81.99 wt.%, 95.70 wt.%, 98.98 wt.%, and 97.67 wt.% were achieved with for reactor lengths of 900 mm PF, 900 mm SM, 700 mm for US, and 900 mm for SM/US, respectively. However, the PF and SM reactors consumed total electricity consumption of 0.189 kWh which is less than eight times of the electricity consumption of US and SM/US reactors.

Somnuk, K. et al. [89] studied three-step continuous process for producing biodiesel from palm fatty acid distillate (PFAD). Helical static mixers (HSM) were performed in three steps of the reactions as shown in Figure 3.2. From the experiment, methyl ester purities of 71.01, 95.94, and 99.96 wt.% from first, second, and third step, respectively were achieved when using 115.1 wt.% of methanol, 13.5 wt.% of H_2SO_4, and 5.0 g/L of KOH. The average energy consumption of HSM was 0.0473 kWh/L.

Additionally, ester purity from three-step process meets the specifications standard for commercial biodiesel.
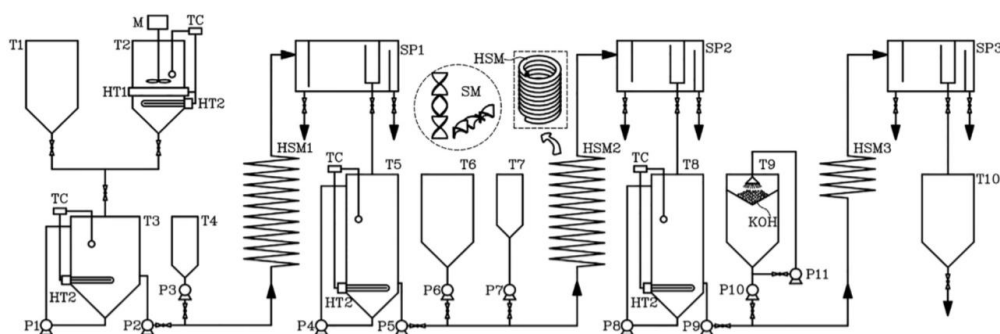
Figure 3.2 Schematic diagram of a three-step continuous process for biodiesel production from PFAD, using helical static mixers as react [89].

3.2.2 Micro-channel reactor

Micro-channel reactor is defined as a miniaturized reactor in sub-micrometers or sub-millimeters. Because of narrow channels within the reactor, excellent performance in liquid-liquid phase reaction, extremely high heat and mass transfer rates, and short molecular diffusion distance are occurred [14, 90]. Thus, higher conversion and selectivity in shorter residence time can be obtained in the micro-channel reactor. Mohadesi, M. et al. [91] reported the investigation of transesterification of waste cooking oil (WCO) with methanol in presence of KOH as the catalyst using a semi-industrial pilot of microreactor with 50 tubes. The optimum condition was obtained methanol to oil molar ratio of 9.4:1, the catalyst concentration of 1.16 wt.%, and the reaction temperature of 62.4 $^{\circ}$C. The highest level of biodiesel purity of 98.26% was obtained using a residence time of 120 s.

A similar study, zigzag micro-channel reactor is a micro-channel reactor which is modified geometric parameters on the performance such as hydraulic diameter and number of turns of the micro-channel reactors to increase the mixing performance. The highest methyl ester yield was 99.5% using the residence time of only 28 s was obtained at the methanol to oil molar ratio of 9:1, 1.2 wt.% of NaOH, and temperature of 56 $^{\circ}$C [17].

3.2.3 Micro mixer reactor

Micro mixer reactor is the micro-channel reactor which is combined with static mixer elements. The transformation of flow direction and disturbance in the boundary layer within reactor generates vortex which results in higher fluid mixing and oil conversion.

Harrson S. et al. [92] reported the evaluation of the biodiesel synthesis using sunflower oil and ethanol in microchannel reactor with static elements. The optimum FAEE yield (99.53%) was obtained at 50 ^oC, catalyst concentration of 1.0%, and ethanol/oil molar ratio of 9.

3.2.4 Liquid-liquid film reactors

Liquid-liquid film reactor (LLFR) is the intensified reactor which is shown in Figure 3.3. A main purpose of LLFR is used to mass transfer within the reactor by increasing interfacial area between oil-rich phase and methanol-rich phase result in high conversion, yield, and productivity. The highest conversion and yield of 99.9 and 97.5%, respectively, were achieved in presence of 1 wt.% of NaOH at 55 ^oC, and methanol to oil molar ratio of 6:1 in LLFR [93].

1) Oil tank.
2) NaOH in methanol solution tank.
3a) Oil metering pump.
3b) NaOH in methanol metering pump.
4a) Oil heat exchanger.
4b) NaOH in methanol heat exchanger.
5a) LLFR oil feeding nozzle.
5b) LLFR NaOH in methanol solution feeding nozzle.
5c) LLFR outlet nozzle and valve.
6) Decanter.
7a) Ester-rich phase output.
7b) Alcoholic phase output.
8) Ester-rich phase tank.
9) Alcoholic phase tank.

Figure 3.3 Diagram of the experimental configuration of the LLFR [93].

3.2.5 Packed tubular reactor

Packed tubular reactors or packed bed reactor (PBR) is one of the process intensification technologies which is suitable for heterogeneous catalyzed reaction process because inside PBR has an empty space for containing solid catalysts. Buasri, A. et al. [94] studied continuous transesterification of free fatty acids (FFA) from acidified oil with methanol using a calcium oxide supported on activated carbon (CaO/AC) as a heterogeneous solid-base catalyst. From the experiment, the yield of FAME was achieved to 94% using methanol to oil molar ratio of 25:1 at the reaction temperature 60 $^{\circ}$C and residence time of 8 h. Moreover, the characteristics of the product under the optimum condition were within the ASTM standard.

3.2.6 Rotating packed bed reactor

Rotating packed bed reactor (PBR), which is a novel technology, is designed to increase mass transfer and micromixing efficiency using centrifugal force [95, 96]. Inside PBR consists of the rotor and stator. During the experiment, liquid flowing through the packing in the rotor is split into droplets, threads, and thin films which contributes to a vast and violently interface. Chen, Y.H. et al. [95] reported a maximum FAME yield of 97.3% and maximum productivity of FAME of 0.828 mol/min were achieved at hydraulic retention time 0.72 min, methanol to oil molar ratio of 6:1, and rotational speed of 900 rpm.

3.2.7 Oscillatory flow reactors

Oscillatory flow reactor (OFR) consists of a tube containing baffles (orifice plates equally spaced). During the operation, pulsed flow within OFR creates eddies in the vicinity of the baffles resulting to enhance heat transfer and mixing efficiency. The OFR technology is especially appropriate for liquid-liquid heterogeneous reactions because the recirculation flow increases the interfacial area in the liquid phase which consequently enhances the rate of mass transfer [13, 97, 98]. García-Martín, J.F. et al. [98] reported that the highest biodiesel yield of OFR (78.8 %) was achieved using 6:1

methanol to waste cooking oil molar ratio, 0.67 Hz oscillation frequency and reaction time of 30 min. The flowchart of the biodiesel production using OFR in the study is shown in Figure 3.4.
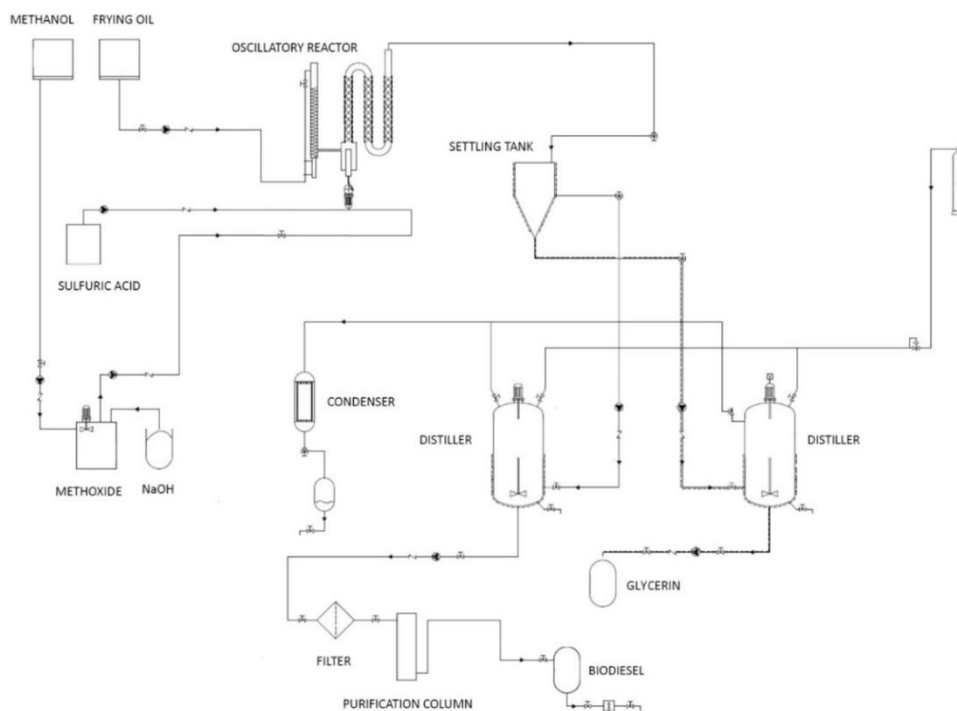
Figure 3.4 Flowchart of the biodiesel production using OFR [98].

3.2.8 Helical tube reactors

Helical coil reactor is the reactor which generates centrifugal force within the reactor. The curvature of the tube can increase heat transfer, mass transfer, and mixing performance between multiphase reactants. Furthermore, a helical coil extends the surface area in a relatively smaller reactor volume and a lesser land area [99]. Madhu Agarwal, M. et al. [100] reported that the maximum yield of 92.3% was obtained at 65∘C reaction temperature, 7:1 methanol to oil molar ratio, 0.8 wt.% of KOH as a catalyst, and 6.6 mL/min flow rate of oil using continuous helical tube reactor.

To modify the helical coil reactor, Gupta, J. et al. [99] studied the efficiency of continuous biodiesel synthesis using reverse flow helical coil reactors (RFHR) and a single flow helical coil reactor (SFHR) as shown in Figure 3.5. The results showed that

a maximum yield of 99.9 % was obtained at the optimum residence time of 5 min, a reaction temperature of 63 °C, in presence of catalyst (KOH) concentration of 2.1 g in RFHR.
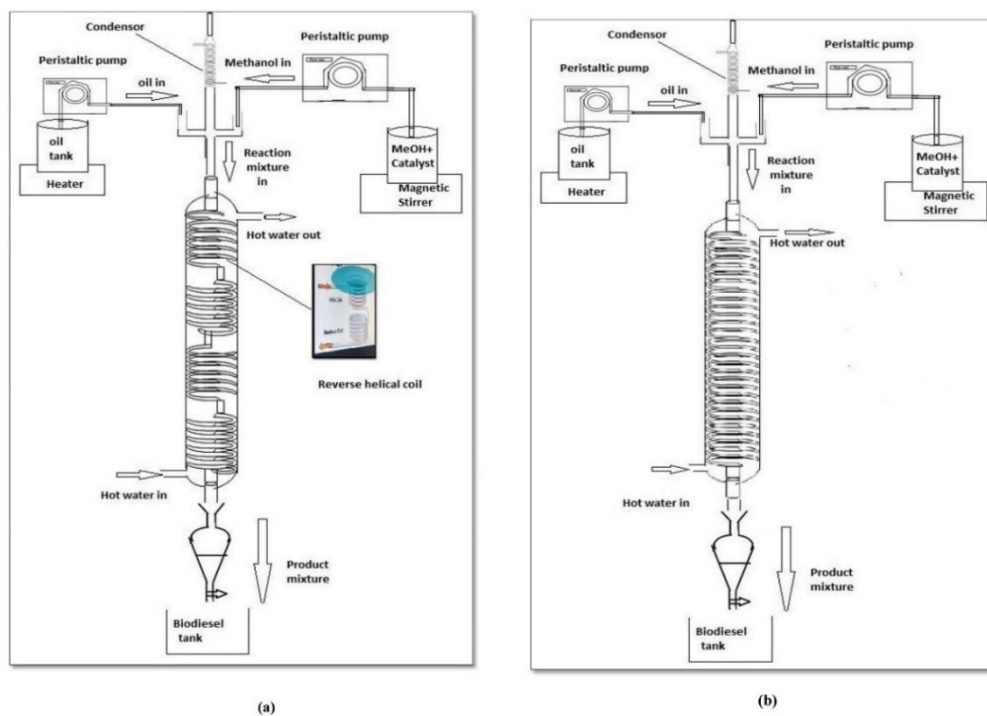
Figure 3.5 Schematic view of the (a) reverse flow helical coil reactor (RFHR) (b) single flow helical coil reactor (SFHR) [99].

3.2.9 Microwave reactors

In conventional process, heating bath that used to generate heat for system is transferred energy from heat source to reaction mixture. Although conduction, convection, and radiation are transferred from the surface of the reactor continuously, heat transfer could be an ineffective since heat loss occurs anytime.

Microwave reactor is remarkable to improve heat transfer. Within microwave reactor, energy transfer from microwave irradiation is more effective than conventional heating [11, 101]. Furthermore, the interaction of the electromagnetic field with the polar molecules and ions in the reaction medium are generated [102, 103]. Hence, the complete reaction is achieved in much shorter time. Lertsathapornsuk, V. et al. [11] reported that the continuous conversion of waste frying palm oil to ethyl ester was

obtained over 97% at the optimum condition of 12:1 ethanol to oil molar ratio, 3 wt.%
NaOH (in ethanol), and residence time of 30 s in a continuous microwave reactor. The
schematic diagram of continuous microwave reactor is shown in Figure 3.6.
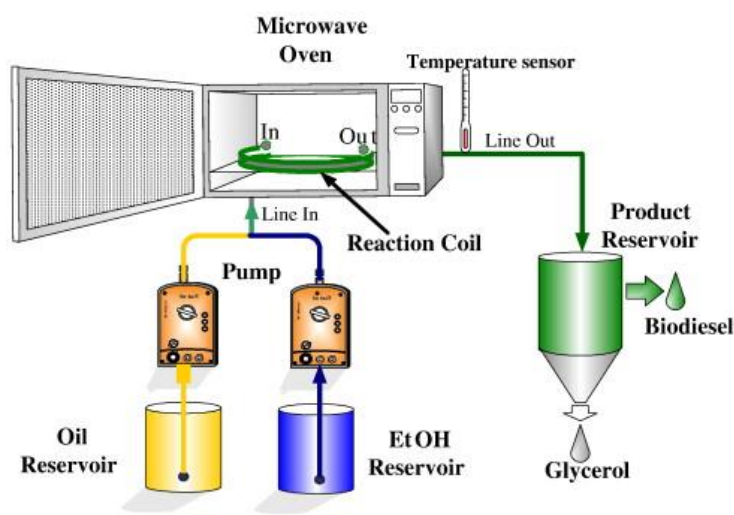
Figure 3.6 Schematic diagram of continuous microwave reactor [11].

3.2.10 Acoustic cavitation reactor/Ultrasonic reactor (US)

Immiscible of vegetable oil and alcohol is the major problem for biodiesel
production because of differences of chemical polarity. Vegetable oil is a non-polar
molecule, but alcohol is a polar molecule.

Acoustic cavitation reactor/ultrasonic reactor (US) is an intensified reactor can
enhance the mixing performance. Using low frequency ultrasonic irradiation is an
application for emulsifying immiscible liquids. The cavitation bubbles from ultrasonic
disrupt the phase boundary between two phases of vegetable oil and alcohol resulting
in a lower mass transfer resistance of liquid-liquid heterogeneous reaction [104, 105].
Moreover, the cavitation bubbles generate intense heating (transient hotspot) to reaction
mixture which leads to higher production efficiency than conventional process [10].
Gole, V.L. and P.R. Gogate [106] and Gole, V.L. et al. [107] reported that the biodiesel
yield and yield efficiency of ultrasonic reactor (see Figure 3.7) were obtained 92.5 %
and 0.1 x 10^{-4} g/J at the optimum condition of 6:1 methanol to oil molar ratio, 1 wt.%

of KOH, temperature of 60 °C at reaction time of 40 min using Nagchampa oil and methanol as feedstocks.
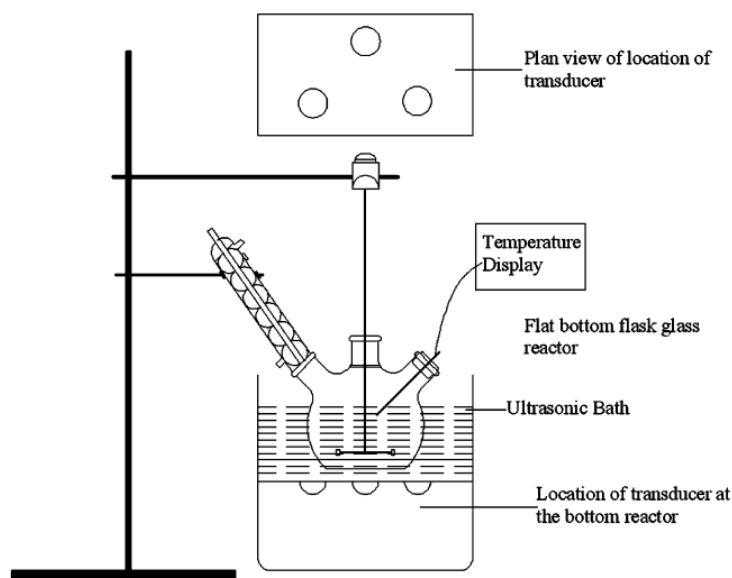
Figure 3.7 Schematic representation of a sonochemical reactor [106, 107].

3.2.11 Hydrodynamic cavitation reactors

Since methyl ester synthesis is constrained by mass transfer, studying the effects of cavitation generation including micro-emulsification and elimination mass transfer resistance of stream is significant for improving this process. Acoustic cavitation and hydrodynamic cavitation can enhance these effects. Acoustic cavitation requires electrical device to generate cavitation bubbles in the reaction medium; in contrast, the cavitation bubbles generated from hydrodynamic cavitation is obtained by the passage of liquid through a constriction such as throttling valve, orifice plate, and venturi [107, 108]. Therefore, hydrodynamic cavitation is cheap alternative for methyl ester synthesis. Ghayal, D. et al. [109] reported the application of a hydrodynamic cavitation reactor for the synthesis of biodiesel with used frying oil as a feedstock. Maximum yield was over 95 % when using 6:1 methanol to oil molar ratio, 1 wt.% KOH at 60 °C, and reaction time of 10 min. Moreover, the yield efficiency of biodiesel production

using hydrodynamic cavitation reactor is 1.28 x 10^{-3} g/J which is higher than acoustic cavitation reactor.

3.2.12 High Speed Homogenizer reactors

High Speed Homogenizer (HSM) is a cavitational reactor which works based on the rotor-stator principle. Because the rotor rapidly rotates and the gap between rotor and stator is narrow, the cavitation bubbles are generated within the reactor [110, 111]. Mohod, A.V. et al. [110] reported that the maximum yield of biodiesel was 97% for using waste cooking oil as feedstock under optimized conditions of methanol to oil molar ratio of 12:1, reaction time of 120 min, 3 wt.% of KOH as the catalyst, and temperature of 50 °C in HSM. The schematic of the flow loop which is used in experiments is shown in Figure 3.8.
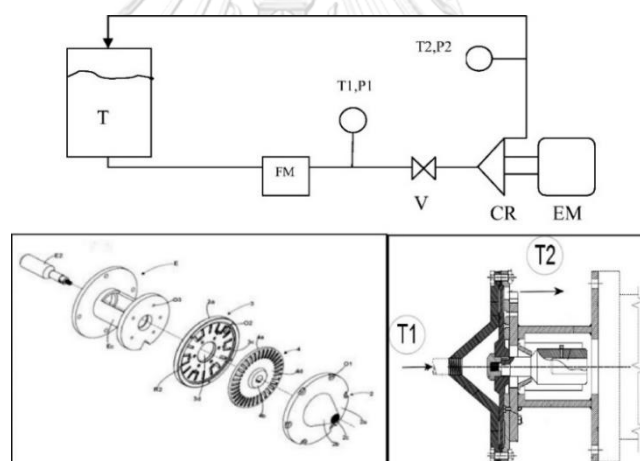
Figure 3.8 Schematic of the flow loop used in experiments: T: tank, FM: flowmeter, V: valve, CR: cavitation reactor, EM: electric motor, Ti: temperature measurement and Pi: pressure measurements [110].

Moreover, Laosuttiwong, T. et al. [112] studied the performance comparison of different cavitation reactors for biodiesel production via transesterification of palm oil. From this experiment, increasing the reaction volume from 165 to 1,000 mL when using homogenizer reactor with constant power input (80 W) did not significantly influence to the rate of FAME formation; in contrast, it decreases the reaction rate of mechanical

stirred and direct ultrasonic reactors. The highest yield efficiency of 169.46×10^{-4} was obtained from homogenizer reactor using sodium hydroxide in the reaction volume of 1,000 mL.

3.2.13 Spinning disk reactors

Spinning disk reactor (SDR) is one of the process intensification technologies employing high gravity fields. Rotational of disk surface generates a high gravity field centrifugal force leading to the dispersion of liquid as a thin film on the surface. Since a thin film dispersed on the surface of reactor is an unsteady film, the shearing action of the rotating surface and the outstanding of micro-mixing is achieved to generate the excellent heat and mass transfer [21, 113]. Chen, K.-J. and Y.-S. Chen [113] studied the continuous transesterification of soybean oil and methanol in a spinning disk reactor (SDR) which the main structure of an SDR is shown in Figure 3.9. From this experiment, the optimal operating condition was obtained methanol to oil molar ratio of 6:1, 1.5 wt.% of KOH as a catalyst at temperature of 60 $^{\circ}$C, rotational speed of 2,400 rpm, and flow rate of 773 mL/min. The highest FAME yield and production were 96.9 % and 1.86 mol/min, respectively.
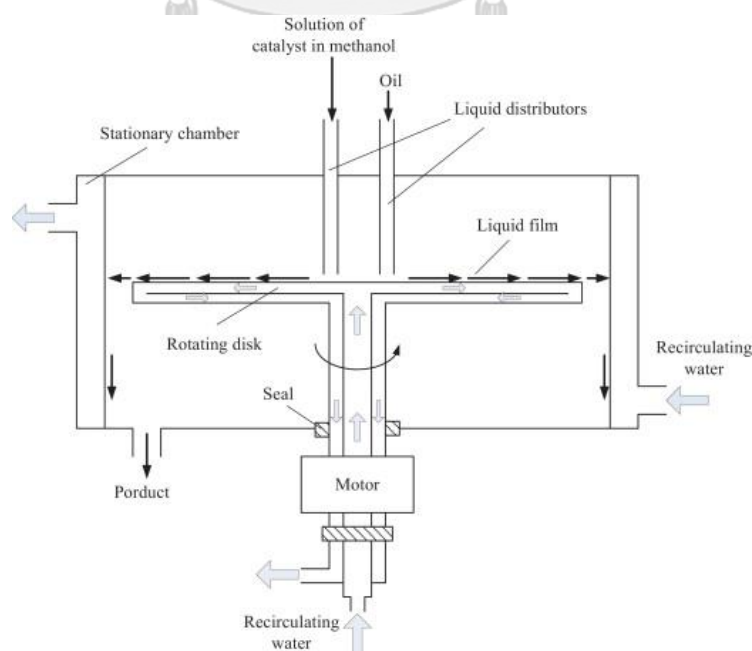
Figure 3.9 The main structure of an SDR [113].

3.2.14 Rotating/spinning tube reactors

Rotating/spinning tube reactor (RTR) is one of the process intensification technologies using the similar operating principle as well as spinning disk reactor (SDR). Because of the rapid rotation within RTR, the generation of centrifugal forces on the rotating tube surface lead to produce shear stress of thin films. Generally, the film thickness varies from 700 to 1,400 μm. The small thickness of thin film providing a very high surface area/volume ratio (∼1,000) can improve the interactions of film on the surface. Thus, heat and mass transfer are increased by spreading in thin film while excellent mixing is also obtained by generating curly films in reaction mixture. Lodha, H. et al. [63] studied the continuous biodiesel production of canola oil and methanol using rotating tube reactor (RTR). The maximum conversion was 97.65% under optimized condition of 6:1 methanol to oil molar ratio, 1.5 wt.% of NaOH, rotational speed at 670 rpm, flow rate of 900 mL/min, and residence time of 45 s.

To consider and compare the performance of biodiesel production in each reactor, the summarization of the process intensification technology for biodiesel production is shown in Table 3.2.

Table 3.2 Summary of the process intensification technologies of biodiesel production.

Type of reactor	Type of process	Reactant	Condition	Purity of methyl ester (%)	Yield eff. (g/J)	Ref.
Static mixer reactor (SM)	Continuous	RPO / methanol	RPO flowrate 20 L/h, 20 vol.% methanol, 12 g/L of KOH	95.70	N/A	[88]
Helical static mixers reactor (HSMs)	Continuous	PFAD / methanol	Two steps esterification, and one step transesterification, 115.1 wt.% methanol, 13.5 wt.% H_2SO_4, 5.0 g/L KOH and total residence time of 147 s in the 3 HSMs	99.96	N/A	[89]
Microchannel reactor	Continuous	WCO / methanol	9.4:1 methanol to oil molar ratio, 1.16 wt.% H_2SO_4 at 62.4 °C and residence time of 120 s	98.26	N/A	[91]
Micromixer with static elements (MES)	Continuous	Sunflower oil / ethanol	9:1 ethanol to oil molar ratio, 1 wt.% of NaOH at 50 °C and residence time 12 s	99.53	N/A	[92]
Liquid-liquid film reactor (LLFR)	Continuous	Soybean oil / methanol	Flow rate of oil 40 g/min, 6:1 methanol to oil molar ratio, 1 wt.% of NaOH at 55 °C	97.5	N/A	[93]
Packed tubular reactor	Continuous	WCO / methanol	25:1 methanol to oil molar ratio, 295 mm packed bed height of CaO/AC catalyst at 60°C and residence time 8 h	94	N/A	[94]

Table 3.2 Summary of the process intensification technologies of biodiesel production. *cont.*

Type of reactor	Type of process	Reactant	Condition	Purity of methyl ester (%)	Yield eff. (g/J)	Ref.
Rotating packed bed (RPB) reactor	Continuous	Soybean oil / methanol	6:1 methanol to oil molar ratio, rotational speed of 900 rpm and hydraulic retention time of 0.72 min	97.3	N/A	[95]
Oscillatory flow reactor (OFR)	Batch	WCO / methanol	6:1 methanol to oil molar ratio, 1 wt.% of NaOH, 0.67 Hz oscillation frequency at 60 ºC and reaction time of 30 min	78.8	N/A	[98]
Helical tube reactor	Continuous	Karanja oil/ methanol	Flow rate of oil 6.6 mL/min, 7:1 methanol to oil molar ratio, 0.8 wt.% of KOH at 65 ºC	92.3	N/A	[100]
Microwave reactor (MW)	Continuous	WCO / ethanol	12:1 ethanol to oil molar ratio, 3 wt.% NaOH and residence time of 30 s	> 97	N/A	[11]
Acoustic cavitation/Ultrasonic reactor (US)	Batch	Nagchampa oil / methanol	6:1 methanol to oil molar ratio, 1 wt.% of KOH at 60 ºC and reaction time of 40 min	92.5	0.1×10^{-4}	[106, 107]
Hydrodynamic cavitation reactor	Batch	UFO / methanol	6:1 methanol to oil molar ratio, 1 wt.% KOH at 60 ºC and reaction time of 10 min	> 95	1.28×10^{-3}	[109]
High Speed Homogenizer (HSM)	Batch	WCO / methanol	12:1 methanol to oil molar ratio, 3 wt.% of KOH at 50 ºC and reaction time of 120 min.	97	N/A	[110]

Table 3.2 Summary of the process intensification technologies of biodiesel production. *cont.*

Type of reactor	Type of process	Reactant	Condition	Purity of methyl ester (%)	Yield eff. (g/J)	Ref.
Spinning disk reactor (SDR)	Continuous	Soybean oil / methanol	Flow rate of 773 mL/min, 6:1 methanol to oil molar ratio, 1.5 wt.% of KOH, rotational speed at 2,400 rpm at 60 °C and residence time of 2–3 s	96.9	N/A	[113]
Rotating/spinning tube reactor (RTR)	Continuous	Canola oil / methanol	Flow rate of 900 mL/min, 6:1 methanol to oil molar ratio, 1.5 wt.% of NaOH, rotational speed at 670 rpm and residence time 45 s	97.65	N/A	[63]

3.3 Spinning tube in tube reactor (STT reactor) and rotating tube reactor (RTR)

Hampton P.D. [114] reported the study of the continuous production of aldehydes using a spinning tube in tube reactor (STT reactor). The Magellan STT reactor which was used as a prototype in this study is manufactured by Kreido Biofuels. The basic design of the Magellan STT reactor specified the narrow gap of 0.25 mm, the working length of 10.1 cm and the reactor volume of 1.43 mL. The modified motor of STT reactor provided a rotational speed of 4,000-6,000 rpm. The result showed that the high yields of $\geq$ 90% was achieved when using sodium hypochlorite/sodium bicarbonate at controlled pH 8.5 with organic solutions (TEMPO/tetrabutylammonium bromide/primary alcohol/toluene or CH_2Cl_2) through the Magellan STT with residence times 1-2 min. Moreover, the design principle of the Magellan STT was used to scale up the reactor volume from 1.43 mL to 38.6 mL.

Moreover, the incomplete reaction is a common chemical reaction which appears in ionic liquid synthesis. The batch process required a longer reaction time, higher temperature and solvent-intensive purification to troubleshoot. Since the reaction rate is the limitation of mass transfer, continuous-flow reactor as the spinning tube in tube (STT reactor) was chosen to eliminate this obstacle. The working volume of Magellan STT and the Innovator STT reactors were 1.29 and 27.1 mL, respectively. They were also used to synthesis of imidazolium ionic liquid. The narrow gap between the rotor and the stator was 0.25-0.44 mm and the rapidly rotational speed was up to 12,000 which induces the creation of thin film fluid inside the reactor. Since the molecular velocity in the thin-film fluid should be proportional to shear rate and depends on the rotation rate and gap size. To hold the constant shear rate, the design specification of both STT reactors was modified to be a suitable STT reactor resulting in the working volume was different around 21 times. The conversion of ionic liquid synthesis using the STT reactor directly depended on shear rate, the scale up into the larger reactor can occurred easily by setting the appropriate shear rate. Moreover, the 1-methylimidazole-based ionic liquids with >99% conversion and the throughput rate around 10 kg/day was achieved by the STT reactor [115].

The rotating tube reactor (RTR) is a novel reactor for continuous production and separation of biodiesel which is based on a thin film system [63]. The operation of

the RTR is similar to the STT reactor due to the emphasis on the thin-film generation inside the narrow gap. In RTR, the film thickness was varied from 700-1,400 μm resulting in a high surface area to volume ratio of around 1,000. The results showed that the biodiesel yield was increased when increase the catalyst loading (NaOH 1-2 wt.%), except at the condition of highest temperature (80ºC), highest (2 wt.%) and highest rotational speed (900 rpm) leading to obtain the saponification as a side reaction. The highest yield of 98% was achieved when catalyst concentration of 1.5 wt.%, rotational speed 670 rpm, temperature 60 ºC, the residence time of 45 s and a surface area to volume ratio of 900 mL/min. Moreover, the generation of centrifugal force inside the RTR results in easy separation between biodiesel and glycerol. Consequently, the development of intensified biodiesel production using RTR is beneficial for energy consumption, reaction time and separation process.

A review of rotating reactors was expressed by Visscher F. [34]. The spinning tube in tube reactor (STT reactor) is classified into a high shear rotating tube group while the rotating tube reactor (RTR) is classified into a low shear rotating tube group. The STT reactor consists of a rotating cylinder inside a stationary cylinder with concentric radial spacing between 0.25 mm and 0.44 mm. When the inner cylinder rotates, the fluid strokes on the inner surface of outer cylinder and generates shear force. The typical rotational speed of the inner cylinder is between 3,000 and 12,000 rpm with a reactor volume from 10 to 1,000 cm^3. The advantage of STT reactor is higher heat transfer rate; however, the lower reactor volume is a limitation of scale-up. The design of RTR is similar to the STT reactor which is the control the fluid flow inside the narrow gap. Since the RTR requires a low shear force, the rotational speed below 1,000 rpm has the typical range. The film thickness between 700 and 1,400 μm was appeared while the inner cylinder rotated. The advantage of RTR is a simple design, low pressure drop over the cylinder and reduced mass transfer limitation.

3.4 Residence time distribution (RTD) for continuous reactor

The study of RTD combined with τ is an essential tool to achieve the accurately prediction of the mixing degree for fluid traveling in the actual reactor as a nonideal flow behavior. Rotational speed and total flowrate are significant parameters which are the directly effect on the mixing degree and the hydrodynamic regime inside the reactor.

The alteration of total flowrate had a dramatic impact on the transformation of fluid regime because of the directly disturbance of axial velocity. Mohammadi, S. [32] studied the effect of flowrate on the RTD curve inside the SDR. The disturbance of fluid flow by increasing flowrate induced the intensive ripple generation on the fluid film surface. The instability of film surface produced the turbulence behavior leading to the increase of transverse mixing and more uniform radial velocity [116]. Moreover, the effect of flowrate is also reflexed in terms of the dispersion number. The RTD curve of higher flowrate that appeared the narrower and sharper peak had the lower value of dispersion number which can be attributed the generation of turbulent flow without dispersion effect in the flow direction.

The rotational speed is the essential parameter which is significantly influenced on the hydrodynamic regime and mixing degree inside RTR. The higher rotational speed induces the degree of mixing causing the increase of primary and secondary flow instabilities and creating more turbulent flow. RTD profile derived from higher rational speed was narrow and sharp. In contrast, the long tails of RTD curve appeared at a lower rotational speed. It may be indicated that insufficient centrifugal force of fluid flow resulted in the generation of dead space or stagnant fluid inside the reactor [74]. However, in the case of lower flowrate condition (lower fluid axial flow), the radial mixing which originated from the turbulence was remarkable parameter for the prediction of hydrodynamic regime because the turbulent 'eddies' is more significant than the axial flow velocity [117].

3.5 Human power device a viable electricity generator for intensification process

Mechtenberg, A.R. et al. [36] reported the usage of human powered device to generate electricity. Table 3.3 shows the general range of the power generation, the total capital cost, and the unitary capital cost of three human powered devices including the bicycle generator, the hand-crank surgical lamp, and the merry-go-round (MGR). The unitary capital cost of bicycle generator is the lowest due to the high power range generating and the low total capital cost.

Table 3.3 Comparison of three human powered devices [36].

Device	Power range (W)	Total capital cost (US $)	Unitary capital cost ($/W)
Bicycle	100 – 150	75 – 500	0.25 – 2.00
Hand-crank	50 – 100	50 – 500	1.00 – 3.00
MGR	100 – 600	500 – 2,400	2.00 – 4.00

A person who bikes at 125 W of power capacity for 1 h generates 125 Wh of electricity. To control the efficiency of storage and the rate of discharge electricity continuously, small battery is required to store the electricity from human powered devices. Since the power range generating of bicycle generator overlaps the power demand for electrical appliances which shown in Figure 3.10. Thus, human powered device is suitable for employing domestic usability and small businesses [36].
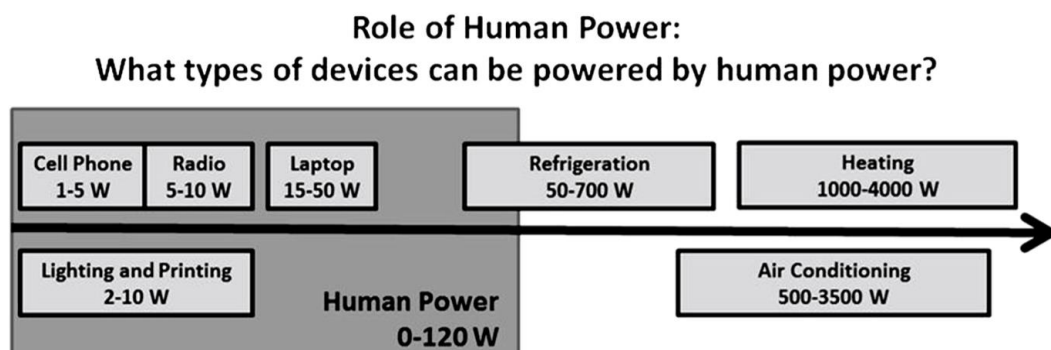
Figure 3.10 Spectrum of electrical devices according to power demand [36].

CHAPTER 4
RESEARCH PROCEDURE

This chapter provides materials and equipment for biodiesel production, the experimental setup, biodiesel analysis and the calculations of hydrodynamic regime in RTR and residence time distribution.

4.1 Materials for biodiesel production

4.1.1 Reactants

There are 2 reactants used to produce biodiesel including of vegetable oil and alcohol. Refined palm oil and waste cooking oil were used in this research as triglyceride sources. Refined palm oil in brand of Morakot industry Co. Ltd. was purchased from local store in Thailand. Analytical grade methanol (99.8% purity) was used in this research and purchased from Loba Chemie Pvt. Ltd. Methanol was preferred for biodiesel production because of its low cost and the physical and chemical advantages (polar and short-chain molecule). Moreover, methanol can easily dissolve the NaOH and can quickly react with triglycerides.

4.1.2 Catalyst

Sodium hydroxide pellet (99.0% purity) which was used as a catalyst in this study was purchased from Merck company Ltd.

4.1.3 Analytical agents

The biodiesel analysis, heptane (99.5% purity) which was used as a solvent for GC analysis was provided by Ajax Finechem Pty Ltd. Moreover, methyl heptadecanoate ($\geq$ 95% purity) which was used as an internal standard for GC analysis following ASTM EN14214 was provided by Sigma-Aldrich.

4.2 Materials for residence time distribution study

To study the residence time distribution of the RTR, the deionized (DI) water which is the major fluid always fed through the reactor. Methylene blue (Sigma-Aldrich) was used as the homogeneous tracer system. Moreover, glycerol was used as the component of the viscous solution and purchased from Elago Enterprises Pty Ltd.

4.3 Equipment

In this research, the RTR system was divided into 2 processes: rotating tube reactor (RTR) process and bicycle power generator system

4.3.1 Rotating tube reactor (RTR) process

The intensification reactors for the continuous biodiesel production are considered its efficiency by increasing of heat, mass and momentum transfers to accelerate reaction rate.

A schematic diagram and general view of continuous biodiesel production using the RTR is presented in Figure 4.1. A 3-phase motor (1/2 HP, 380 V) directly connected to the rotating tube reactor was used to operate the rotor (cylindrical core) inside the reactor. The rotational speed of the motor was controlled by an inverter. Two peristaltic pumps were used to feed substances while three vessels were used to contain refined palm oil (RPO), methanol-NaOH mixture and products. A heating system derived from a heating bath was an optional function used to control the reaction temperature.
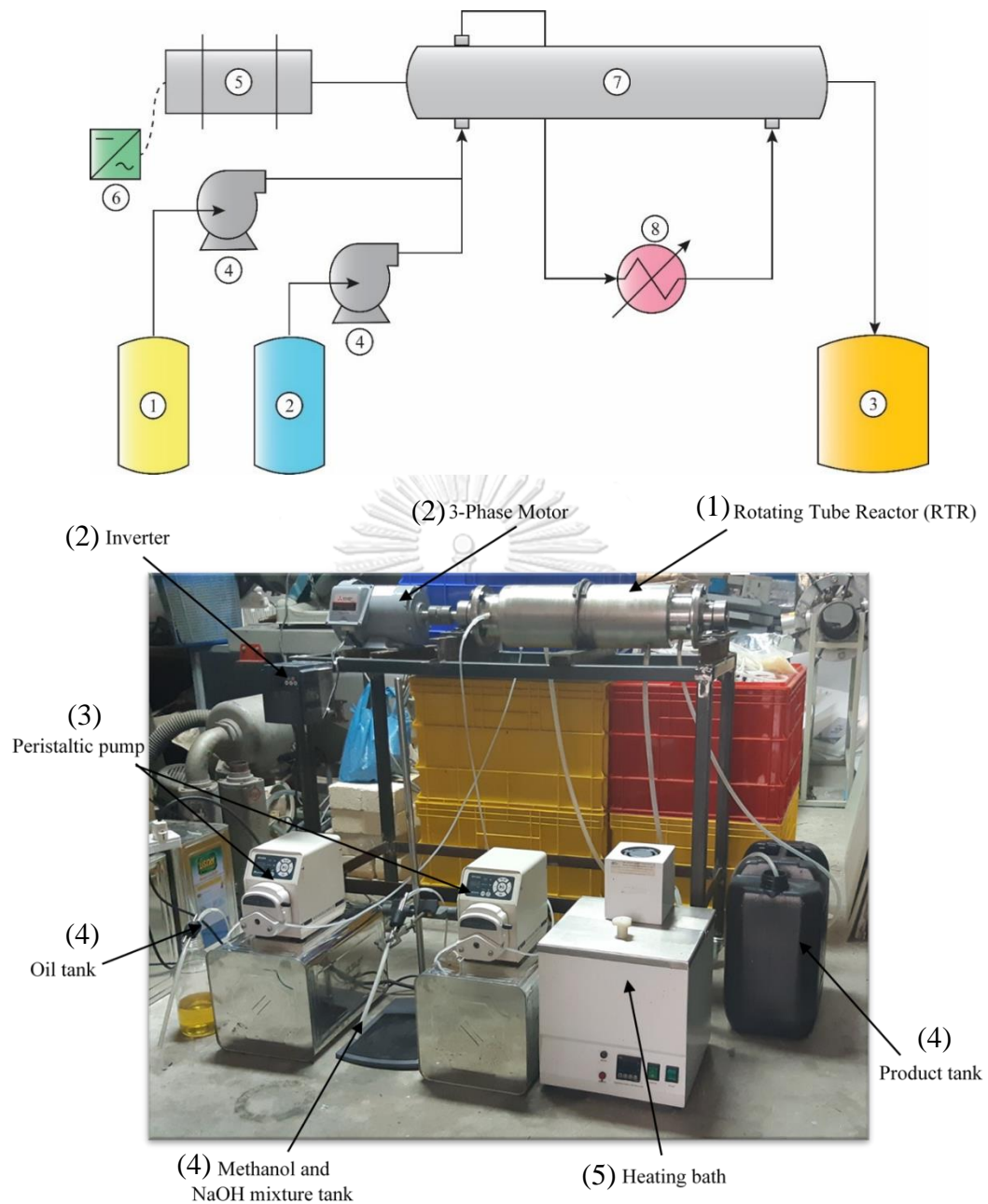
Figure 4.1 RTR prototype for continuous biodiesel production system including:
(1) RTR, (2) AC motor and inverter, (3) peristaltic pumps, (4) storage tank and
(5) heating bath.
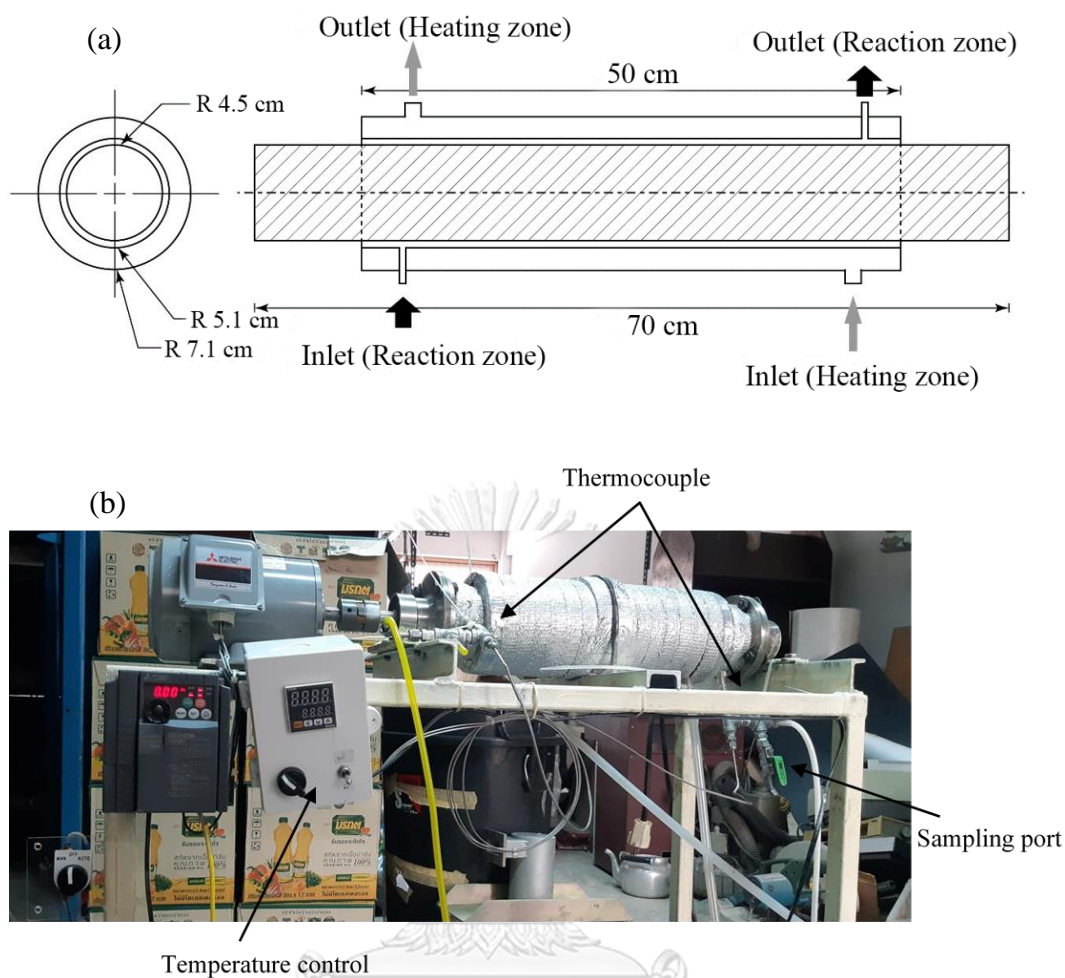
Figure 4.2 Schematic view of rotating tube reactor (RTR)
(a) drawing and (b) RTR photograph.

The schematic view and photograph view inside the RTR presented in Figure 4.2 consists of 3 tubes: (1) an inner tube which acted as the rotor that rotated rapidly inside a concentric stationary; (2) a middle tube which acted as the stator; and (3) an outer tube containing heating/cooling fluid to control the reaction temperature. The RTR consisted of two concentric zones (i.e., reaction and heating/cooling zones). The reaction zone was a small gap between the inner and the middle tubes. The heating/cooling source was a larger gap between the middle and the outer tubes. Rotation of the rotor generated a thin film in the reaction zone to increase the interfacial surface area of substances. The RTR was made from 316L stainless steel. The inner,

middle and outer tube diameters were 8.9, 9.4 and 13.5 cm, respectively. The radial spacing of the reaction zone was 2.35 mm obtained from the gap between the inner and the middle tubes. The reactor length and volume were 0.5 m and 0.337 L, respectively. Owing to the limitation of RTR construction, 2 thermocouples were installed between rotor and stator at inlet and outlet of RTR to measure the reaction temperature during biodiesel production process. The steady state temperature (T_{ss}) was calculated from the average of measured inlet and outlet temperature of RTR at the steady state conditions during the reaction.

4.3.2 Bicycle power generator system

The design of the power generation system is divided into two parts: the production of electricity from the bicycle power generator and the solar cell system as presented in Figure 4.3. The bicycle power generator system, which is a mechanical power generation system, was first developed because it was a simple design with few components and low production cost. The components of the bicycle power generator included [118].

(1) Bicycle, which is an essential device in the system connected to the axis of the motor. It serves to rotate the generator shaft.

(2) Generator, which generates electricity based on the principle of electromagnetic induction inside the device to convert the mechanical rotation to direct current (DC).

(3) Battery, which is the energy storage of the system, holding the electrical current produced by the generator and feeding the DC current to various devices.

(4) Inverter, which is a device converting DC current to AC current to be used with other electrical appliances.

The principle of the bicycle power generator system begins when it was cycling. As a result, the axis of the generator spins, resulting in electromagnetic induction within the device. The mechanical energy is converted into electrical energy in the form of direct current. Then, the DC current is sent to the battery to be used. When an electrical

device is connected, the DC current flows through the inverter to convert from DC-current to AC-current and sent to the device.

Although the DC power generation principle of the generator and RTR is the same, both equipment cannot be connected directly. This is due to the limitation that the generator rotation depended on human with nonuniform rotation speed. The RTR cannot work with a non-uniform current supplying to the motor of the RTR.
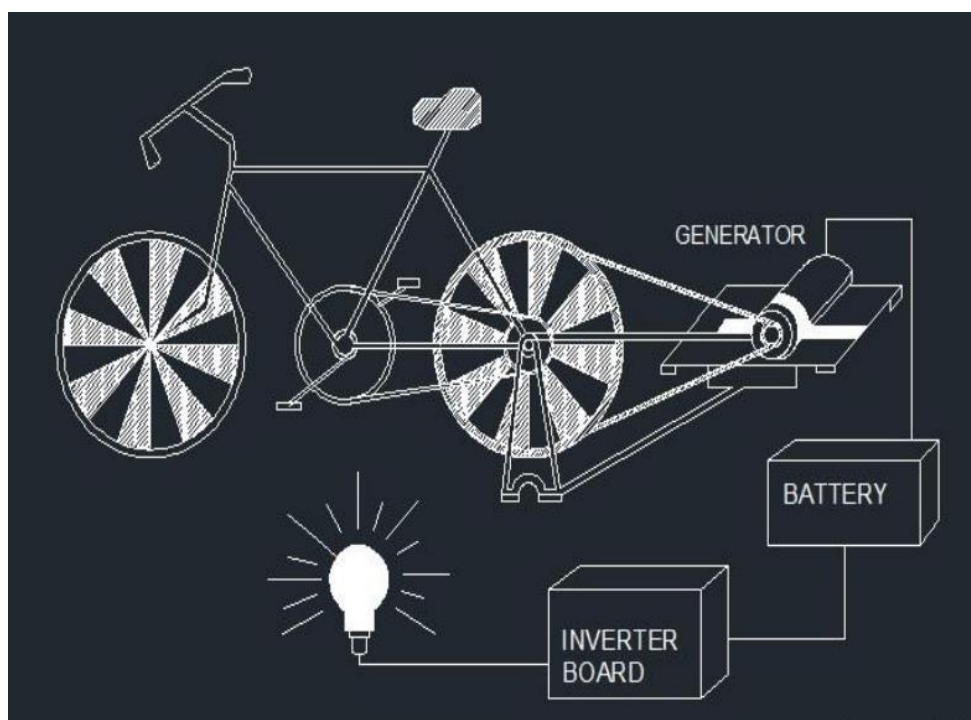
Figure 4.3 Schematic diagram of the bicycle powered generator system [118].

From the preliminary study, it was found that if the bicycle power generator system was the only system applied to the continuously operating RTR, the system operating could not be controlled as expected. This is because the power generation is not very high and it is difficult to have continuous electricity production from this system. Therefore, another power generation system has been introduced, which is a photovoltaic system.

The photovoltaic system is the most popular power generation system nowadays due to its low cost (compared to the service life), non-complicated system, as well high power generation efficiency. The photovoltaic system comprises the following [119]:

(1) Solar panel, which is a connection of several solar cells into one circuit to receive the solar irradiation.

(2) Battery, which is an energy storage device that stores electricity in the form of DC current.

(3) Inverter, which is a device converting DC current into AC current to be used with electrical appliances.

The operating principle of the photovoltaic system starts when light impinges on a semiconductor in the solar cell. The semiconductor converts light, which is an electromagnetic wave, into electrical energy in the form of DC current. Then, the DC current is stored in the battery. When an appliance is connected, the DC current is sent to the inverter to convert to AC current.

Although the performance of the photovoltaic system is high, there are several limitations, both in terms of installation space, climate conditions and working time. Therefore, implementing such a system as stand-alone may not be appropriate.

Combining the bicycle power generator system and the photovoltaic system is a good approach to increase the efficiency of the power generation system, as they both use DC current and have relatively similar sets of equipment. Besides, both systems have advantages that complement the performance of the system, making the system more complete. However, connecting the two systems has never been reported before; therefore, the combination of the two systems must be designed with a focus on safety to cover a wide range of applications.

The design of the combination of the bicycle power generator-photovoltaic system is shown in Figure 4.4. The principle of operation of the system starts from electricity generation in the form of DC current from the solar cell and bicycle power generator. However, the electrical power from the bicycle power generator is lower than that of the photovoltaic system, the voltage needs to be adjusted using a DC-DC

converter. The DC current is then sent to the hybrid solar inverter and is stored in the connected 12 V DC battery. When an AC electrical appliance is connected, the DC current from the battery is passed through the inverter to convert from DC to AC current to 220 V AC output. A DC electrical appliance can also be connected to the 12 V DC output. Figure 4.5 and Figure 4.6 show the solar panel and bicycle power generate prototype as developed in this research.
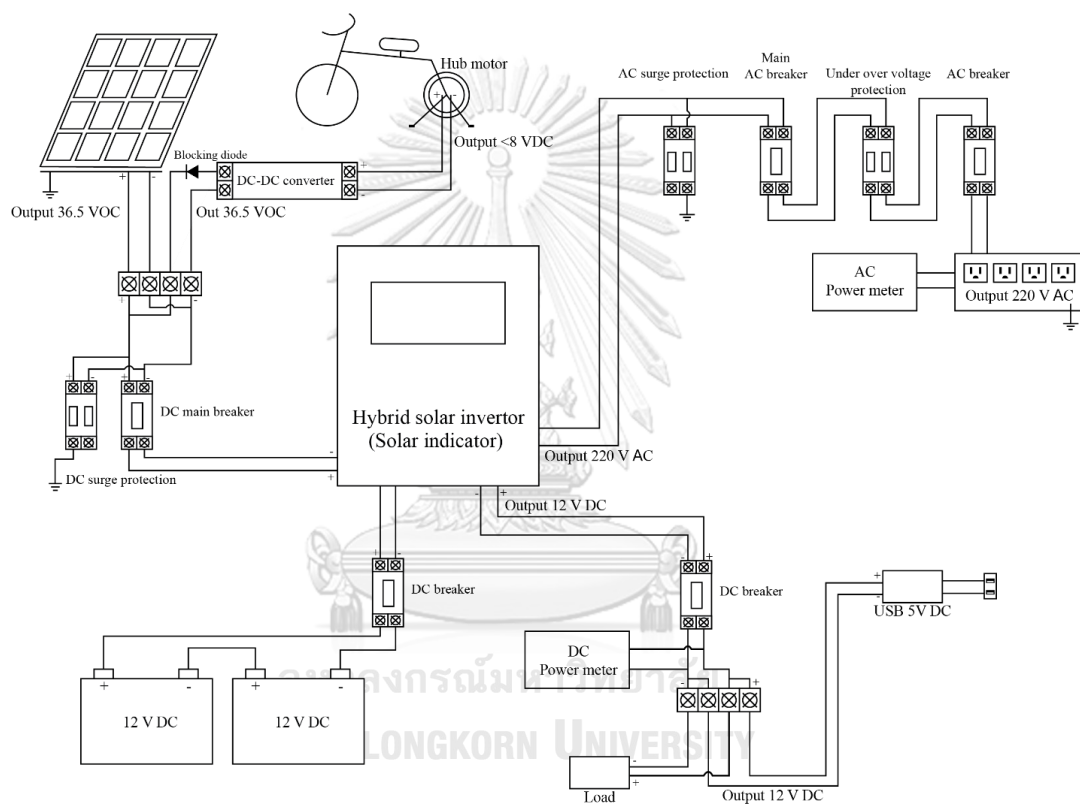
Figure 4.4 Solar-bicycle power generator system.

Figure 4.5 Solar panel location.

Figure 4.6 Bicycle power generator prototype.

4.4 Experimental procedure

This topic presents the operating condition of biodiesel production using batch reactor and RTR.

4.4.1 Continuous biodiesel production using RTR

The RTR performance test via the transesterification process was carried out by using a NaOH catalyst (0.5, 1 and 1.5 wt.%) which was homogeneously mixed with methanol. Then, the container of the methanol-NaOH mixture and RPO was connected to the inlet port of the RTR. Two peristaltic pumps were used to feed the substances into the RTR. The total flow rate was set at 30, 45, 60 and 75 mL/min. The methanol-to-oil molar ratios of 3:1, 4.5:1, 6:1 and 9:1 were investigated. The rotational speed of the RTR controlled by the inverter was examined from 900 to 1,200 rpm. The reaction was operated at atmospheric pressure, and the temperature was controlled in the range of room temperature (around 30°C), 45 and 60°C for 3 h. Samples were collected at 15, 30, 45, 60, 90, 120, 150 and 180 min to ensure the steady-state condition. The samples were quenched to stop the reaction and then were centrifuged to separate biodiesel (FAME) from the mixture and were purified by washing process before being analyzed by gas chromatography (GC). Triplicated experiment for transesterification of palm oil in RTR were performed to confirm the obtained results. All experimental results were expressed as the mean with ± standard deviation.

4.4.2 Separation and purification process for biodiesel production

Washing process is an essential process for increasing biodiesel purity. After the reaction mixture is centrifuged, methanol, biodiesel, and glycerol are separated into upper phase, middle phase, and lower phase, respectively. Biodiesel phase is washed with 20 vol.% of deionized water (around 50 $^{\circ}$C). After the solution settles, the separation of biodiesel from water is occurred. Washing process should repeat around 4 - 5 times to confirm that the catalyst or impurity in biodiesel does not existed. Then,

biodiesel is dried over 105 - 110 °C for 1 – 2 h, and finally, biodiesel is filtered by paper filter to obtain the final product.

4.4.3 Residence time distribution experiment

The tracer experiment was used to analyze the residence time distribution (RTD). Methylene blue was used as a tracer for this RTD study. However, transesterification reaction mixture (palm oil, methanol, FAME and glycerol) could not use for the RTD experiment due to the tracer of methylene blue could not dissolve in this reaction mixture. Therefore, the 50 wt.% of water-glycerol solution was selected as model fluid for RTD experiment because of its similar viscosity. A 2 mL pulse of 3 mmol/L of methylene blue in 50 wt.% of glycerol-water solution was rapidly injected into the RTR at the entrance of reactor in a minute to produce the pulsed injection. At the outlet of the RTR was sampling every minute. The absorbance value of methylene blue sampling solution was measured at the wavelength of 664.5 nm using a UV-vis spectrophotometer (Cary 5000 UV-Vis-NIR Spectrophotometer from Agilent). Rotational speed and total flow rate as the main parameters determined in this study were investigated in the range of 300-1,200 rpm and 30-75 mL/min, respectively. All experiments were controlled by the constant total time at 30 min to assure the steady pattern of flow regimes. A full factorial DOE was conducted to manage the experimental plan which includes 21 experimental runs as shown in Table 4.1.

Table 4.1 The DOE of residence time distribution experiment.

Experiment	Rotational speed (rpm)	Flowrate (mL/min)
1	900	45
2	300	75
3	1,200	75
4	600	60

Table 4.1 The DOE of residence time distribution experiment. *cont.*

Experiment	Rotational speed (rpm)	Flowrate (mL/min)
5	1,200	60
6	300	30
7	1,200	30
8	600	30
9	600	75
10	900	60
11	1,200	45
12	900	75
13	600	45
14	300	60
15	300	45
16	900	30
17	0	30
18	0	45
19	0	60
20	0	75
21	1,000	30

The absorbance value was converted to the concentration of methylene blue solution using the calibration curve of the measured absorbance with methylene blue concentration (Figure 4.7). The linear fitted was divided into 2 range at low and high concentration as presented in Figure 4.7. The concentration versus time of methylene

blue solution was used to calculate the age distribution functions $(E(t))$, the dimensionless formulation of the residence time distribution density $(E(\theta))$, mean residence time (τ) and dimensionless time parameter (θ) resulting in the evaluation of the variance of the residence time (σ_t^2) and the normalized variance (σ_θ^2), respectively.
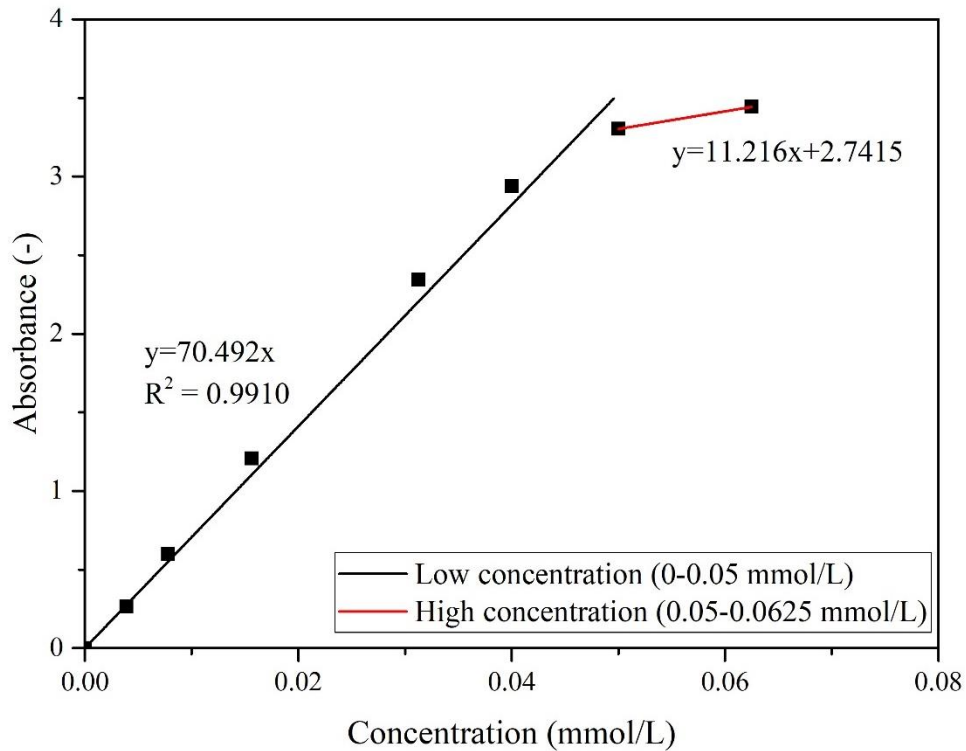
Figure 4.7 Calibration curve of methylene blue concentration with the measure absorbance.

4.5 Biodiesel analysis

The biodiesel yield is analyzed following EN14103 using Shimadzu GC-2010 Plus, with DB-WAX capillary column with 30 m (length), 0.32 mm (diameter) and 0.25 µm (film coating) and detected by flame ionization detector (FID). Helium and Nitrogen are used as carrier and make up gas. For GC analysis, the initial temperature was 150°C with a holding time of 5 min. Then, the temperature programming rate of 3°C/min was used to increase the temperature from 150 to 190°C and hold for 5 min.

Finally, the temperature was increased from 190 to 220°C using the temperature programming rate of 3°C/min and hold for 5 min.

4.5.1 Biodiesel yield calculation

Biodiesel yield which is defined as the methyl ester purity of biodiesel is calculated by Equation (10).

$$\text{Biodiesel yield}(\%) = ((\textstyle\sum A - A_{\text{IS}})/A_{\text{IS}}) \times (C_{IS} \times V_{\text{IS}}/m_{\text{S}}) \times 100 \qquad (10)$$

where $\sum A$ Total area of fatty acid methyl ester

A_{IS} Area of methyl heptadecanoate (internal standard)

C_{IS} Concentration of methyl heptadecanoate (mg/mL)

V_{IS} Volume of methyl heptadecanoate (mL)

m_{S} Mass of biodiesel sample (mg)

4.5.2 Yield efficiency calculation

Yield efficiency is defined in Equation (11).

$$\text{Yield efficiency} = \text{Amount of biodiesel produced (g)/Energy required for reaction (J)} \qquad (11)$$

4.6 Hydrodynamic regime in the RTR

The physical properties such as kinematic viscosity and density of the reaction mixture which are dependent on the temperature in the RTR were also calculated by using the correlations as follows:

(1) The composition of biodiesel derived from palm oil comprised of 38.73 wt.% methyl palmitate, 10.20 wt.% methyl stearate, 46.73 wt.% methyl oleate and 4.34 wt.% methyl linoleate obtained from Chaiyaso's report [120] was used to calculated the kinematic viscosity and density of the produced biodiesel at different temperature. The calculated kinematic viscosity at 40°C was similar to the experimental

value of the produced biodiesel of 4.502×10^{-6} m^2/s. The density of produced biodiesel at 15°C was also calculated based on the mass fraction of fatty acid methyl ester following the previous report, which was found to be 875.1 kg/m^3 being similar to the measured values due to its similar feedstock (palm oil) [121].

(2) Aspen Plus simulation was used to calculate the temperature-dependent kinematic viscosity and density of methyl palmitate, methyl stearate, methyl oleate and methyl linoleate as presented in Appendix A (Figures. A1 and A2), respectively. The dynamic viscosity of palm oil was measured using a Brookfield viscometer at desired temperatures which yielded similar values to the information obtained from Lipico Technologies Pte. Ltd [122]. The kinematic viscosity and density of palm oil were obtained from Lipico Technologies Pte. Ltd. in the temperature range of 25 to 60°C as illustrated in Figure A3. The dynamic viscosity and density of methanol in the temperature range of 0 to 62°C were obtained from Anton Paar GmbH company [123] as expressed in Figure A4. The dynamic viscosity and density of glycerol were obtained from the previous research [124] as shown in Figure A5.

(3) Gambill method [125] was used to calculate the kinematic viscosity of the produced biodiesel in the RTR based on the composition from the previous study [126] as expressed in Equation (12).

$$\nu^{(1/3)} = x_a \nu_a^{(1/3)} + x_b \nu_b^{(1/3)} \tag{12}$$

(4) The fraction of the reaction mixture was calculated based on the measurement of biodiesel yield obtained from Equation (10). The resulting solution was composed of the produced biodiesel, the unreacted palm oil and methanol because the produced glycerol was earlier separated from the resulting solution. The quantity of produced glycerol was assumed to be 10% of produced biodiesel. For instance, the biodiesel yield of 67.4 wt.% referred to the unreacted palm oil and methanol were 32.6 wt.%. Based on the molar ratio of methanol to palm oil of 6:1, the calculated mass fractions of palm oil and unreacted methanol were 26.5 and 6.1 wt.%, respectively. The produced glycerol was calculated to be 6.74 wt.% based on 10 wt.% of produced biodiesel. The total composition of the reaction mixture in the RTR as produced

biodiesel, glycerol, unreacted palm oil and methanol was 63.1, 6.3, 24.8 and 5.7 wt.%, respectively. The calculated mass fraction was further used to calculate temperature-dependent kinematic viscosity (Gambill method) and average density of the reaction mixture in the RTR.

จุฬาลงกรณ์มหาวิทยาลัย
CHULALONGKORN UNIVERSITY

CHAPTER 5
RESULTS AND DISCUSSION

This chapter presents the results and discussion of all experiments which is divided into 4 sections: transesterification of biodiesel production in RTR, correlation of hydrodynamic regimes in RTR, residence time distribution analysis for thin film flow in RTR and solar-bicycle powered electricity generator to supply RTR.

5.1 Transesterification for biodiesel production in RTR

5.1.1 Effect of methanol-to-oil molar ratio

The effect of methanol-to-oil molar ratio was investigated in the range of 3:1 to 9:1 on a steady-state biodiesel yield for biodiesel production in the continuous RTR as illustrated in Figure 5.1.

As expected, the lowest steady-state biodiesel yield was around $44.3 \pm 4.4\%$ when using the methanol-to-oil molar ratio of 3:1, as well as the theoretical stoichiometric transesterification of triglycerides. This result can be explained that when the reaction was carried out, 3 mol of methanol reacted with 1 mol of triglyceride to produce 3 mol of FAME (biodiesel) and 1 mol of glycerol. A soap formation was observed at this condition which could be due to the excessive alkali catalyst concentration compared to the small amount of methanol in the reaction mixture, which can react with triglyceride via saponification resulting in the generation of soap and the reduction of biodiesel yield [127, 128].
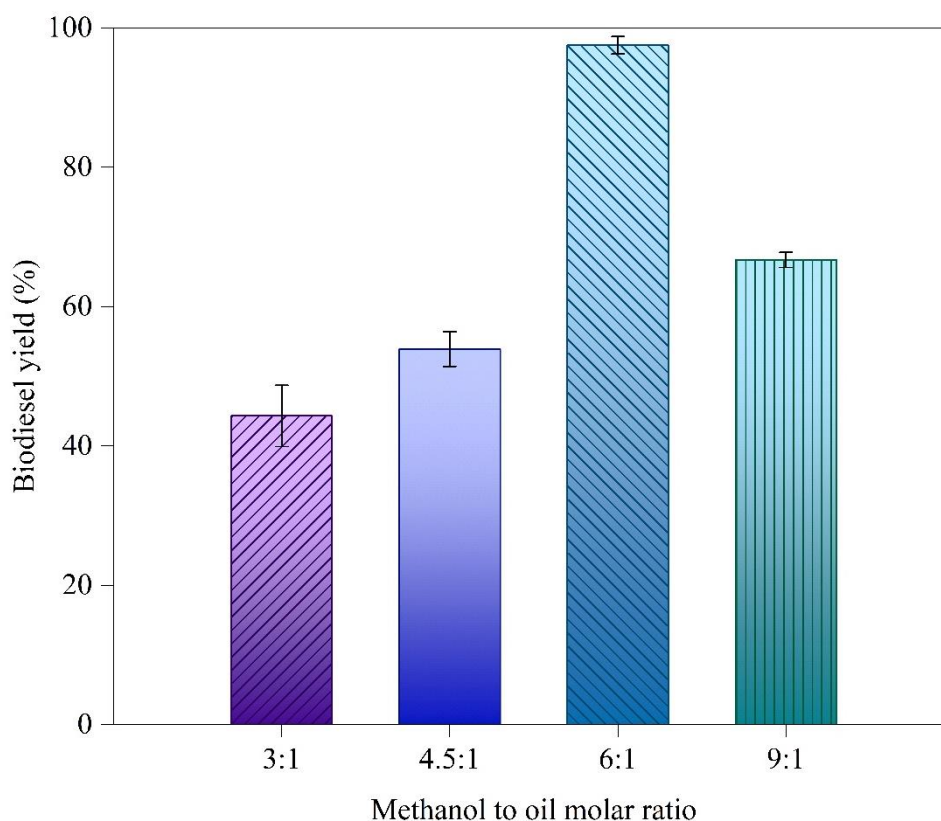
Figure 5.1 Effect of methanol-to-oil molar ratio on steady-state biodiesel yield using NaOH loading of 1 wt.%, total flow rate of 30 mL/min and rotational speed of 1,000 rpm operated in continuous RTR at room temperature.

Moreover, transesterification is a reversible reaction that causes the dynamic equilibrium in the reaction mixture. Therefore, the reaction will shift to the forward direction when using excess methanol resulting in increasing biodiesel yield [127]. Based on these results, increasing the methanol-to-oil molar ratio to 4.5:1 and 6:1 enhanced biodiesel yield to 53.9 ± 2.5 and $97.5 \pm 1.3\%$, respectively.

Nevertheless, biodiesel yield decreased when the methanol-to-oil molar ratio was increased to 9:1. There are several potential hypotheses. For instance, the difference in molecular polarity between biodiesel and glycerol tended to separate the reaction mixture into two layers. Being a polar compound, as well as a short-chain and amphiphilic molecule, excessive methanol remaining in the reaction mixture can dissolve in both biodiesel and glycerol layers. A high concentration of methanol in the biodiesel layer could raise the polarity of biodiesel in the reaction mixture. Accordingly,

some glycerol can dissolve in the biodiesel leading to more turbidity in the biodiesel layer. Moreover, the biodiesel can also dissolve in the excess methanol layer to reduce biodiesel yield in its layer [129-131] The second hypothesis is that glycerol and biodiesel in each layer can reverse the reaction to monoglyceride and diglyceride resulting in the decrease of biodiesel yield and the increase of emulsion formation [130]. Based on the same total flow rate of the liquid, the excess methanol could reduce the concentration of triglyceride leading to a decreased transesterification rate [132]. According to the result in Figure 5.1, this RTR can operate at room temperature to provide a high biodiesel yield comparable to the previous work [63] without any external heat source. Only shear force can generate sufficient heat for this reaction. It can be suggested that the optimal methanol-to-oil molar ratio for NaOH catalyzed transesterification of refined palm oil using the continuous RTR was 6:1.

5.1.2 Effect of NaOH loading

The effect of NaOH loading (0.5, 1 and 1.5 wt.% based on the weight of oil) was examined using methanol-to-oil molar ratio of 6:1, total flowrate of 30 mL/min and rotational speed of 1,000 rpm at room temperature as shown in Figure 5.2.

The lowest biodiesel yield occurred when using the smallest amount of NaOH (0.5 wt.%). The lowest NaOH loading generates the lowest amount of the methoxide anion as an active site leading to the incomplete reaction indicated by the lowest biodiesel yield [95, 133]. When the NaOH loading was increased to 1 wt.%, biodiesel yield increased which can be attributed to more active sites to accelerate the transesterification rate [127]. However, biodiesel yield was reduced when using the highest NaOH loading of 1.5 wt.%. This can be explained that the excess alkali catalyst generates an emulsion phase within the reaction mixture resulting in increasing saponification of triglycerides and biodiesel [134]. Saponification is an undesirable reaction for biodiesel production because this reaction produces soap as an emulsifier for biodiesel and glycerol layer resulting in the generation of strong film barriers of glycerol and the difficulty in the biodiesel purification process [127, 134, 135].

Therefore, the optimal NaOH loading was 1 wt.% for transesterification of refined palm oil using this RTR.
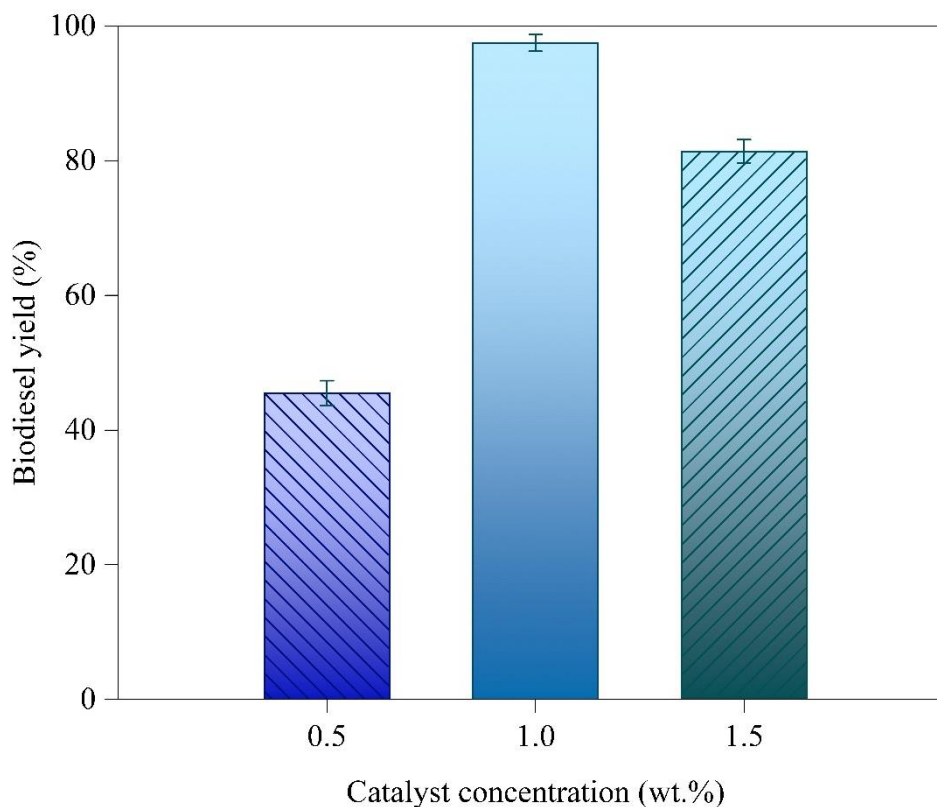
Figure 5.2 Effect of NaOH loading on steady-state biodiesel yield using methanol-to-oil molar ratio of 6:1, total flow rate of 30 mL/min and rotational speed of 1,000 rpm operated in continuous RTR at room temperature.

5.1.3 Effect of rotational speed

The rotational speed is a crucial operating parameter of using the RTR for biodiesel production to enhance mass transfer of immiscible oil and methanol. To provide a sufficient shear rate and shear stress, the effect of rotational speed on biodiesel yield was investigated in the range of 900 to 1,200 rpm as presented in Figure 5.3.
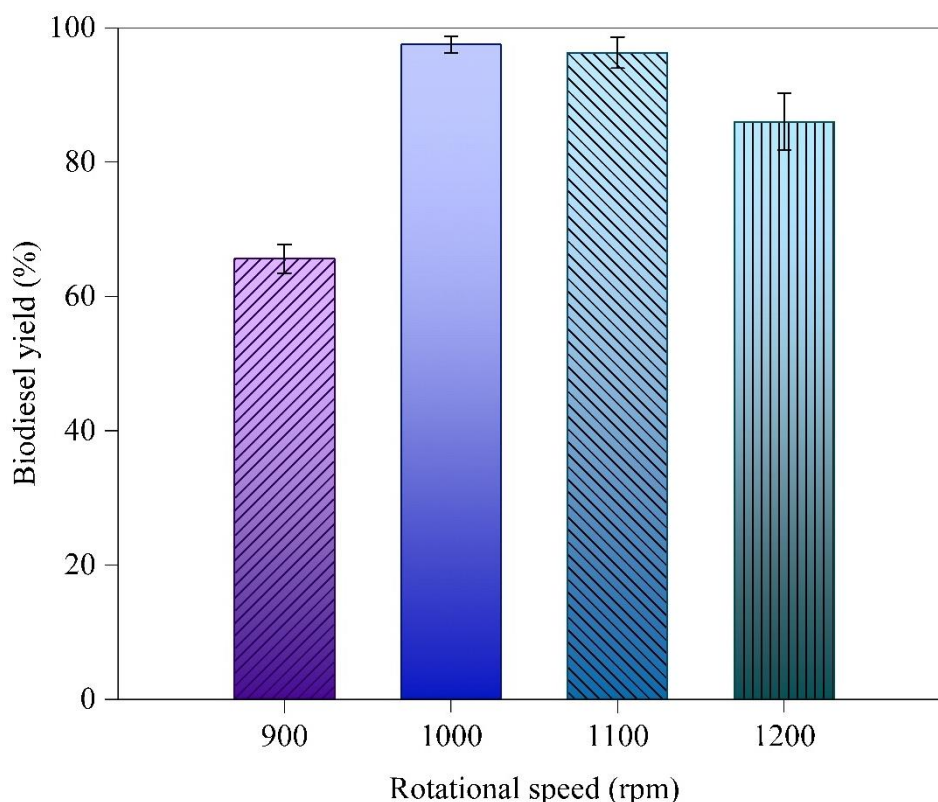
Figure 5.3 Effect of rotational speed on steady-state biodiesel yield using methanol-to-oil molar ratio of 6:1, NaOH loading of 1 wt.% and total flow rate of 30 mL/min operated in continuous RTR at room temperature.

When the rotational speed was increased from 900 to 1,000 rpm, the biodiesel yield was raised from 65.6 ± 2.1 to 97.5 ± 1.3%. Poor flow occurred at the low rotational speed (900 rpm) owing to the lower centrifugal force which might be present in the two layers of methanol and oil with less solubility. As the density of methanol is lower than that of palm oil, it stayed near the inner tube while palm oil stayed near the outer tube based on the centrifugal force. The calculated shear rate was 3,300 s $^{-1}$ which is lower than the range of the design specification [22]. Increasing the rotational speed results in the enhancement of shear force and the interfacial contact area of thin-film reactants in the narrow gap of the reaction vessel [63, 127]. Methanol and oil came into more perfect contact to produce more biodiesel yield due to the nature of homogeneous alkali catalyzed transesterification that is limited by the mass transfer resistance between the methanol and oil phases [136]. However, the biodiesel yield was slightly decreased by about 10% when the rotational speed was increased to 1,200 rpm. The

calculated shear rate was higher than 3,670 s $^{-1}$ within the range of the design specification [22]. This should be remarked that the increase in rotational speed can have a counterbalancing effect on the shear force with the increase of the rotation velocity and the decrease of the reaction mixture viscosity, resulting in reduced biodiesel yield. Moreover, the increase of the rotational speed as proportional to shear rate (friction force) can increase the heat dissipation of viscous force on the interfacial contact of the reaction mixture and the surface of the RTR [137, 138] to enhance the vaporization rate of methanol which should decrease biodiesel yield [139, 140].

5.1.4 Effect of total flowrate

The total flowrate, as well as the residence time, is one of the important parameters for continuous biodiesel production which indicated the efficiency of the reactor [141]. The effect of total flowrate on a steady-state biodiesel yield was studied using the methanol-to-oil molar ratio of 6:1, NaOH concentration of 1 wt.% and rotational speed of 1,000 rpm at room temperature as presented in Figure 5.4.

The investigation on the total flowrate was in the range of 30 – 75 mL/ min corresponding to the residence time of 11.23 to 4.49 min, respectively. Since the short residence time was insufficient for the reaction mixture, a low biodiesel yield was obtained [30]. This RTR provides a shorter residence time as compared to the previous report using KOH catalyzed transesterification with similar methanol to palm oil molar ratio in a CSTR [69]. In addition, the axial velocity was increased with an increasing total flowrate which might disturb the hydrodynamic regime inside the gap of RTR [142].

Figure 5.4 Effect of total flow rate on steady-state biodiesel yield using methanol-to-oil molar ratio of 6:1, NaOH loading of 1 wt.% and rotational speed of 1,000 rpm operated in continuous RTR at room temperature.
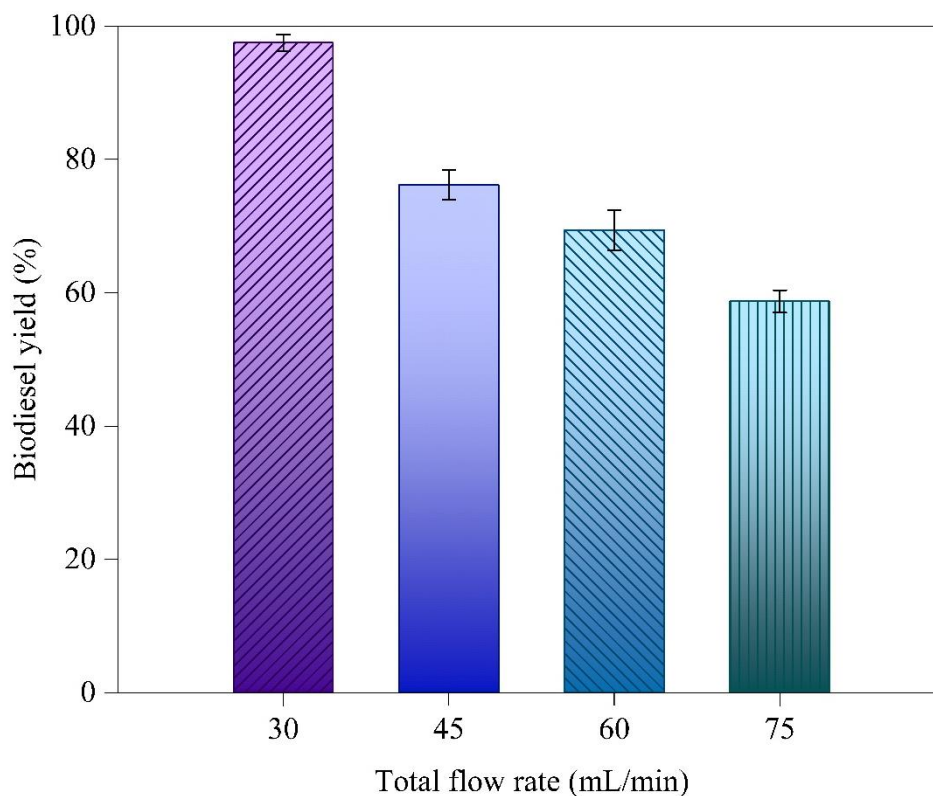
5.1.5 Effect of temperature on biodiesel production

Based on the chemical kinetics, the reaction temperature is one of the main parameters to increase both the reaction rate and biodiesel yield. Moreover, the increased reaction temperature also influences the physical properties of the reaction mixture especially viscosity which can affect the hydrodynamics regime [138]. Therefore, the effect of temperature was investigated using the reaction temperatures of 30, 45 and 60 °C as illustrated in Figure 5.5. As mentioned before, heat can be self-generated during the RTR operation. Based on the total flowrate of 30 mL/min, the increase in reaction temperate could decrease the RTR performance as indicated by biodiesel yield. Therefore, the effect of reaction temperature using different total flowrates of 30 and 60 mL/min was also investigated.
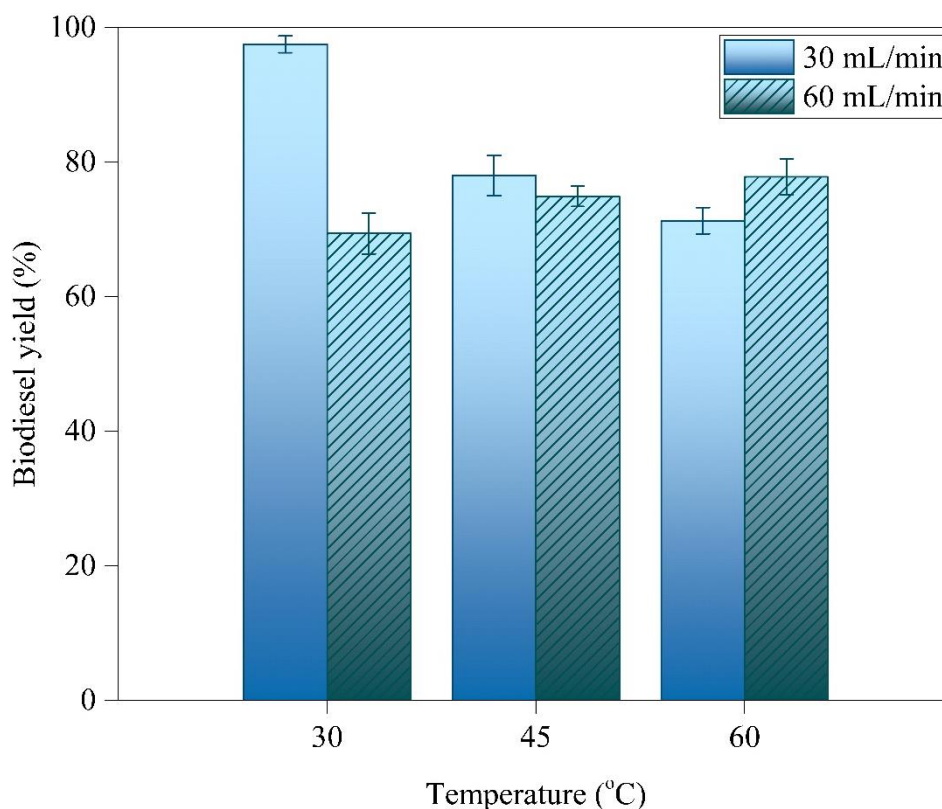
Figure 5.5 Effect of temperature on steady-state biodiesel yield using methanol-to-oil molar ratio of 6:1, NaOH loading of 1 wt.%, total flow rate of 30 and 60 mL/min, rotational speed of 1,000 rpm with various reaction temperature of 30, 45 and 60°C.

The effect of the temperature parameter can be explained based on the two total flowrates as follows.

(1) At a low total flowrate and low reaction temperature condition, the high viscosity of the reaction mixture was obtained as derived from refined palm oil as the major component in the reaction mixture. When the rotor rapidly rotates inside the reactor, the high viscosity of the reaction mixture drives the high shear force and generates a thin film layer of the reaction mixture with a larger interfacial contact area [140]. The generation of shear force increased mass transfer and heat transfer in the reaction mixture leading to high biodiesel yield at a low total flowrate and low reaction temperature in the RTR. In contrast, when the reaction temperature was increased, the generated excess heat in the reaction mixture derived from shear force and the external heating source accelerated the methanol vaporization and reduced the reaction mixture viscosity. Therefore, the lower biodiesel yield occurred [143]. This finding

corresponded with the previous research [144-146] which described that the dynamic viscosity was proportional to the negative exponential of temperature.

(2) At a high total flowrate, the self-heating intensity derived from the shear force of the RTR might be insufficient to accelerate transesterification [147]. The increase in reaction temperature by additional heat from a heating source could drive the transesterification rate to produce a higher biodiesel yield. Moreover, the initial time to reach steady-state was significantly decreased from 30 to 15 min with the increase in the reaction temperature using the total flowrate of 60 mL/min. In addition, biodiesel yield was slightly increased with increasing reaction temperature by using a high total flowrate of 60 mL/min which reduced the residence time from 11.23 to 5.61 min and equally reduced the heating contact time, resulting in less observed methanol vaporization. However, as mentioned above, the higher heat intensity for transesterification of palm oil in the RTR tended to reduce biodiesel yield due to the vaporization of methanol and reduction of reaction mixture viscosity. It can be concluded that the optimal condition for using the RTR at room temperature to produce biodiesel (according to the EN standard) was methanol-to-oil molar ratio of 6:1, NaOH loading of 1 wt.%, rotational speed of 1,000 rpm and total flowrate of 30 mL/min based on the highest biodiesel yield.

5.1.6 Yield efficiency

Biodiesel yield is one of the main targets to determine the intensification process instead of the conventional process. The economics of biodiesel production that relates to the other parameters such as reaction time and input energy should be considered to evaluate the costs of biodiesel production. Therefore, yield efficiency was used to evaluate the reactor performance based on the amount of biodiesel production, energy consumption and also reaction time [112]. The measurement of total energy consumption included the electrical power input to the RTR and peristaltic pump. In practice, the purity of biodiesel was increased after the purification process [148]. When using the reaction mixture with biodiesel yield higher than 90%, the FAME content after the purification process should conform to the EN 14214 standard, which requires

the minimum FAME content of 96.5%. Therefore, the condition produce biodiesel yield greater than 90% was selected to calculate yield efficiency. Figure 5.6 depicts that the values of yield efficiency were 3.75×10^{-3} and 3.06×10^{-3} g/J for biodiesel production in the RTR using the rational speed of 1,000 and 1,100 rpm, respectively.
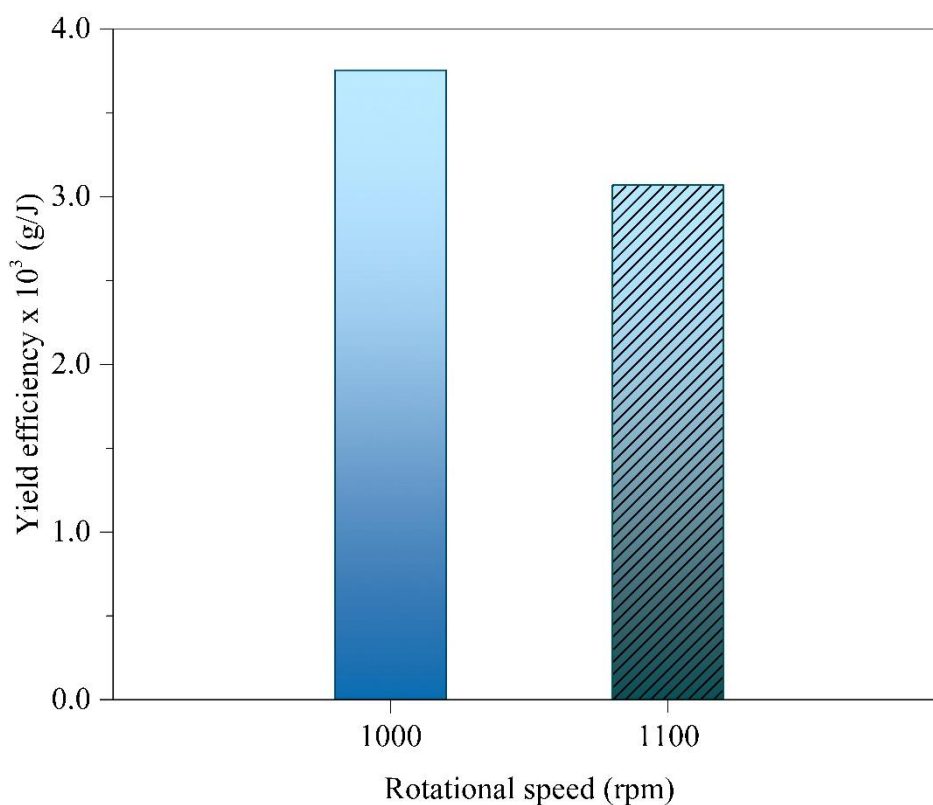
Figure 5.6 Yield efficiency of biodiesel production in RTR based on 90% biodiesel yield.

The comparison of the intensification processes for biodiesel production via transesterification using alkali catalyst obtained from previous studies were also presented in Table 5.1.

Table 5.1 shows the yield efficiency obtained from this study was mostly higher compared to the other ultrasound-based reactors and hydrodynamic cavitation reactors. This is because this RTR operated at room temperature without any additional heating source which can significantly reduce the energy consumption for biodiesel production. This finding proves that an RTR is a promising reactor for biodiesel production. In addition, the operating hydrodynamic regime of MWVT in the RTR can produce the

highest biodiesel yield with the highest yield efficiency. Although the yield efficiency of biodiesel production using a homogenizer was higher than that of the RTR, the drawback of the homogenizer is that it is mainly used in a batch process which might be a limitation of the production scale-up.

Table 5.1 Comparison study of yield efficiency of the intensification processes for biodiesel production via transesterification using alkaline catalyst.

Type of reactor	Process	Feedstock	Condition	Time (min)	Yield (%)	Yield efficiency (g/J) x 10³	Ref.
Acoustic cavitation reactor	Batch	Vegetable oil	4 g of vegetable oil is mixed with 4 mL of methanol in the presence of 0.5% NaOH as a catalyst	10	99.0	0.086	[108]
Hydrodynamic cavitation reactor	Batch	Vegetable oil	4,000 g of oil is mixed with 4000 mL of methanol (4:4 ratio (wt./vol.) of oil to alcohol) in the presence of 1% NaOH as a catalyst	15	98.0	3.370	[108]
Hydrodynamic cavitation reactor	Batch	Used frying oil	6:1 methanol to oil molar ratio in the presence of 1% KOH as a catalyst at temperature of 60 °C	60	95.0	1.280	[109]
Hydrodynamic cavitation reactor	Batch	Nagchampa oil	6:1 methanol to oil molar ratio in the presence of 1% KOH as a catalyst at temperature of 60 °C	20	92.1	0.870	[107]
Ultrasonic reactor	Batch	Nagchampa oil	6:1 methanol to oil molar ratio in the presence of 1% KOH as a catalyst at temperature of 40 °C	40	92.5	0.010	[106]
Hydrodynamic cavitation reactor	Batch	Refined cooking oil	6:1 methanol to oil molar ratio in the presence of 1% KOH as a catalyst at temperature of 60 °C	15	98.0	1.275	[149]
Hydrodynamic cavitation reactor	Batch	WCO	6:1 methanol to oil molar ratio in the presence of 1% KOH as a catalyst at temperature of 60 °C	15	98.0	1.250	[149]

Table 5.1 Comparison study of yield efficiency of the intensification processes for biodiesel production via transesterification using alkaline catalyst. *cont.*

Type of reactor	Process	Feedstock	Condition	Time (min)	Yield (%)	Yield efficiency (g/J) x 10^3	Ref.
Ultrasonic reactor	Batch	Refined palm oil	6:1 methanol to oil molar ratio in the presence of 1% NaOH as a catalyst at temperature of 60 °C	180	93.0	1.090	[112, 149]
Homogenizer reactor	Batch	Refined palm oil	6:1 methanol to oil molar ratio in the presence of 1% NaOH as a catalyst at temperature of 60 °C	180	94.0	8.450	[112, 149]
Hydrodynamic cavitation reactor	Continuous	Cannabis sativa oil	6:1 methanol to oil molar ratio in the presence of 1% KOH as a catalyst at temperature of 60 °C	120	97.5	1.100	[149, 150]
Rotating tube reactor	Continuous	Refined palm oil	6:1 methanol to oil molar ratio in the presence of 1% NaOH as a catalyst at ambient temperature (around 30 °C)	180	97.5	3.750	This study

5.1.7 Properties of biodiesel derived from transesterification of palm oil in RTR

Biodiesel produced from the intensification RTR at the optimal condition was further analyzed on the important properties for diesel engines including density, flash point, calorific value, kinematic viscosity and oxidation stability. It was found that the properties of the obtained biodiesel followed the ASTM standard as can be seen in Table 5.2. Biodiesel properties should also be of concern for a commercial production process. Although some of the processes show a high production rate, biodiesel properties do not conform to the standard so it cannot be readily used in a real diesel engine.

Viscosity is a measure of the resistance of the fluid to flow which leads to opposing the dynamic change of fluid motion [151]. In this study, the kinematic viscosity of biodiesel at 40 $^{\circ}$C was 4.502 ($\pm$ 0.003) $\times 10^{-6}$ m^2/s which is within the allowable range according to the ASTM standard of approximately 1.9–6 $\times 10^{-6}$ m^2/s.

Density is one of the main physical properties which is a measure of mass per unit volume of fluid [152-154]. From this study, the density was approximately 875.1 $\pm$ 0.1 kg/m^3 which is within the range of the ASTM standard (approximately 860–900 kg/m^3).

Flash point is the lowest temperature at which some of the fuel can vaporize into the air and the vapor mixture can be ignited when exposed to flame. In this study, the flash point of biodiesel was about 163 $^{\circ}$C which was within the range of the ASTM standard (higher than approximately 130 $^{\circ}$C).

Calorific value is an amount of thermal energy released or produced by the combustion of a unit quantity of fuel. In the ASTM standard, the calorific value is limited to between 35 and 45 MJ/kg. From this study, the calorific value was around 38.175 $\pm$ 0.067 MJ/kg which is in agreement with the ASTM standard.

Acid value (AV) is a measure of free fatty acids (FFAs) present in fat or oil which is defined by the neutralization of organic acids with the KOH solution. In this

study, the acid value of biodiesel was 0.1337 ± 0.0025 mg KOH/g which is lower than the maximum allowable in the ASTM standard.

Oxidation stability refers to the tendency to generate chemical reactions when the fuel combines with oxygen at ambient temperature [155]. In the ASTM standard, the minimum oxidation stability is 3 h. The oxidation stability from this study was 12.67 h which is substantially higher than the minimum value of the ASTM standard.

Table 5.2 Biodiesel properties according to ASTM D6751 standard.

Property	Biodiesel	
	ASTM standard	This study
Kinematic viscosity at 40 °C (m^2/s) x10^6	1.9 – 6	4.502 ± 0.003
Density (kg/m^3)	860 – 900	875.1 ± 0.1
Flash point (°C)	> 130	163
Calorific value (MJ/kg)	35 – 45	38.175 ± 0.067
Acid value (mg KOH/g)	Max 0.5	0.1337 ± 0.0025
Oxidation stability at 110 °C (h)	Min 3	12.67

5.2 Correlation of hydrodynamic regimes in RTR using various operating parameters

Several parameters influence the RTR performance. This section proposed the hydrodynamic regime inside the gap of the RTR to gain more understanding of using the RTR to enhance biodiesel production efficiency. The operating principle of the RTR resembles the general Taylor-Couette device which increases the capability of mixing two or more than two immiscible substances by increasing interfacial contact area and generating a turbulent flow pattern (perfect mixing). The critical Taylor number (Ta_{cr}) is proportional to the axial Reynolds number (Re_x). The critical Taylor number is defined for the transition from circular Couette flow of hydrodynamic regimes to the

Taylor vortex regime. The higher value of Ta induces a higher turbulence level. At the same Re_x, the values of the Taylor number greater than Ta_{cr} represent the hydrodynamic regime in a Taylor vortex flow [25, 156, 157] This regime can generate a higher degree of mixing in the gap of the RTR. In contrast, the Ta below the Ta_{cr} represents only the circular Couette flow of hydrodynamic regimes. The effect operating parameters on the hydrodynamic regime in terms of methanol-to-oil molar ratio, NaOH loading, rotational speed, total flow rate, and reaction temperature were investigated in Figure 5.7 (a) – (f).
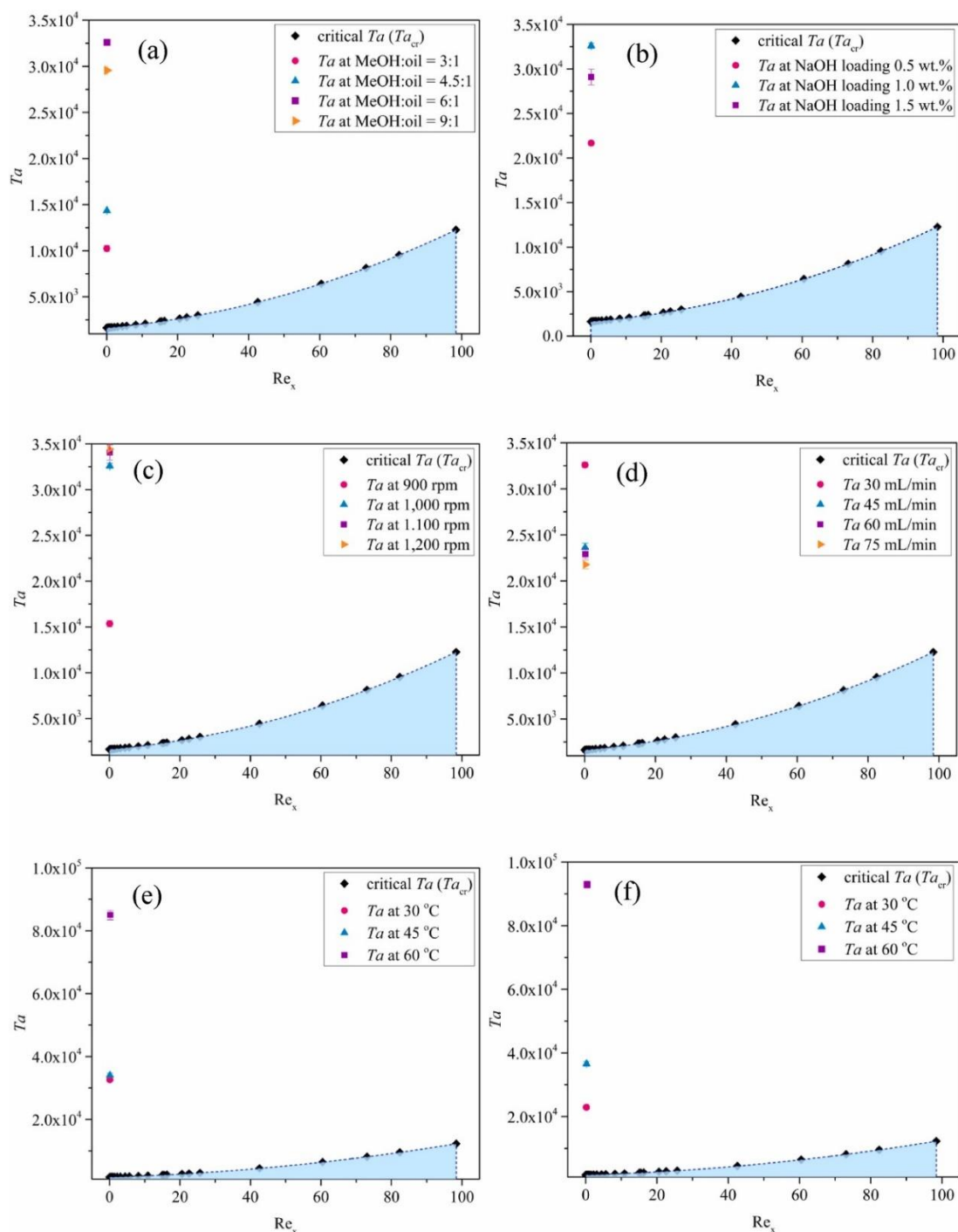
Figure 5.7 Taylor number versus axial Reynolds number for $\eta = 0.95$ based on (a) methanol-to-oil molar ratio, (b) NaOH loading, (c) rotational speed, (d) total flow rate (e) reaction temperature at 30 mL/min and (f) reaction temperature at 60 mL/min in RTR.

The calculated value of Ta obtained from various operating conditions were greater than the critical Ta (Ta_{cr}) [156] while the Re_x were quite similar which was

related to the flow rate. This was found that increase methanol-to-oil molar ratio from 3:1 to 6:1 and NaOH loading from 0.5 to 1.0 wt.% gave rising the Ta as well as biodiesel yield as present in Figure 5.7 (a) and (b) respectively. However, when the methanol-to-oil and NaOH were further increased to 9:1 and 1.5 wt.%, the Ta were decreased corresponded to biodiesel yield. The rotational speed as important parameter to facilitate the degree of mixing in the RTR. As expected, the Ta values were propotional to the rotational speed well as the reaction temperature as depicted in Figure 5.7 (c), (e) and (f). The increase of reaction temperature can decrease the viscosity of reaction mixture resulting to increase the Ta as corresponding to the previous research [138]. The effect of total flow rate was reversed results as illustrated in Figure 5.7 (d), the Ta and biodiesel yield were decreased with increasing of total flow rate from 30 to 75 mL/min. This was due to the residence time was reduced with increase of total flow rate. However, the Ta were greater than 1,713 based on the highest Re_x in this study ($Re_x = 0.42$) for all operating condition which can generate the Taylor vortex flow regime providing a sufficient degree of mixing to produce biodiesel via transesterification.

Generally, the flow dynamics in the conventional tube are divided into 3 regimes including laminar flow ($Re < 2,300$), transitional flow ($2,300 < Re < 4,000$) and turbulent flow ($Re > 4,000$). With a similar concept of the hydrodynamic regime in the RTR, the hydrodynamic regime transforms from laminar to turbulent when the rotation rate of the RTR increases through the generation of unstable laminar asymmetric flow and hydrodynamic instabilities, respectively [25]. The major factor for the transformation of flow regimes is rotational speed which relates to the rotating Reynolds number [69]. Beyond the critical rotating Reynolds number ($Re_{r,\text{cr}}$) associated with the laminar-turbulent configuration, the formation of steady toroidal vortices since the pure azimuthal Couette flow at the critical condition occurred, namely, Taylor vortex flow (TVF). At higher Re_r, a secondary instability causes the deformation of vortices resulting in the next flow regime, known as wavy vortex flow (WVF). When Re_r further increases, the WVF transforms to modulated wavy vortex flow (MWVF) and eventually becomes turbulent Taylor vortex flow (TTVF) [158].

Moreover, the gap width is one of the major factors affecting the hydrodynamic regimes in addition to the rotation rate. The narrow gap (higher η) induces the transformation of the flow regime to turbulent Taylor vortex flow more than the larger gap (smaller η) [70]. For the rotating inner cylinder and stationary outer cylinder, secondary instability appears when the radius ratio (ratio of inner diameter to outer diameter) is greater than 0.714 resulting in the generation of a secondary vortex [159, 160]. In the present study, the radius ratio of the RTR was approximately 0.95; therefore, the flow regime should be in the range of WVF to TTVF regime.

Unfortunately, there was no report regarding the flow regime related to Re_r using ($\eta = 0.95$). Therefore, the flow characteristics for the Taylor-Couette flow device based on ($\eta = 0.9$) was adopted to compare the flow regime of this study as presented in Table 5.3. The hydrodynamic regimes are divided into 4 patterns including TVF regime indicated by Re_r with $Re_{r,cr}$ of 125 and WVF regime corresponding to Re_r between 165 and 680. Re_r in the range of 680 to 1,150 represented a MWVF regime, while Re_r greater than 1,150 provided TTVF regime. The TVF regime occurs when the fluid flows through a narrow gap which is the cause of secondary instability and generation of secondary vortices, respectively. Secondary vortices improve the mixing efficiency because of the increase in both axial and radial dispersions. At higher Re_r a secondary instability causes the deformation of the secondary vortices resulting in the WVF regime [4]. As Re_r further increases, the disorder of the WVF regime results in the MWVF regime. When Re_r increases to greater than 1,150, the secondary flow is more complex because the small tertiary vortices are produced between the inner cylinder and the corners of the secondary vortices and the wall which is in the TTVF regime [52].

In this study, the Re_x was quite similar for all operating conditions as determined from the axial velocity as can be seen in Table 5.3. This is worth mentioning that the operating parameters including methanol-to-oil molar ratio, NaOH loading, rotational speed and reaction temperature gave the positive effect on the increase in the calculated Ta, as well as the degree of mixing of the hydrodynamic regime in the RTR.
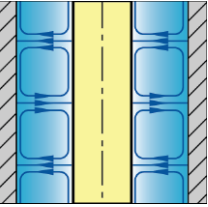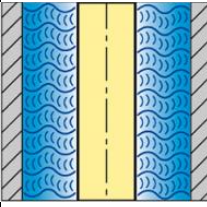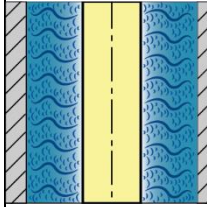
The effect of total flowrate posed the negative effect as decreasing Ta with the increase of total flowrate from 30 to 75 mL/min due to their difference in residence time. However, only the Ta value could not fully describe the deviation of biodiesel yield based on different Ta values. Re_r was calculated to gain more insight into the hydrodynamic regimes related to biodiesel yield. This study found that Re_r was in the range of 440 – 1,326 corresponding to the hydrodynamic regimes in the RTR as WVF, MWVF and TTVF derived from different operating conditions. Low biodiesel yields were observed in the presence of the WVF regime except at the total flowrate of 45 and 60 mL/min, while the MWVF regime can enhance biodiesel yield in the range of 66.7 – 97.5%. Aforementioned, the Re_r value of 669 and 658 based on total flowrate of 45 and 60 mL/ min provided high biodiesel of 76.2 and 69.4%, respectively. Based on the obtained biodiesel yield, the hydrodynamic regime should be MWVF instead of WVF. This can suggest that the residence times were different and that the range of transformation of the hydrodynamic regime might not be accurate for this study because of the different radius ratio (Re_r) from the previous report [4]. Unexpectedly, the biodiesel yield of 66.7% was obtained from the methanol-to-oil molar ratio of 9:1 with the MWVF regime. The explanation should be that the high methanol concentration in the reaction mixture can 1) increase the solubility of biodiesel in the glycerol phase to reduce the biodiesel content and 2) reduce the triglyceride concentration to minimize the transesterification rate [126]. Moreover, the biodiesel yield was decreased by 10% when using the rotational speed of 1,200 rpm within the MWVF regime. This finding confirms that using a higher rotational speed increased the shear force together with excessive heat dissipation in the RTR [58]. Unfortunately, the average steady-state temperature of the reaction mixture in this research was measured at the inlet and the outlet of the gap in the RTR which might not be the exact reaction temperature during the transesterification process. The presence of the TTVF regime providing more mixing degrees should enhance the biodiesel yield. However, this study found that the biodiesel yields obtained from the reaction temperature 60 $^\circ$C were significantly dropped by about 20% based on the highest biodiesel yield of 97.5% with the presence of the MWVF regime. The transesterification rate should be proportional to the reaction temperature based on the Arrhenius equation. Therefore, the hypothesis of the excessive heat dissipation was carried out inside the RTR to reduce viscous force and to vaporize
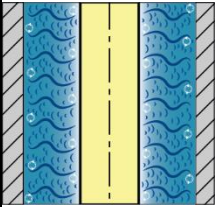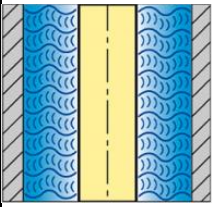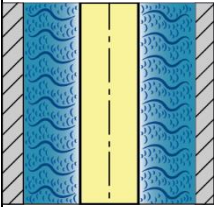
methanol resulting in the vapor-liquid two-phase mixture. This Re_r could be used to determine the optimal operating condition to obtain the MWVF regime with high biodiesel yield via a single liquid-phase transesterification in the Taylor-Couette flow device. To reduce the methanol vaporization rate, using cooling system might be applied for the higher rotational speed of the RTR (> 1,200 rpm). However, the yield efficiency was also reduced because it required more energy for cooling system circulation. This should be noted that the presence of the vapor-liquid phase might be a limitation to achieve economical biodiesel production as expected from the TTVF regime in the Taylor-Couette flow device.

จุฬาลงกรณ์มหาวิทยาลัย
CHULALONGKORN UNIVERSITY

Table 5.3 Summary of flow characteristics for Taylor-Couette flow device ($\eta = 0.9$) using different operating condition and produced biodiesel yield.

Parameter	T_{ss} (°C)	Re_x	Re_r	Ta	Type of flow regime with Re_r for transition	Flow regime[a]	Biodiesel yield (%)
-	-	-	-	-	TVF $Re_{r,cr} = 125$	TVF	-
Effect of methanol-to-oil molar ratio							
3:1	32.8 ±1.0	0.07 ±0.00	440 ±6.8	10,248 ±311.4	WVF $1.32Re_{r,cr} < Re_r < 5.44Re_{r,cr}$ 165 − 680	WVF	44.3 ±4.4
4.5:1	32.3 ±1.0	0.08 ±0.00	521 ±0.4	14,352 ±24.3			53.9 ±2.5
6:1	38.9 ±1.6	0.13 ±0.00	785 ±3.5	32,598 ±286.7	MWVF $5.44Re_{r,cr} < Re_r < 9.2Re_{r,cr}$ 680 − 1,150	MWVF	97.5 ±1.3
9:1	36.2 ±0.8	0.12 ±0.00	748 ±0.2	29,566 ±12.3			66.7 ±1.1

Table 5.3 Summary of flow characteristics for Taylor-Couette flow device ($\eta = 0.9$) using different operating condition and produced biodiesel yield. *cont.*

Parameter	T_{ss} (°C)	Re_x	Re_r	Ta	Type of flow regime with Re_r for transition	Flow regime[a]	Biodiesel yield (%)
-	-	-	-	-	TTVF $Re_r > 9.2Re_{r,cr}$ $Re_r > 1,150$	TTVF	-
Effect of NaOH loading							
0.5 wt.%	39.0 ±1.3	0.10 ±0.00	640 ±4.0	21,679 ±267.3	WVF $1.32Re_{r,cr} < Re_r < 5.44Re_{r,cr}$ $165 - 680$	WVF	45.5 ±1.8
1.0 wt.%	38.9 ±1.6	0.13 ±0.00	785 ±3.5	32,598 ±286.7	MWVF $5.44Re_{r,cr} < Re_r < 9.2Re_{r,cr}$ $680 - 1,150$	MWVF	97.5 ±1.3
1.5 wt.%	39.1 ± 1.4	0.12 ±0.00	742 ±11.2	29,091 ±880.1		MWVF	81.4 ±1.7

Table 5.3 Summary of flow characteristics for Taylor-Couette flow device ($\eta = 0.9$) using different operating condition and produced biodiesel yield. *cont.*

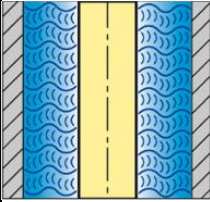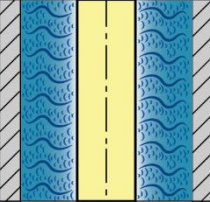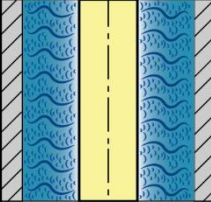| Parameter	T_{ss} (°C)	Re_x	Re_r	Ta	Type of flow regime with Re_r for transition	Flow regime[a]	Biodiesel yield (%)
Effect of rotational speed							
900 rpm	34.3 ±1.6	0.10 ±0.00	539 ±6.2	15,366 ±352.2	WVF $$1.32Re_{r,cr} < Re_r < 5.44Re_{r,cr}$$ $165 - 680$	WVF	65.6 ±2.1
1,000 rpm	38.9 ±1.6	0.13 ±0.00	785 ±3.5	33,000 ±286.7	MWVF $$5.44Re_{r,cr} < Re_r < 9.2Re_{r,cr}$$ $680 - 1,150$	MWVF	97.5 ±1.3
1,100 rpm	39.5 ±1.2	0.12 ±0.00	803 ±9.7	34,049 ±827.2			96.3 ±2.3
1,200 rpm	40.1 ±1.3	0.11 ±0.00	807 ±6.9	34,423 ±588.1			86.0 ±4.2
Effect of total flow rate*							
30 mL/min (residence time = 11.23 min)	38.9 ±1.6	0.13 ±0.00	785 ±3.5	33,000 ±286.7	MWVF $$5.44Re_{r,cr} < Re_r < 9.2Re_{r,cr}$$ $680 - 1,150$	MWVF	97.5 ±1.3
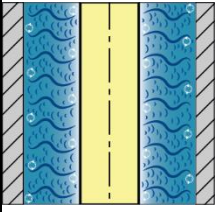
Table 5.3 Summary of flow characteristics for Taylor-Couette flow device ($\eta = 0.9$) using different operating condition and produced biodiesel yield. *cont.*

Parameter	T_{ss} (°C)	Re_x	Re_r	Ta	Type of flow regime with Re_r for transition	Flow regime[a]	Biodiesel yield (%)
45 mL/min (residence time = 7.49 min)	36.6 ±0.8	0.16 ±0.00	669 ±6.5	23,627 ±460.4	WVF $1.32Re_{r,cr} < Re_r < 5.44Re_{r,cr}$ 165 – 680	WVF	76.2 ±2.3
60 mL/min (residence time = 5.61 min)	34.9 ±0.6	0.21 ±0.00	658 ±7.6	22,906 ±529.4			69.4 ±3.0
75 mL/min (residence time = 4.49 min)	35.2 ±0.7	0.26 ±0.00	642 ±6.7	21,772 ±455.6			58.7 ±1.7
Effect of temperature (flowrate 30 mL/min)							
30°C	38.9 ±1.6	0.13 ±0.00	785 ±3.5	33,000 ±286.7	MWVF $5.44Re_{r,cr} < Re_r < 9.2Re_{r,cr}$ 680 – 1,150	MWVF	97.5 ±1.3
45°C	44.7 ±1.2	0.13 ±0.00	803 ±8.2	34,077 ±696.7			78.0 ±3.0

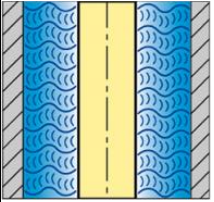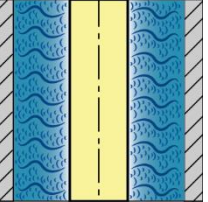**Table 5.3** Summary of flow characteristics for Taylor-Couette flow device ($\eta = 0.9$) using different operating condition and produced biodiesel yield. *cont.*

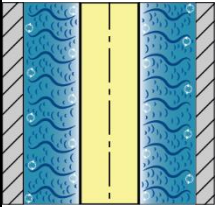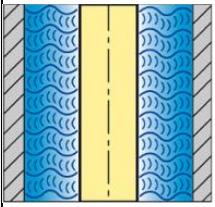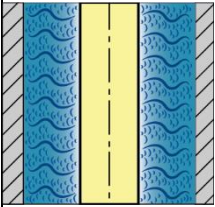| Parameter	T_{ss} (°C)	Re_x	Re_r	Ta	Type of flow regime with Re_r for transition	Flow regime[a]	Biodiesel yield (%)
60°C*b	61.9 ±1.4	0.20 ±0.00	1,268 ±11.2	85,031 ±1502.5	TTVF $Re_r > 9.2Re_{r,cr}$ $Re_r > 1,150$	TTVF	71.3 ±2.0
Effect of temperature (flowrate 60 mL/min)							
30°C	34.9 ±0.6	0.21 ±0.00	658 ±7.6	22,906 ±529.4	WVF $1.32Re_{r,cr} < Re_r < 5.44Re_{r,cr}$ $165 - 680$	WVF	69.4 ±3.0
45°C	43.1 ±1.2	0.27 ± 0.00	832 ±8.9	36,583 ±785.5	MWVF $5.44Re_{r,cr} < Re_r < 9.2Re_{r,cr}$ $680 - 1,150$	MWVF	74.9 ±1.5

Table 5.3 Summary of flow characteristics for Taylor-Couette flow device ($\eta = 0.9$) using different operating condition and produced biodiesel yield. *cont.*

Parameter	T_{ss} (°C)	Re_x	Re_r	Ta	Type of flow regime with Re_r for transition	Flow regime[a]	Biodiesel yield (%)
60°C*[b]	58.3 ±1.0	0.42 ±0.00	1,326 ±7.4	92,952 ±1039.4	TTVF $Re_r > 9.2Re_{r,cr}$ $Re_r > 1,150$	 TTVF	77.8 ±2.7

[a] flow regimes were modified from [67].

[b] appeared vapor-liquid phase mixture due to methanol vaporization

Generally, the hydrodynamic regime is also dependent on the velocity profile and torque generation by adjusting the rotational speed for the concentric RTR. However, the eccentricity of the RTR can also influence the hydrodynamic regime based on similar parameters such as temperature (related to viscosity and density of the liquid mixture) and rotational speed, etc. Due to the mechanical design limitation, the effect of RTR eccentricity was not investigated. The characteristic of the hydrodynamic regimes depends not only on the rotational speed but also on the different physical properties of the reaction mixture in the RTR; therefore, the effects of operating parameters on the correlation between $\sqrt{Ta}$, toque and biodiesel yield were also examined in this study. This should be noted that the effect of total flowrate was excluded for this consideration because of different residence time as already stated.

Figure 5.8 shows the correlation between $\sqrt{Ta}$, toque and biodiesel yield which indicated the difference in the hydrodynamic regime, as well as the value of Re_r. The results illustrated the different slopes derived from different operating conditions. At the low value of $\sqrt{Ta}$, the first slope of the linear plot was generated from the operating condition of methanol-to-oil malar ratio of 3:1 and 4.5:1, NaOH loading of 0.5 wt.% and rotational speed of 900 rpm. This indicated the hydrodynamic regime of WVF with the slope of $2,449\sqrt{Ta}$ corresponding to low biodiesel yield. For the moderate value of $\sqrt{Ta}$, the change of the slope of the liner plot ($3,053\sqrt{Ta}$) was observed to indicate the presence of the MWVF regime, providing high biodiesel yield. Furthermore, for the high value of $\sqrt{Ta}$, the third slope of the linear plot ($3,790\sqrt{Ta}$) was acquired from the operating condition of reaction temperature of 60 °C to indicate the change of the hydrodynamic regime from MWVF to TTVF. However, the biodiesel yield produced from this operating condition was reduced due to the vaporization of methanol from the excessive heat generation inside the RTR as evident from the steady-state temperature of 58 – 62 °C. These calculated values including Re_r and the correlation between torque and $\sqrt{Ta}$ can be used as indicators to improve biodiesel production efficiency in the RTR. It should be concerned that the requirement of a more turbulent TTVF hydrodynamic regime by increasing the rotational speed or the reaction temperature might not provide the high biodiesel yield because of the redundant heat generation inside the RTR to vaporize methanol, leading to lower biodiesel yield.
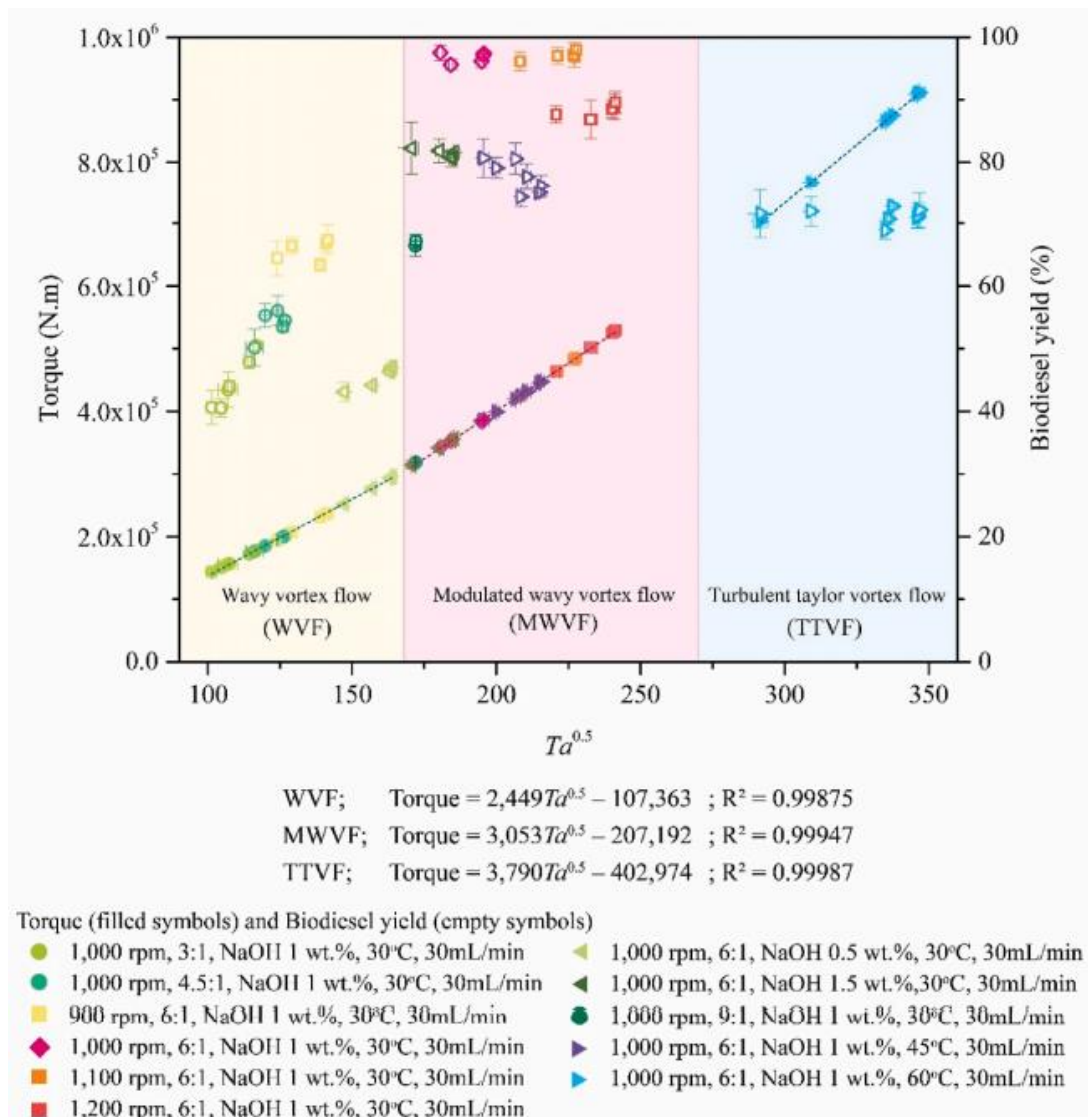
Figure 5.8 Relation of torque and Taylor number for various rotational speeds using ($\eta = 0.95$) (yellow zone: wavy vortex flow, pink zone: modulated wavy vortex flow and blue zone: turbulent Taylor vortex flow).

5.3 Residence time distribution (RTD) of thin film flow in RTR

Residence time is one of the most critical parameters for reactor design and scale up as referred to the average time that fluid travels in a reactor during a continuous process. Residence time distribution (RTD) analysis combines the chemical kinetics, momentum and mass transfer which can be used to predict the chemical reaction conversion [161]. The basic calculation of residence time by the ratio of total volume to total flowrate might be inaccurate since the operating principle of RTR based on a

nonideal flow reactor depends on the dispersion and turbulence intensity of fluid. The study of residence time distribution (RTD) and mean residence time (τ) can estimate accurate residence time and express the appearance of fluid flow behavior/pattern based on the conventional RTD models (ideal PFR or ideal CSTR behaviors). This section investigated the effect of rotational speed and total flowrate of RTR on the RTD and τ to examine the fluid flow behavior inside the RTR. The transesterification reaction mixture (palm oil, methanol, FAME and glycerol) could not be used in the RTD experiment because the tracer of methylene blue could not dissolve in this reaction mixture. Therefore, the 50 wt.% of water-glycerol solution was selected as model fluid for RTD experiment because of its similar viscosity.

จุฬาลงกรณ์มหาวิทยาลัย

CHULALONGKORN UNIVERSITY

5.3.1 Effect of rotational speed
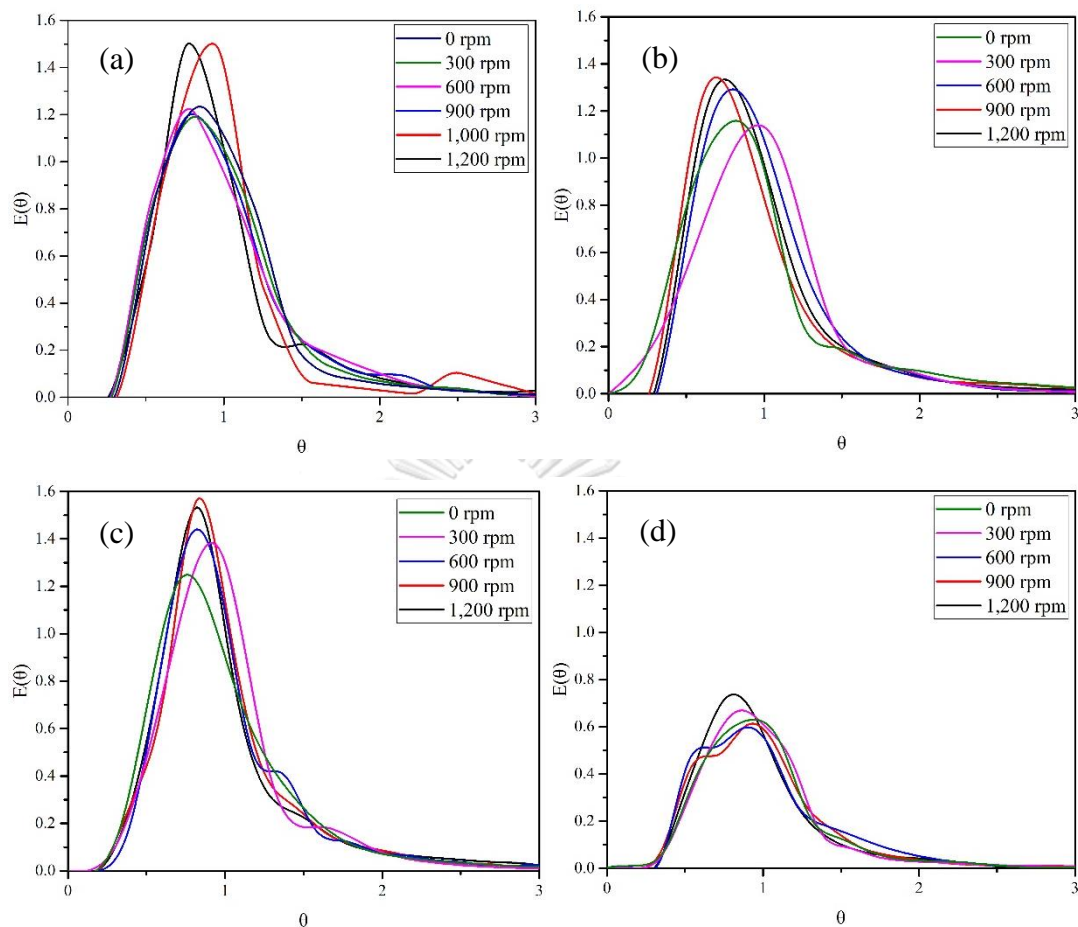
Figure 5.9 Influence of rotational speed on RTD using (a) 30 mL/min,
(b) 45 mL/min, (c) 60 mL/min and (d) 75 mL/min for 50 wt.% of water-glycerol
solution system in RTR.

Figure 5.9 shows the influence of rotational speed on RTD using (a) 30 mL/min, (b) 45 mL/min, (c) 60 mL/min and (d) 75 mL/min of 50 wt.% of water-glycerol solution in RTR, respectively. All feed flowrate showed the similar RTD profiles for different rotational speeds except the highest feed flowrate of 75 mL/min. At lower rotational speed, the RTD curve was broader while the magnitude of peak was lower, resulting in the similar flow behavior to the ideal CSTRs. When the rotational speed was increased, the obtained RTD curve became sharp and narrow with higher magnitude. The effect of flowrate on the RTD profile was also corresponding to Mohammadi, S. [32] work who studied the effect of flowrate on the RTD curve inside the SDR. In addition, the characteristics of RTD curve became more turbulence as can

be seen in Figure 5.10. However, the long tails were occurred in all rotational speed because the viscous fluid could resist the movement of the fluid flow.
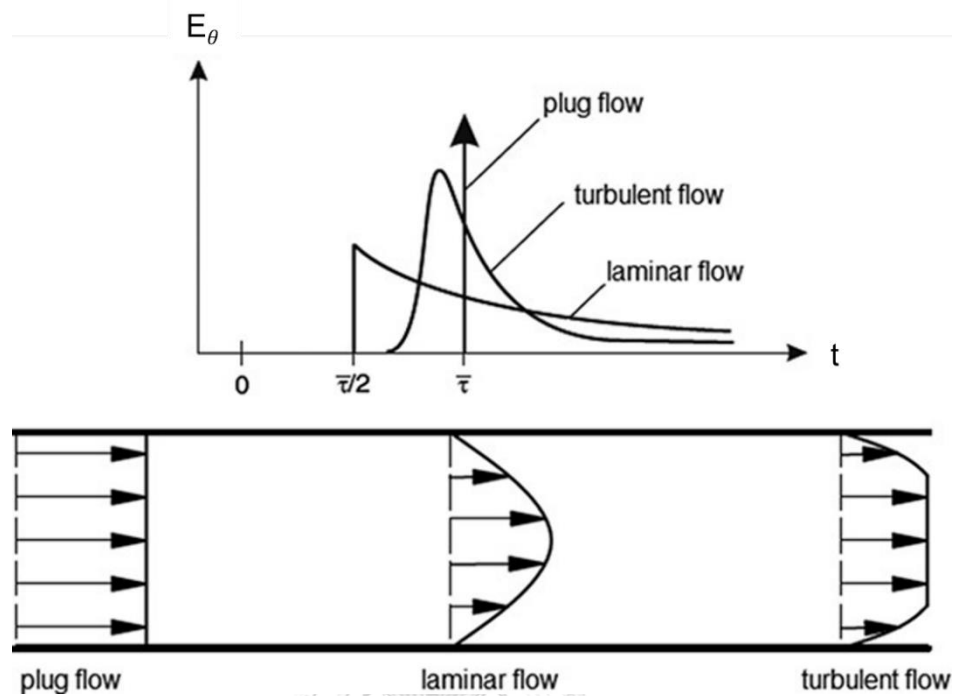
Figure 5.10 The relation between output concentration profile of tracer and average flow velocity profile [126].

5.3.2 Effect of total flowrate
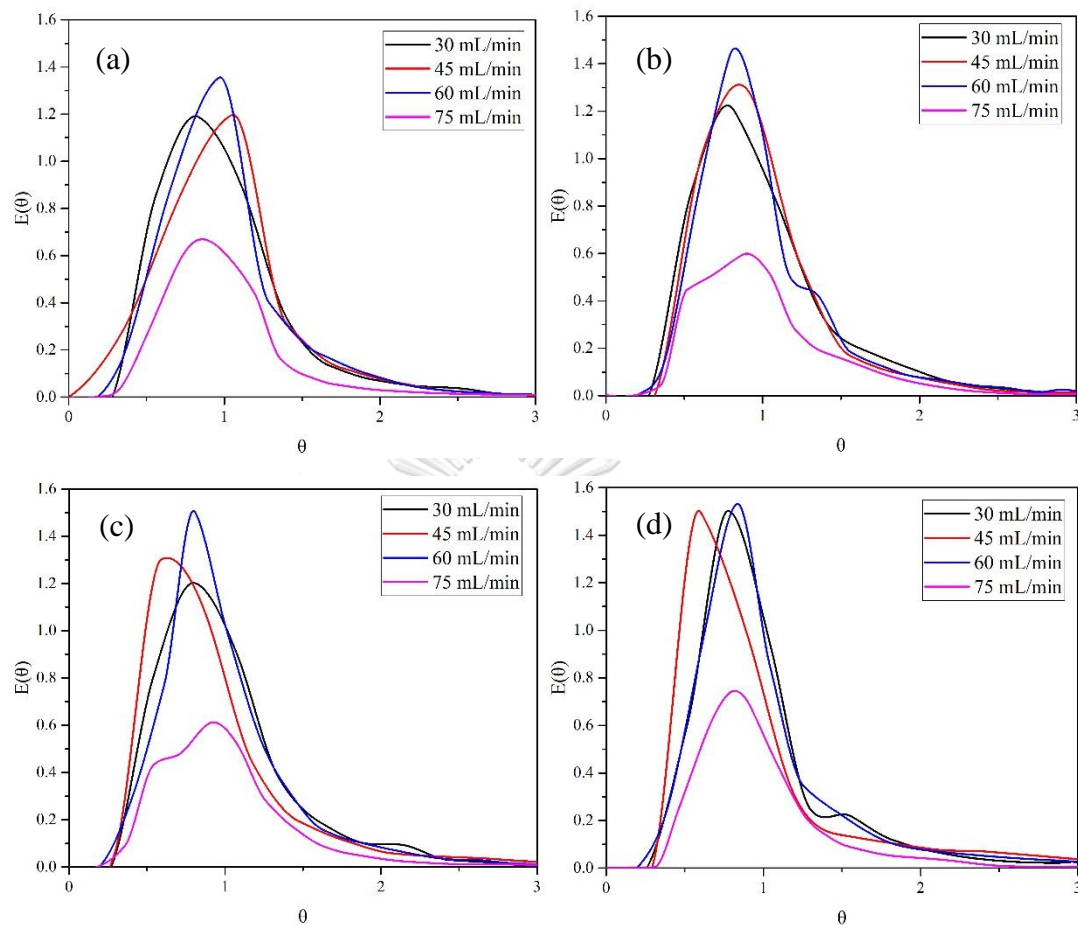
Figure 5.11 Influence of total flowrate on RTD using (a) 300 rpm, (b) 600 rpm, (c) 900 rpm and (d) 1,200 rpm in RTR for 50 wt.% of water-glycerol solution system in RTR.

Figure 5.11 presents the influence of total flowrate on RTD using (a) 300 rpm, (b) 600 rpm, (c) 900 rpm and (d) 1,200 rpm in RTR for 50 wt.% of water-glycerol solution, respectively. The higher total flowrate induced more ripples on the surface of the fluid film and more turbulence inside the reactor. The narrower RTD curves were found when the total flowrate was increased from 30 to 60 mL/min. This indicated the characteristic peak of turbulence RTD curves [32]. However, the RTD curve was broader when the total flowrate was increased from 60 to 75 mL/min. This could be implied that the significant effect of axial velocity derived from the higher flowrate disturbed the fluid traveling in RTR.

Moreover, the dispersion and mean residence time were also calculated to gain more insight on the RTD analysis inside the RTR with different rotational speed and flowrate. Table   5.4 shows the operating mean residence time (τ), the normalized variance (σ_θ^2) and dispersion number (D/uL) corresponding to the RTD measurement. From the results of this study, at 30 mL/min without rotation (0 rpm), the D/uL value was lower than the other flowrates. This could be attributed that the generation of laminar flow was occurred with negligible effect of axial and radial mixing. When increasing the flowrate from 45 – 75 mL/min without rotation, the D/uL values were decreased from 0.257 to 0.147 which confirmed the decreased dispersion at high flowrates [117]. The mean residence times (τ) of 30, 45, 60 and 75 mL/min with rotation for 50 wt.% of the water-glycerol solution were 3.18 – 3.70, 2.86 – 3.38, 3.11 – 5.11 and 2.78 – 3.25 min, respectively. This can be concluded that at a low flowrate (30 – 45 mL/min), the mean residence time (τ) decreased when increasing the total flowrate which implied the fluid have a shorter time to spend inside the reactor. On the other hand, the results obtained at high flowrate conditions (75 mL/min) showed the broader peak with long tail appearing in the RTD curve which represented that the fluid flow through RTR might be inhomogeneity due to the tracer was slowly diffused as presence of dead zone derived from the higher flowrate of 75 mL/min [32, 162]. The increase of rotational speed extended the role of strong radial mixing and consequently increased more turbulent flow behavior inside the reactor [116]. To summary the results, the increase of σ_θ^2 and D/uL values exhibited the hydrodynamic regime to be more turbulence.

Table 5.4 Operating mean residence time (τ), the normalized variance (σ_θ^2) and dispersion number (D/uL) corresponding to the RTD measurement of 50 wt.% of water/glycerol

Rotational speed (rpm)	τ	σ_θ^2	D/uL
Flowrate 30 mL/min			
0	3.35	0.176	0.098
300	3.57	0.182	0.101
600	3.65	0.189	0.106
900	3.70	0.183	0.102
1,000	3.18	0.198	0.111
1,200	3.85	0.225	0.139
Flowrate 45 mL/min			
0	4.10	0.385	0.257
300	2.86	0.193	0.109
600	3.21	0.179	0.099
900	3.38	0.425	0.298
1,200	3.32	0.388	0.260
Flowrate 60 mL/min			
0	2.83	0.260	0.153
300	3.11	0.177	0.098
600	5.11	0.193	0.109
900	4.93	0.192	0.107
1,200	4.80	0.241	0.140
Flowrate 75 mL/min			
0	2.71	0.250	0.147
300	2.94	0.266	0.158
600	2.89	0.270	0.161
900	2.78	0.274	0.163
1,200	3.25	0.418	0.290

5.4 Bicycle powered electricity generator for RTR

From the previous sections, the biodiesel production in RTR can be operated at mild condition without external heating source with less energy consumption as compared with other intensified processes. Utilization of an alternative power source to replace the conventional power source is a better way to add the value of the production process and reduce the production cost. A mechanical power generator, especially a bicycle power generator, is a remarkable device for an alternative power generation system because of easy invention, user-friendliness, less requirement of area and low cost. The major limitation of the device is less power generation which is insufficient for the operation in a continuous process. Therefore, the photovoltaic system is also used to integrate with a mechanical power source as the alternative power source for power supply to the RTR operating system.

The data of power generation was collected into 2 sections including electric power from the photovoltaic cell and the bicycle generator. The power generation from the photovoltaic cell is accumulated between 8:00 am to 6:00 pm every day. Both the maximum power and the average power were presented through the hybrid inverter every 30 min. Figure 5.12 shows that the values of maximum power were 141.0, 190.0, 156.0, 151.0 and 148.0 W at 9:00, 9:30, 10:00, 10:30 and 11:00 am, respectively, while the average power was in a range of 80 – 120 W at the same time. The actual efficiency of the photovoltaic system was higher than that of the bicycle generator during daytime. The limitation of the location which has sunlight only before noon results in reducing the performance of the PV system. When combining the photovoltaic system with the bicycle generator, the operation faced the main obstacle from the different power generations, resulting in depressing the performance of bicycle generation. Accordingly, the bicycle generator was a suitable power generation system in the case of a lack of sunlight. The high performance of the bicycle generator was around 25-30 W, which was calculated from the difference between the total power generation and the photovoltaic system. The best times to analyze the power generation from bicycle generation were 7:00 am – 9:00 am and 3:00 pm – 6:00 pm when less power generation from the photovoltaic system was obtained.
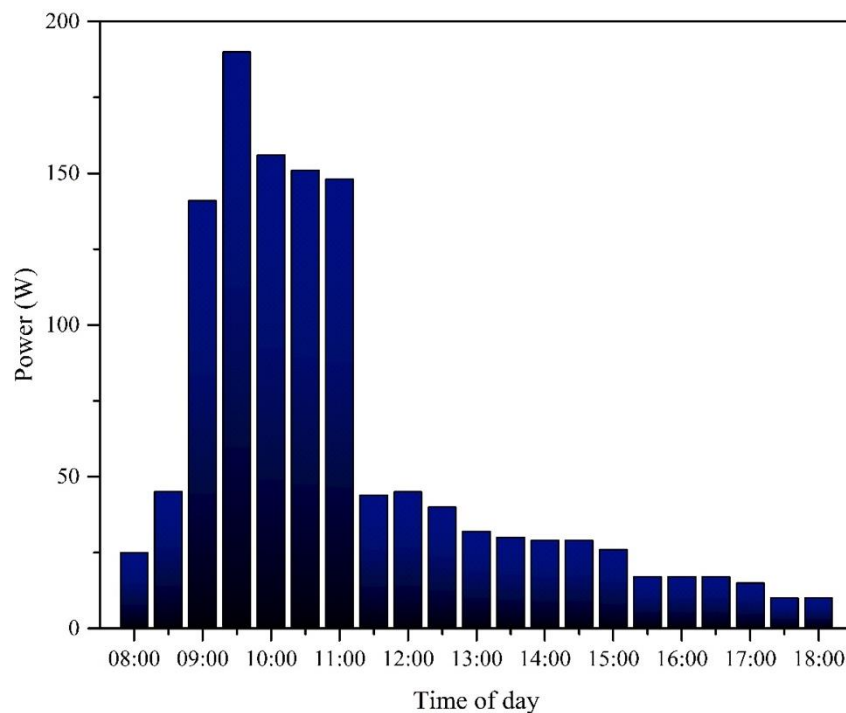
Figure 5.12 Maximum power data from 8:00 a.m. - 6:00 p.m. (in March 2021).

The energy consumption for biodiesel production using the RTR based on methanol-to-oil molar ratio of 6:1, NaOH concentration of 1.0 wt.%, rotation speed of 1,000 rpm and total flowrate of 30 mL/min at room temperature are shown in Figure 5.13. The electricity was connected to two units of 12VDC 12Ah batteries to store the electrical energy. As mentioned before, the accumulated electrical energy from a mechanical power generation (bicycle) was insufficient, and the solar energy is an interesting alternative resource which is used to combine with the mechanical power generator. Initially, the system can be continuously operated for 7 h with approximately 1.07 kWh of energy consumed, divided into 0.73 kWh for the reactor motor power and 0.34 kWh for power used to feed and control system. Figure 5.13 shows that this solar-bicycle generator provided the sufficient energy derived from the energy storage in the battery for biodiesel capacity of 9.87 L per 7 h production time using RTR. However, the solar panel system was designed to be able to produce continuous energy to replace the energy used. Consequently, this was possible to produce more energy than the energy the battery can store.
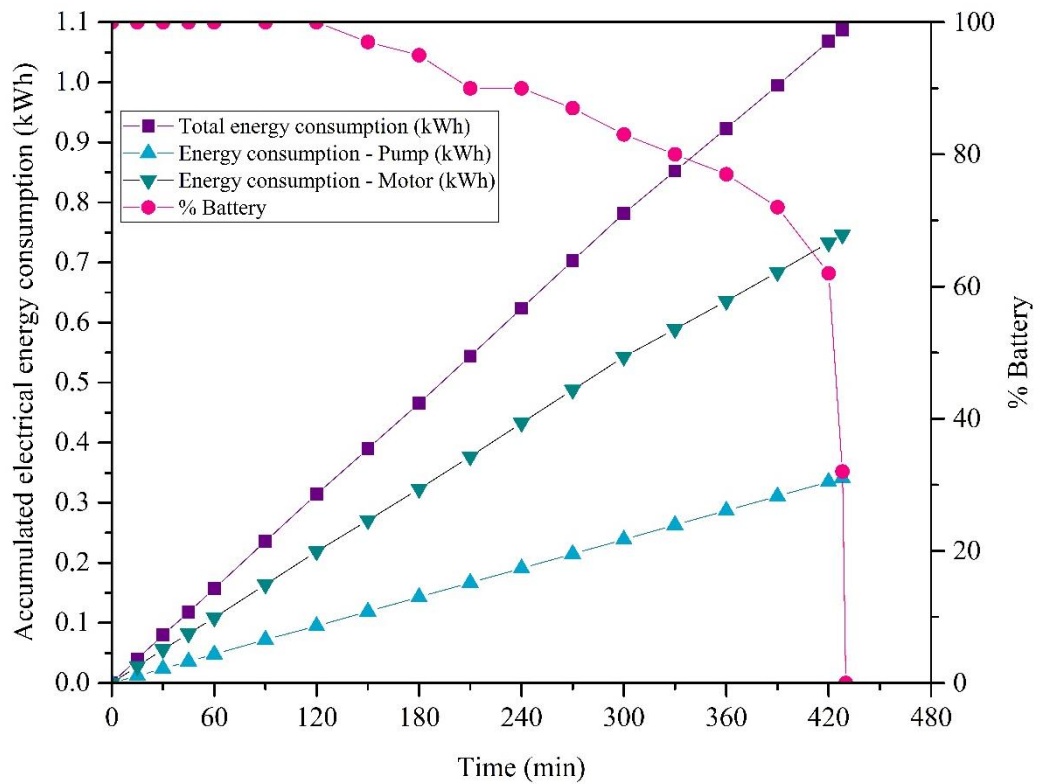
Figure 5.13 Cumulative power consumption using RTR for biodiesel production.

CHAPTER 6
CONCLUSIONS AND RECOMMENDATIONS

Conclusions

In this work, the RTR was constructed based on the design specification to produce biodiesel using alkali-catalyzed transesterification of palm oil. The diameters of the inner, middle, and outer tubes were 8.9, 10.2 and 14.1 cm, respectively. The radius ratio (η) was 0.95 and the reactor length was 0.5 m resulting in a total volume of approximately 0.337×10^{-3} g/L. The highest biodiesel yield of 97.5% with yield efficiency of 3.75×10^{-3} g/J was obtained by using a methanol-to-oil molar ratio of 6:1, 1 wt.% NaOH, total flowrate of 30 mL/min, and rotational speed of 1,000 rpm operated continuously at room temperature. The hydrodynamic regime in the RTR was firstly proposed using two dimensionless numbers, rotating Reynolds number (Re_r) and Tayler number (Ta), as well as torque, which was correlated to biodiesel yield using various operating conditions. Ta expresses the ratio of centrifugal force to viscous force while Re_r characterizes the hydrodynamic flow regime inside the reactor. To classify the Taylor vortex flow regimes, Re_r is the specific value to separate the type of flow regimes. In this study, Re_r was in the range of 440–1,326 corresponding to the WVF, MWVF and TTVF for all operating conditions. Moreover, the difference between the derivative of the torque and the square root of the Taylor number correlation conforms to the classification of Taylor vortex flow regimes using Re_r. Based on the calculated Re_r, Ta and torque, the MWVF flow regime was suggested to produce cost-effective biodiesel in the RTR while methanol vaporization could occur in the TTVF flow regime which should be avoided to reduce biodiesel yield. Using the higher rotational speed, as well as higher reaction temperature, can generate excessive heat from shear force, resulting in a negative effect on biodiesel production. The cooling system should be applied to reduce the methanol vaporization rate for the higher rotational speed of the RTR (>1,200 rpm). However, this is not favorable due to lowering in yield efficiency. This can be concluded that the RTR provided low energy consumption and low cost for biodiesel production at room temperature. Moreover, the important properties of

produced biodiesel including viscosity, density, flash point, calorific value, acid value and oxidation stability conformed to the ASTM standard of biodiesel.

The mean residence time (τ) and residence time distribution (RTD) were used to determine the flow characteristics inside the RTR. It was found that RTD curve of RTR presented the nonideal flow behavior. The rotational speed and total flowrate were the crucial parameters which can influence the fluid flow in the reactor. The higher rotational speed and total flowrate promoted turbulence and suppressed the effect of dispersion in the viscous fluid. The resistant flow of viscous solution induced the generation of turbulent flow within the RTR to achieve the perfect mixing.

In addition, the utilization of solar-bicycle powered electricity generator for biodiesel production in RTR was achieved. The energy derived from the energy storage in the battery was sufficient for biodiesel capacity of 9.87 L per 7 h production time using RTR. Furthermore, the knowledge of design, construction and operation was the essential tool for improving this system in the future.

Recommendations

- For better improvement of the RTD study, the parameter which is sensitive to the hydrodynamic regime should be selected such as fluid viscosity.

- The other effects which can impact the mixing efficiency should be investigated i.e., mass transfer coefficient and heat transfer coefficient

- Since the highlight of RTR provide high degree of mixing based on shear force, it can be used in other processes dealing with the same limitation as biodiesel production.

REFERENCES

[1]   Hajjari M, Tabatabaei M, Aghbashlo M, Ghanavati H. A review on the prospects of sustainable biodiesel production: A global scenario with an emphasis on waste-oil biodiesel utilization. Renewable and Sustainable Energy Reviews. 2017;72:445-464.

[2]   Energy and Climate Outlook, MIT Joint Program on the Science and Policy of Global Change.2014.; 20th November 2016.

[3]   Kumar M, Sharma MP. Selection of potential oils for biodiesel production. Renewable and Sustainable Energy Reviews. 2016;56:1129-1138.

[4]   Aghbashlo M, Tabatabaei M, Hosseini SS, Younesi H, Najafpour G. Exergy analysis for decision making on operational condition of a continuous photobioreactor for hydrogen production via WGS reaction. International Journal of Hydrogen Energy. 2016;41(4):2354-2366.

[5]   Gerpen JV. Biodiesel processing and production. Fuel Processing Technology. 2005;86(10):1097-1107.

[6]   Szulczyk KR, Atiqur Rahman Khan M. The potential and environmental ramifications of palm biodiesel: Evidence from Malaysia. Journal of Cleaner Production. 2018;203:260-272.

[7]   Mandolesi de Araújo CD, de Andrade CC, de Souza e Silva E, Dupas FA. Biodiesel production from used cooking oil: A review. Renewable and Sustainable Energy Reviews. 2013;27:445-452.

[8]   Pisarello ML, Dalla Costa B, Mendow G, Querini CA. Esterification with ethanol to produce biodiesel from high acidity raw materials. Fuel Processing Technology. 2010;91(9):1005-1014.

[9]   Canakci M, Van Gerpen J. Biodiesel production via acid catalysis. Transactions of the ASAE. 1999;42(5):1203-1210.

[10]   Stavarache C, Vinatoru M, Nishimura R, Maeda Y. Fatty acids methyl esters from vegetable oil by means of ultrasonic energy. Ultrasonics Sonochemistry. 2005;12(5):367-372.

[11]   Lertsathapornsuk V, Pairintra R, Aryusuk K, Krisnangkura K. Microwave assisted in continuous biodiesel production from waste frying palm oil and its performance in a 100 kW diesel generator. Fuel Processing Technology. 2008;89(12):1330-1336.

[12]   Demirbas A. Biodiesel from waste cooking oil via base-catalytic and supercritical methanol transesterification. Energy Conversion and Management. 2009;50(4):923-927.

[13]   Phan AN, Harvey AP, Eze V. Rapid production of biodiesel in mesoscale oscillatory baffled reactors. Chemical Engineering & Technology. 2012;35(7):1214-1220.

[14]   Sun J, Ju J, Ji L, Zhang L, Xu N. Synthesis of biodiesel in capillary microreactors. Industrial & Engineering Chemistry Research. 2008;47(5):1398-1403.

[15]   Boucher MB, Weed C, Leadbeater NE, Wilhite BA, Stuart JD, Parnas RS. Pilot scale two-phase continuous flow biodiesel production via novel laminar flow reactor‒separator. Energy & Fuels. 2009;23(5):2750-2756.

[16]   Noriega MA, Narváez PC, Habert AC. Simulation and validation of biodiesel production in Liquid-Liquid Film Reactors integrated with PES hollow fibers membranes. Fuel. 2018;227:367-378.

[17]   Wen Z, Yu X, Tu ST, Yan J, Dahlquist E. Intensification of biodiesel synthesis using zigzag micro-channel reactors. Bioresource Technology. 2009;100(12):3054-3060.

[18]   Kalu EE, Chen KS, Gedris T. Continuous-flow biodiesel production using slit-channel reactors. Bioresource Technology. 2011;102(6):4456-4461.

[19]   Kraai GN, Schuur B, van Zwol F, van de Bovenkamp HH, Heeres HJ. Novel highly integrated biodiesel production technology in a centrifugal contactor separator device. Chemical Engineering Journal. 2009;154(1-3):384-389.

[20]   Farobie O, Sasanami K, Matsumura Y. A novel spiral reactor for biodiesel production in supercritical ethanol. Applied Energy. 2015;147:20-29.

[21]   Qiu Z, Petera J, Weatherley LR. Biodiesel synthesis in an intensified spinning disk reactor. Chemical Engineering Journal. 2012;210:597-609.

[22]   Richard AH, inventor. Spinning tube in tube reactors and their methods of operation. 2010.

[23]   Qiu Z, Zhao L, Weatherley L. Process intensification technologies in continuous biodiesel production. Chemical Engineering and Processing: Process Intensification. 2010;49(4):323-330.

[24]   Tang Z, Kim W-S, Yu T. Studies on morphology changes of copper sulfide nanoparticles in a continuous Couette-Taylor reactor. Chemical Engineering Journal. 2019;359:1436-1441.

[25]   Tan W.H. EKDv, Lim T.T., Soria, J., editor Stability of Taylor-Couette flow with axial flow. 14th Australasian Fluid Mechanics Conference; 2001.

[26]   Kataoka KK, Ohmura N, Kouzu M, Simamura Y, Ökubo M. Emulsion polymerization of styrene in a continuous Taylor vortex flow reactor. Chemical Engineering Science. 1995;50(9):1409-1413, 1415-1416.

[27]   Dutta PK, Ray AK. Experimental investigation of Taylor vortex photocatalytic reactor for water purification. Chemical Engineering Science. 2004;59(22-23):5249-5259.

[28]   Nguyen A-T, Yu T, Kim W-S. Couette-Taylor crystallizer: Effective control of crystal size distribution and recovery of l-lysine in cooling crystallization. Journal of Crystal Growth. 2017;469:65-77.

[29]   Park S, Kim W-S. Influence of fluid motions on polymorphic crystallization of l-Histidine: Taylor vortex flow and turbulent eddy flow. Crystal Growth & Design. 2018;18(2):710-722.

[30]   Lee S, Choi A, Kim W-S, Myerson AS. Phase transformation of sulfamerazine using a Taylor vortex. Crystal Growth & Design. 2011;11(11):5019-5029.

[31]   Park S-A, Lee S, Kim W-S. Polymorphic crystallization of sulfamerazine in Taylor vortex flow: Polymorphic nucleation and phase transformation. Crystal Growth & Design. 2015;15(8):3617-3627.

[32]   Mohammadi S, Boodhoo KVK. Online conductivity measurement of residence time distribution of thin film flow in the spinning disc reactor. Chemical Engineering Journal. 2012;207-208:885-894.

[33]   Zhang H, Tang S, Liang B. Residence time distribution in two-phase flow mini-channel reactor. Chemical Engineering Journal. 2011;174(2-3):652-659.

[34]   Visscher F, van der Schaaf J, Nijhuis TA, Schouten JC. Rotating reactors – A review. Chemical Engineering Research and Design. 2013;91(10):1923-1940.

[35]   Agee BM, Mullins G, Swartling DJ. Use of solar energy for biodiesel production and use of biodiesel waste as a green reaction solvent. Sustainable Chemical Processes. 2014;2(1):21.

[36]   Mechtenberg AR, Borchers K, Miyingo EW, Hormasji F, Hariharan A, Makanda JV, et al. Human power (HP) as a viable electricity portfolio option below 20W/Capita. Energy for Sustainable Development. 2012;16(2):125-145.

[37]   Doman LE. EIA's International Energy Outlook 2017 (IEO2017). U.S. Energy Energy Information Administration. 2017.

[38]   Sheehan J, Camobreco V, Duffield J, Graboski M, Shapouri H. Life cycle inventory of biodiesel and petroleum diesel for use in an urban bus. U.S. Department of Agriculture and U.S. Department of Energy. 1998.

[39]   Lapuerta M, Armas O, Rodriguezfernandez J. Effect of biodiesel fuels on diesel engine emissions. Progress in Energy and Combustion Science. 2008;34(2):198-223.

[40]   Wu X, Leung DYC. Optimization of biodiesel production from camelina oil using orthogonal experiment. Applied Energy. 2011;88(11):3615-3624.

[41]   McCormick RL, Graboski MS, Alleman TL, Herring AM, Tyson KS. Impact of biodiesel source material and chemical structure on emissions of criteria pollutants from a heavy-duty engine. Environmental Science & Technology. 2001;35(9):1742-1747.

[42]   He H, Yu Y. Selective catalytic reduction of NOx over Ag/Al_2O_3 catalyst: from reaction mechanism to diesel engine test. Catalysis Today. 2005;100(1-2):37-47.

[43]   Ciardelli C, Nova I, Tronconi E, Chatterjee D, Bandl-Konrad B, Weibel M, et al. Reactivity of $NO/NO_2–NH_3$ SCR system for diesel exhaust aftertreatment: Identification of the reaction network as a function of temperature and NO_2 feed content. Applied Catalysis B: Environmental. 2007;70(1-4):80-90.

[44]   Grossale A, Nova I, Tronconi E. Study of a Fe–zeolite-based system as NH_3-SCR catalyst for diesel exhaust aftertreatment. Catalysis Today. 2008;136(1-2):18-27.

[45]   Avhad MR, Marchetti JM. A review on recent advancement in catalytic materials for biodiesel production. Renewable and Sustainable Energy Reviews. 2015;50:696-718.

[46]   ASTM. Standard Specification for Biodiesel Fuel (B100) Blend Stock for Distillate Fuels. American Society for Testing and Materials. 2002.

[47]   ACEA. Biodiesel Guidelines. European Automobile Manufacturers Association, Brussels, Belgium. 2009.

[48]   Ambat I, Srivastava V, Sillanpää M. Recent advancement in biodiesel production methodologies using various feedstock: A review. Renewable and Sustainable Energy Reviews. 2018;90:356-369.

[49]   Schuchardt U, Sercheli R, Matheus V. Transesterification of vegetable oils: A review. Journal of the Brazilian Chemical Society. 1998;9.

[50]   Meher L, Vidyasagar D, Naik S. Technical aspects of biodiesel production by transesterification—a review. Renewable and Sustainable Energy Reviews. 2006;10(3):248-268.

[51]   Chanthon N, Ngaosuwan K, Kiatkittipong W, Wongsawaeng D, Appamana W, Assabumrungrat S. A review of catalyst and multifunctional reactor development for sustainable biodiesel production. ScienceAsia. 2021;47(5):1-11.

[52]   Abdullah SHYS, Hanapi NHM, Azid A, Umar R, Juahir H, Khatoon H, et al. A review of biomass-derived heterogeneous catalyst for a sustainable biodiesel production. Renewable and Sustainable Energy Reviews. 2017;70:1040-1051.

[53]   Ouachab N, Tsoutsos T. Study of the acid pretreatment and biodiesel production from olive pomace oil. Journal of Chemical Technology & Biotechnology. 2013;88(6):1175-1181.

[54]   Zhang Y, Wong W-T, Yung K-F. Biodiesel production via esterification of oleic acid catalyzed by chlorosulfonic acid modified zirconia. Applied Energy. 2014;116:191-198.

[55]   Leung DYC, Guo Y. Transesterification of neat and used frying oil: Optimization for biodiesel production. Fuel Processing Technology. 2006;87(10):883-890.

[56]   Noiroj K, Intarapong P, Luengnaruemitchai A, Jai-In S. A comparative study of KOH/Al_2O_3 and KOH/NaY catalysts for biodiesel production via transesterification from palm oil. Renewable Energy. 2009;34(4):1145-1150.

[57]   Watanabe Y, Shimada Y, Sugihara A, Tominaga Y. Enzymatic conversion of waste edible oil to biodiesel fuel in a fixed-bed bioreactor. Journal of the American Oil Chemists' Society. 2001;78(7):703-707.

[58]   Alhassan FH, Rashid U, Taufiq-Yap YH. Synthesis of waste cooking oil-based biodiesel via effectual recyclable bi-functional $Fe_2O_3MnOSO_4^{2-}/ZrO_2$ nanoparticle solid catalyst. Fuel. 2015;142:38-45.

[59]   Dehghani S, Haghighi M. Sono-dispersion of MgO over Al-Ce-doped MCM-41 bifunctional nanocatalyst for one-step biodiesel production from acidic oil: Influence of ultrasound irradiation and Si/Ce molar ratio. Ultrasonics Sonochemistry. 2019;54:142-152.

[60]   Hu N, Ning P, He L, Guan Q, Shi Y, Miao R. Near-room temperature transesterification over bifunctional CunO-Bs/SBA-15 catalyst for biodiesel production. Renewable Energy. 2021;170:1-11.

[61]   Ngaosuwan K, Chaiyariyakul W, Inthong O, Kiatkittipong W, Wongsawaeng D, Assabumrungrat S. La_2O_3/CaO catalyst derived from eggshells: Effects of preparation method and La content on textural properties and catalytic activity for transesterification. Catalysis Communications. 2021;149:106247.

[62]   Cowen G, Norton-Berry P, Steel ML, inventors; Imperial Chemical Industries Limited, London, England, assignee. Chemical process on the surface of a rotating body, the subsequent discharging of the reaction product and the reactor used. England. 1979 Feb 21.

[63]   Lodha H, Jachuck R, Suppiah Singaram S. Intensified biodiesel production using a rotating tube reactor. Energy & Fuels. 2012;26(11):7037-7040.

[64]   Gonzalez-Avila SR, Klaseboer E, Khoo BC, Ohl C-D. Cavitation bubble dynamics in a liquid gap of variable height. Journal of Fluid Mechanics. 2011;682:241-260.

[65]   Gonzalez-Avila SR, Blokland ACv, Zeng Q, Ohl C-D. Cavitation bubble collapse and wall shear stress generated in a narrow gap. Proceedings of the 10th International Symposium on Cavitation (CAV2018). 2008.

[66]   Zeng Q, Gonzalez-Avila SR, Dijkink R, Koukouvinis P, Gavaises M, Ohl C-D. Wall shear stress from jetting cavitation bubbles. Journal of Fluid Mechanics. 2018;846:341-355.

[67]   Ting DSK. Introducing flow turbulence. Basics of Engineering Turbulence. 2016:3-18.

[68]   Childs PRN. Rotating cylinders, annuli, and spheres. Rotating Flow. 2011:177-247.

[69]   Grossmann S, Lohse D, Sun C. High–Reynolds number Taylor-Couette turbulence. Annual Review of Fluid Mechanics. 2016;48(1):53-80.

[70]   Nemri M, Charton S, Climent E. Mixing and axial dispersion in Taylor–Couette flows: The effect of the flow regime. Chemical Engineering Science. 2016;139:109-124.

[71]   Deng D, Braun MJ. Taylor vortices induced instability and turbulence in Jjurnal bearing microscale flow. Tribology Transactions. 2008;50(3):415-426.

[72]   Seo D, Kim W-S, Kim DH. Numerical simulation of Taylor-Couette fluidic device for the exfoliation of two-dimensional materials. Chemical Engineering Journal. 2020;399.

[73]   Chanthon N, Ngaosuwan K, Kiatkittipong W, Wongsawaeng D, Appamana W, Quitain AT, et al. High-efficiency biodiesel production using rotating tube reactor: New insight of operating parameters on hydrodynamic regime and biodiesel yield. Renewable and Sustainable Energy Reviews. 2021;151.

[74]   Feng X, Patterson DA, Balaban M, Emanuelsson EAC. Characterization of liquid flow in the spinning cloth disc reactor: Residence time distribution, visual study and modeling. Chemical Engineering Journal. 2014;235:356-367.

[75]   Conesa JA. Chemical reactor design: Mathematical modeling and applications. 2019.

[76]   Levenspiel O. Chemical Reaction Engineering. Industrial & Engineering Chemistry Research. 1999;38(11):4140-4143.

[77]   Dias JM, Alvim-Ferraz MCM, Almeida MF. Comparison of the performance of different homogeneous alkali catalysts during transesterification of waste and virgin oils and evaluation of biodiesel quality. Fuel. 2008;87(17-18):3572-3578.

[78]   Sinha S, Agarwal AK, Garg S. Biodiesel development from rice bran oil: Transesterification process optimization and fuel characterization. Energy Conversion and Management. 2008;49(5):1248-1257.

[79]   Georgogianni KG, Kontominas MG, Pomonis PJ, Avlonitis D, Gergis V. Conventional and in situ transesterification of sunflower seed oil for the production of biodiesel. Fuel Processing Technology. 2008;89(5):503-509.

[80]   Rashid U, Anwar F. Production of biodiesel through optimized alkaline-catalyzed transesterification of rapeseed oil. Fuel. 2008;87(3):265-273.

[81]   Ali EN, Tay CI. Characterization of biodiesel produced from palm oil via base catalyzed transesterification. Procedia Engineering. 2013;53:7-12.

[82]   Al-Hamamre Z, Yamin J. Parametric study of the alkali catalyzed transesterification of waste frying oil for Biodiesel production. Energy Conversion and Management. 2014;79:246-254.

[83]   Uzun BB, Kılıç M, Özbay N, Pütün AE, Pütün E. Biodiesel production from waste frying oils: Optimization of reaction parameters and determination of fuel properties. Energy. 2012;44(1):347-351.

[84]   Leevijit T, Tongurai C, Prateepchaikul G, Wisutmethangoon W. Performance test of a 6-stage continuous reactor for palm methyl ester production. Bioresource Technology. 2008;99(1):214-221.

[85]   Santori G, Di Nicola G, Moglie M, Polonara F. A review analyzing the industrial biodiesel production practice starting from vegetable oil refining. Applied Energy. 2012;92:109-132.

[86]   Thompson J, He B. Biodiesel production using static mixers. Transactions of the ASABE. 2007;50.

[87]   Frascari D, Zuccaro M, Pinelli D, Paglianti A. A pilot-scale study of alkali-catalyzed sunflower oil transesterification with static mixing and with mechanical agitation. Energy & Fuels. 2008;22(3):1493-1501.

[88]   Somnuk K, Prasit T, Prateepchaikul G. Effects of mixing technologies on continuous methyl ester production: Comparison of using plug flow, static mixer, and ultrasound clamp. Energy Conversion and Management. 2017;140:91-97.

[89]   Somnuk K, Soysuwan N, Prateepchaikul G. Continuous process for biodiesel production from palm fatty acid distillate (PFAD) using helical static mixers as reactors. Renewable Energy. 2019;131:100-110.

[90]   Tiwari A, Rajesh VM, Yadav S. Biodiesel production in micro-reactors: A review. Energy for Sustainable Development. 2018;43:143-161.

[91]   Mohadesi M, Aghel B, Maleki M, Ansari A. Production of biodiesel from waste cooking oil using a homogeneous catalyst: Study of semi-industrial pilot of microreactor. Renewable Energy. 2019;136:677-682.

[92]   Santana HS, Tortola DS, Silva JL, Taranto OP. Biodiesel synthesis in micromixer with static elements. Energy Conversion and Management. 2017;141:28-39.

[93]   Noriega MA, Narváez PC, Cadavid JG, Habert AC. Modeling of biodiesel production in liquid-liquid film reactors including mass transfer effects. Fuel Processing Technology. 2017;167:524-534.

[94]   Buasri A, Ksapabutr B, Panapoy M, Chaiyut N. Biodiesel production from waste cooking palm oil using calcium oxide supported on activated carbon as catalyst in a fixed bed reactor. Korean Journal of Chemical Engineering. 2012;29(12):1708-1712.

[95]   Chen Y, Huang Y, Lin R, Shang N. A continuous-flow biodiesel production process using a rotating packed bed. Bioresource Technology. 2010;101(2):668-673.

[96]   Xu J, Liu C, Wang M, Shao L, Deng L, Nie K, et al. Rotating packed bed reactor for enzymatic synthesis of biodiesel. Bioresource Technology. 2017;224:292-297.

[97]   Harvey AP, Mackley MR, Seliger T. Process intensification of biodiesel production using a continuous oscillatory flow reactor. Journal of Chemical Technology & Biotechnology. 2003;78(2-3):338-341.

[98]   García-Martín JF, Barrios CC, Alés-Álvarez F-J, Dominguez-Sáez A, Alvarez-Mateos P. Biodiesel production from waste cooking oil in an oscillatory flow reactor. Performance as a fuel on a TDI diesel engine. Renewable Energy. 2018;125:546-556.

[99]   Gupta J, Agarwal M, Dalai AK. Intensified transesterification of mixture of edible and nonedible oils in reverse flow helical coil reactor for biodiesel production. Renewable Energy. 2019;134:509-525.

[100]   Agarwal M, Soni S, Singh K, Chaurasia SP, Dohare RK. Biodiesel yield assessment in continuous-flow reactors using batch reactor conditions. International Journal of Green Energy. 2013;10(1):28-40.

[101]   Barnard TM, Leadbeater NE, Boucher MB, Stencel LM, Wilhite BA. Continuous-flow preparation of biodiesel using microwave heating. Energy & Fuels. 2007;21(3):1777-1781.

[102]   Azcan N, Danisman A. Alkali catalyzed transesterification of cottonseed oil by microwave irradiation. Fuel. 2007;86(17-18):2639-2644.

[103]   Chee Loong T, Idris A. One step transesterification of biodiesel production using simultaneous cooling and microwave heating. Journal of Cleaner Production. 2017;146:57-62.

[104]   Ji J, Wang J, Li Y, Yu Y, Xu Z. Preparation of biodiesel with the help of ultrasonic and hydrodynamic cavitation. Ultrasonics. 2006;44:e411-e414.

[105]   Chand P, Chintareddy VR, Verkade JG, Grewell D. Enhancing biodiesel production from soybean oil using ultrasonics. Energy & Fuels. 2010;24(3):2010-2015.

[106]   Gole VL, Gogate PR. Intensification of synthesis of biodiesel from nonedible oils using sonochemical reactors. Industrial & Engineering Chemistry Research. 2012;51(37):11866-11874.

[107]   Gole VL, Naveen KR, Gogate PR. Hydrodynamic cavitation as an efficient approach for intensification of synthesis of methyl esters from sustainable feedstock. Chemical Engineering and Processing: Process Intensification. 2013;71:70-76.

[108]   Gogate PR. Cavitational reactors for process intensification of chemical processing applications: A critical review. Chemical Engineering and Processing: Process Intensification. 2008;47(4):515-527.

[109]   Ghayal D, Pandit AB, Rathod VK. Optimization of biodiesel production in a hydrodynamic cavitation reactor using used frying oil. Ultrasonics Sonochemistry. 2013;20(1):322-328.

[110]   Mohod AV, Gogate PR, Viel G, Firmino P, Giudici R. Intensification of biodiesel production using hydrodynamic cavitation based on high speed homogenizer. Chemical Engineering Journal. 2017;316:751-757.

[111]   Joshi S, Gogate PR, Moreira PF, Jr., Giudici R. Intensification of biodiesel production from soybean oil and waste cooking oil in the presence of heterogeneous catalyst using high speed homogenizer. Ultrasonics Sonochemistry. 2017;39:645-653.

[112]   Laosuttiwong T, Ngaosuwan K, Kiatkittipong W, Wongsawaeng D, Kim-Lohsoontorn P, Assabumrungrat S. Performance comparison of different cavitation reactors for biodiesel production via transesterification of palm oil. Journal of Cleaner Production. 2018;205:1094-1101.

[113]   Chen K-J, Chen Y-S. Intensified production of biodiesel using a spinning disk reactor. Chemical Engineering and Processing: Process Intensification. 2014;78:67-72.

[114]   Hampton PD, Whealon MD, Roberts LM, Yaeger AA, Boydson R. Continuous Organic Synthesis in a Spinning Tube-in-Tube Reactor: TEMPO-Catalyzed Oxidation of Alcohols by Hypochlorite. Organic Process Research & Development. 2008;12(5):946-949.

[115]   Gonzalez MA, Ciszewski JT. High Conversion, Solvent Free, Continuous Synthesis of Imidazolium Ionic Liquids In Spinning Tube-in-Tube Reactors. Organic Process Research & Development. 2009;13(1):64-66.

[116]   Klutz S, Kurt SK, Lobedann M, Kockmann N. Narrow residence time distribution in tubular reactor concept for Reynolds number range of 10–100. Chemical Engineering Research and Design. 2015;95:22-33.

[117]   Kacker R, Regensburg SI, Kramer HJM. Residence time distribution of dispersed liquid and solid phase in a continuous oscillatory flow baffled crystallizer. Chemical Engineering Journal. 2017;317:413-423.

[118]   Sunil J, Priyan B, Anish L, Muthuvel A, Daniel T, editors. Bicycle power generation and its feasibility. International Conference on Advanced Technological Innovations, INCATI'15; 2015; SCAD College of Engineering and Technology, Tirunelveli.

[119]   Huang H, Ding X, Tong L. Photovoltaic power generation system. 2017.

[120]   Chaiyaso T. Synthesis of Sugar esters and fatty acid methyl esters from palm oil and palm fatty acid distillates by two bacterial lipases. 2007.

[121]   Baroutian S, Aroua MK, Raman AAA, Sulaiman NMN. Density of palm oil-based methyl ester. Journal of Chemical & Engineering Data. 2008;53(3):877-880.

[122]   Technologies L. Technical References - Palm Oil Properties. 2008. [Available from: http://www.lipico.com/technical_references_palm_oil_properties.html.

[123]   Kaye & Laby EE, RoyMech and Dynesonline. Viscosity of Methanol [Available from: https://wiki.anton-paar.com/th-th/methanol/.

[124]   Association GP. Physical properties of glycerine and its solutions: New York. 1963.

[125]   How to estimate mixtures viscosities [press release]. Chemical Engineering. 1959.

[126]   Bogatykh I, Osterland T. Characterization of residence time distribution in a plug flow reactor. Chemie Ingenieur Technik. 2019;91(5):668-672.

[127]   Gnanaprakasam A, Sivakumar VM, Surendhar A, Thirumarimurugan M, Kannadasan T. Recent strategy of biodiesel production from waste cooking oil and process influencing parameters: A review. Journal of Energy. 2013;2013:1-10.

[128]   Eevera T, Kaliaperumal R, Saradha S. Biodiesel production process optimization and characterization to assess the suitability of the product for varied environmental conditions. Renewable Energy. 2009;34(3):762-765.

[129]   Oh PP, Chong MF, Lau HLN, Chen J, Choo YM. Liquid–liquid equilibrium (LLE) study for six-component transesterification system. Clean Technologies and Environmental Policy. 2013;15(5):817-822.

[130]   Musa IA. The effects of alcohol to oil molar ratios and the type of alcohol on biodiesel production using transesterification process. Egyptian Journal of Petroleum. 2016;25(1):21-31.

[131]   Zhang M, Wu H. Phase behavior and fuel properties of bio-oil/glycerol/methanol blends. Energy & Fuels. 2014;28(7):4650-4656.

[132]   Ngaosuwan K, Mo X, Goodwin Jr JG, Praserthdam P. Effect of solvent on hydrolysis and transesterification reactions on tungstated zirconia. Applied Catalysis A: General. 2010;380(1-2):81-86.

[133]   Tabatabaei M, Aghbashlo M, Dehhaghi M, Panahi HKS, Mollahosseini A, Hosseini M, et al. Reactor technologies for biodiesel production and processing: A review. Progress in Energy and Combustion Science. 2019;74:239-303.

[134]   Chanakaewsomboon I, Tongurai C, Photaworn S, Kungsanant S, Nikhom R. Investigation of saponification mechanisms in biodiesel production: Microscopic visualization of the effects of FFA, water and the amount of alkaline catalyst. Journal of Environmental Chemical Engineering. 2020;8(2).

[135]   Efavi JK, Kanbogtah D, Apalangya V, Nyankson E, Tiburu EK, Dodoo-Arhin D, et al. The effect of NaOH catalyst concentration and extraction time on the yield and properties of *Citrullus*

vulgaris seed oil as a potential biodiesel feed stock. South African Journal of Chemical Engineering. 2018;25:98-102.

[136]   Poosumas J, Ngaosuwan K, Quitain AT, Assabumrungrat S. Role of ultrasonic irradiation on transesterification of palm oil using calcium oxide as a solid base catalyst. Energy Conversion and Management. 2016;120:62-70.

[137]   Ovarlez G, Bertrand F, Rodts S. Local determination of the constitutive law of a dense suspension of noncolloidal particles through magnetic resonance imaging. Journal of Rheology. 2006;50(3):259-292.

[138]   Serov AF, Nazarov AD, Mamonov VN, Terekhov VI. Experimental investigation of energy dissipation in the multi-cylinder Couette-Taylor system with independently rotating cylinders. Applied Energy. 2019;251.

[139]   Rotimi D. Effect of the temperature on dynamic viscosity, density and flow rate of some vegetable oils. Journal of Scientific Research in Engineering & Technology. 2016;1:14-24.

[140]   Sitepu EK, Jones DB, Tang Y, Leterme SC, Heimann K, Zhang W, et al. Continuous flow biodiesel production from wet microalgae using a hybrid thin film microfluidic platform. Chemical Communications. 2018;54(85):12085-12088.

[141]   Kaye GWC LT. Viscosity of methanol: RoyMech and Dynesonline. 2016. [Available from: https://wiki.anton-paar.com/th-th/methanol/.

[142]   Lueptow RM, Docter A, Min K. Stability of axial flow in an annulus with a rotating inner cylinder. Physics of Fluids A: Fluid Dynamics. 1992;4(11).

[143]   Bot P, Mumtaz M, Adnan A, Mahmood Z, Mukhtar H, Danish M, et al. Biodiesel production using *Eruca Sativa* oil: Optimization and characterization. Pakistan Journal of Botany. 2012;44:1111-1120.

[144]   Hlavác P, Boziková M, Regrut T, Ardonová V. Comparison of selected vegetable oils rheologic properties. Journal on Processing and Energy in Agriculture. 2017;21(3):131-135.

[145]   Fasina OO, Colley Z. Viscosity and specific heat of vegetable oils as a function of temperature: 35°C to 180°C. International Journal of Food Properties. 2008;11(4):738-746.

[146]   Tangsathitkulchai C, Sittichaitaweekul Y, Tangsathitkulchai M. Temperature effect on the viscosities of palm oil and coconut oil blended with diesel oil. Journal of the American Oil Chemists' Society. 2004;81:401–405.

[147]   Chilakpu K, Egwuonwu C, V.C O, Okafor K. Biodiesel production from Jatropha Curcas seed oil in a modified batch-reactor using sodium-hydroxide as catalyst. International Journal of Scientific and Research Publications. 2018;8.

[148]   Visscher F, Nijhuis RTR, de Croon MHJM, van der Schaaf J, Schouten JC. Liquid–liquid flow in an impeller–stator spinning disc reactor. Chemical Engineering and Processing: Process Intensification. 2013;71:107-114.

[149]   Chuah LF, Yusup S, Abd Aziz AR, Bokhari A, Abdullah MZ. Cleaner production of methyl ester using waste cooking oil derived from palm olein using a hydrodynamic cavitation reactor. Journal of Cleaner Production. 2016;112:4505-4514.

[150]   Khan IA, Prasad N, Pal A, Yadav AK. Efficient production of biodiesel from *Cannabis sativa* oil using intensified transesterification (hydrodynamic cavitation) method. Energy Sources, Part A: Recovery, Utilization, and Environmental Effects. 2019;42(20):2461-2470.

[151]   Keera ST, El Sabagh SM, Taman AR. Castor oil biodiesel production and optimization. Egyptian Journal of Petroleum. 2018;27(4):979-984.

[152]   Chhetri A, Watts K, Islam M. Waste cooking oil as an alternate feedstock for biodiesel production. Energies. 2008;1(1):3-18.

[153]   Sahar, Sadaf S, Iqbal J, Ullah I, Bhatti HN, Nouren S, et al. Biodiesel production from waste cooking oil: An efficient technique to convert waste into biodiesel. Sustainable Cities and Society. 2018;41:220-226.

[154]   Mahmudul HM, Hagos FY, Mamat R, Adam AA, Ishak WFW, Alenezi R. Production, characterization and performance of biodiesel as an alternative fuel in diesel engines – A review. Renewable and Sustainable Energy Reviews. 2017;72:497-509.

[155]   Pullen J, Saeed K. An overview of biodiesel oxidation stability. Renewable and Sustainable Energy Reviews. 2012;16(8):5924-5950.

[156]   Snyder HA. Experiments on the Stability of Spiral Flow at Low Axial Reynolds Numbers. Proceedings of the Royal Society of London Series A, Mathematical and Physical Sciences,. 1962;265:198-214.

[157]   Drazin P, Reid WH. Centrifugal Instability. Hydrodynamic Stability: Cambridge University Press; 2010. p. 69-123.

[158]   Nemri M, Climent E, Charton S, Lanoë J-Y, Ode D. Experimental and numerical investigation on mixing and axial dispersion in Taylor–Couette flow patterns. Chemical Engineering Research and Design. 2013;91(12):2346-2354.

[159]   Coles D. Transition in circular Couette flow. Journal of Fluid Mechanics. 1965;21:385-425.

[160]   Campero RJ, Vigil RD. Axial dispersion during low Reynolds number Taylor-Couette flow: intra-vortex mixing effects. Chemical Engineering Science. 1997;52(19):3303-3310.

[161]   Fogler HS. Essentials of chemical reaction engineering. 2 ed: Pearson Education. 2011.

[162]   Wang J, Yang J, Sunden B, Wang Q. Assessment of flow pattern and temperature profiles by residence time distribution in typical structured packed beds. Numerical Heat Transfer, Part A: Applications. 2020;77:1-20.

[163]   Dubois J, Tremblay L, Lepage M, Vermette P. Flow dynamics within a bioreactor for tissue engineering by residence time distribution analysis combined with fluorescence and magnetic resonance imaging to investigate forced permeability and apparent diffusion coefficient in a perfusion cell culture chamber. Biotechnology and Bioengineering. 2011;108(10):2488-2498.

[164]   Gutierrez CGCC, Dias EFTS, Gut JAW. Investigation of the residence time distribution in a plate heat exchanger with series and parallel arrangements using a non-ideal tracer detection technique. Applied Thermal Engineering. 2011;31(10):1725-1733.

[165]   Schrimpf M, Esteban J, Warmeling H, Färber T, Behr A, Vorholt AJ. Taylor‐Couette reactor: Principles, design, and applications. AIChE Journal. 2021;67(5).

[166]   Desmet G, Verelst H, Baron GV. Local and global dispersion effects in Couette-Taylor flo—II. Quantitative measurements and discussion of the reactor performance. Chemical Engineering Science. 1996;51:1299-1309.

[167]   Desmet G, Verelst H, Baron GV. Local and global dispersion effects in Couette-Taylor flow—I. Description and modeling of the dispersion effects. Chemical Engineering Science. 1996;51(8):1287-1298.
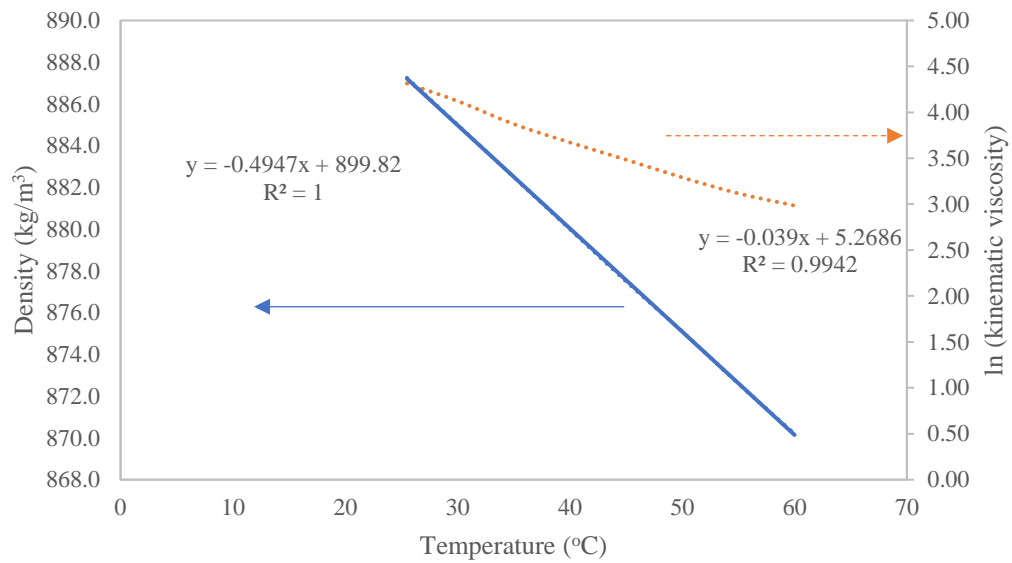
APPENDIX A

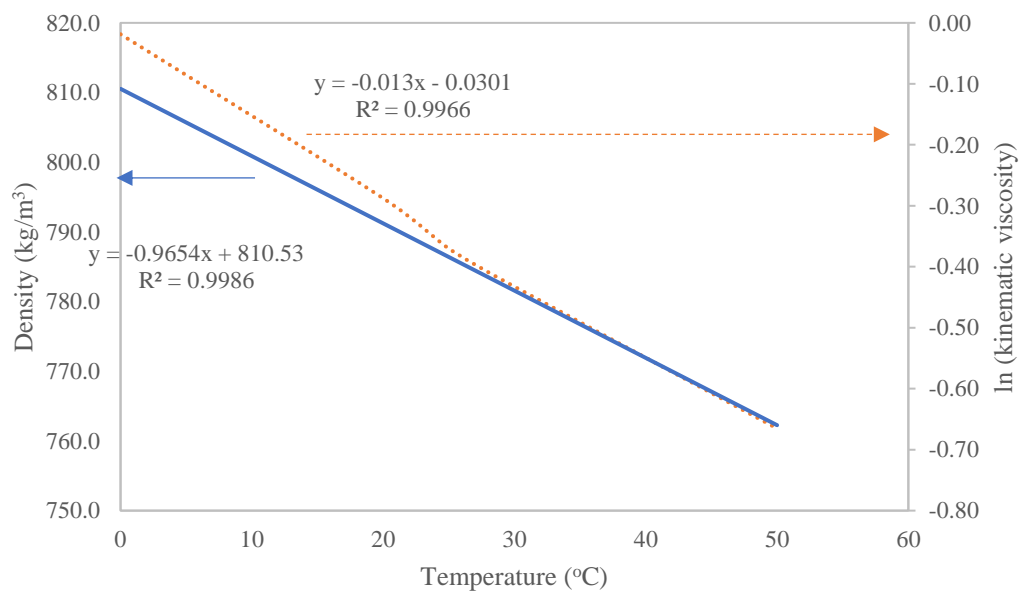# THE CORRELATION BETWEEN DENSITY, KINEMATIC VISCOSITY AND TEMPERATURE
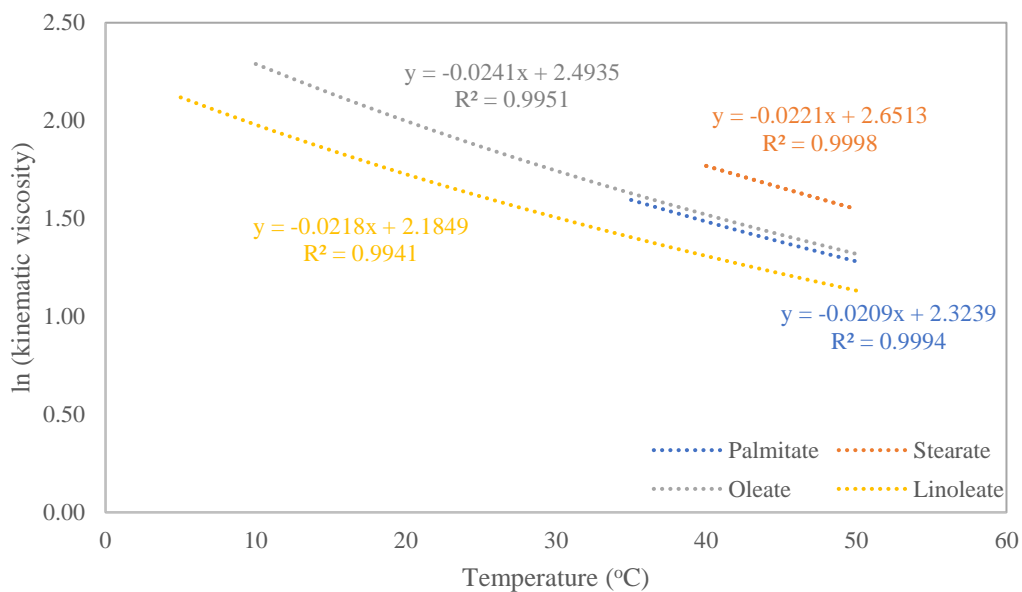
Figure A1 Temperature dependence of predicted value of kinematic viscosity of methyl esters.
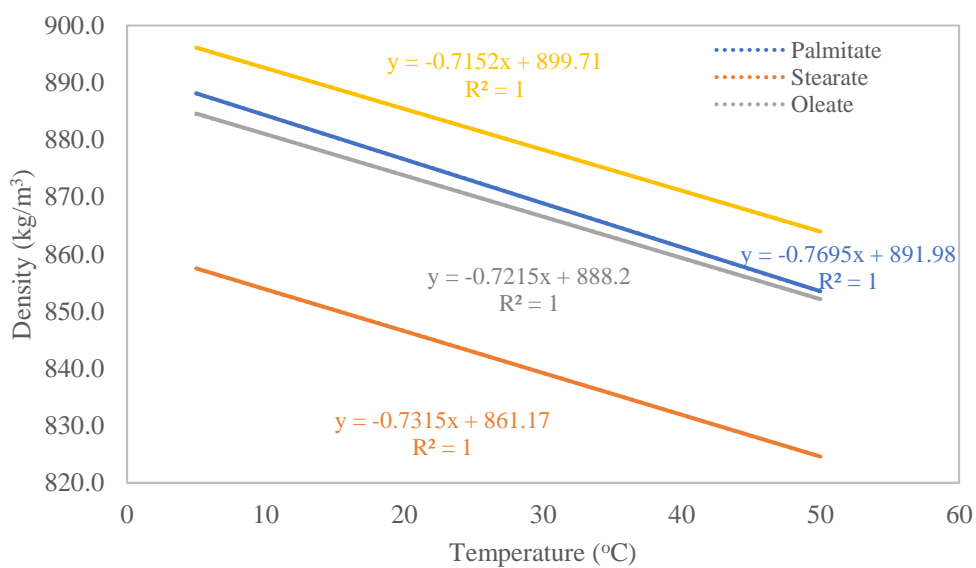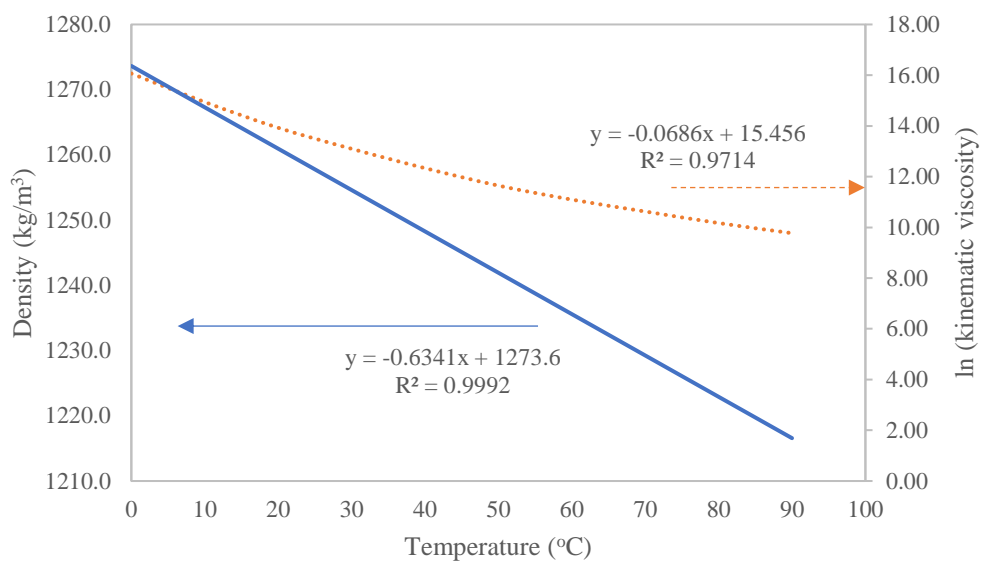

Figure A2 Temperature dependence of density of methyl esters.

Figure A3 Correlation of density and kinematic viscosity of palm oil

with various temperatures (25 to 60°C).

Figure A4 Density and kinematic viscosity of methanol
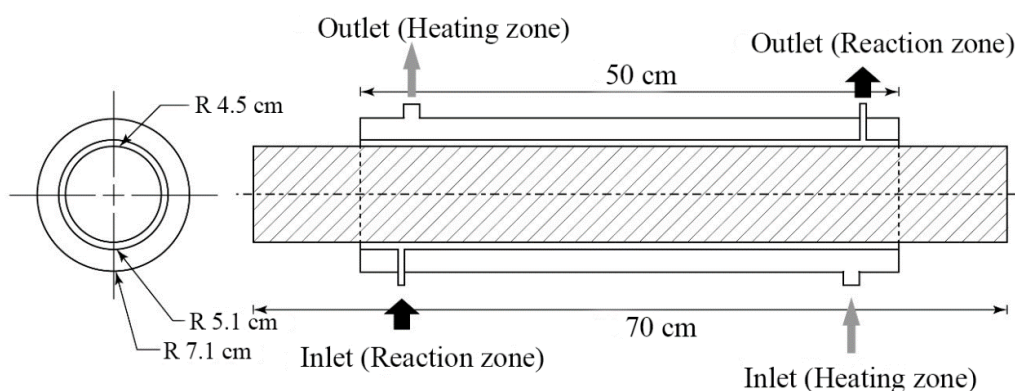
in temperature range of 0 to 50°C.

Figure A5 Density and kinematic viscosity of glycerol
in temperature range of 0 to 90°C.

จุฬาลงกรณ์มหาวิทยาลัย

CHULALONGKORN UNIVERSITY

APPENDIX B

DESIGN SPECIFICATION OF RTR

Figure B1 Schematic view of rotating tube reactor (RTR).

RTR was designed based on the patent of spinning tube in tube reactors and their methods of operation [22]. The details were presented below;

Type of tube: Stainless steel 316L

Inner cylinder: OD 9.0 cm, ID 8.9 cm

Middle cylinder: OD 10.1 cm, ID 9.4 cm

Outer cylinder: OD 14.1 cm, ID 13.5 cm

Radial spacing: 2.35 mm

    (The distance between outer surface of inner cylinder and the inner surface of middle cylinder)

Length (reaction zone):   50 cm

Volume: 0.337 L

Radius ratio: 0.95

    (The ratio of inner diameter to outer diameter of reaction zone)

APPENDIX C
TRACER STUDY OF PURE WATER

Table C1 The DOE of residence time distribution experiment using pure water.

| Experiment	Rotational speed (rpm)	Flowrate (mL/min)
1	900	45
2	300	75
3	1,200	75
4	600	60
5	1,200	60
6	300	30
7	1,200	30
8	600	30
9	600	75
10	900	60
11	1,200	45
12	900	75
13	600	45
14	300	60
15	300	45
16	900	30

Table C1 The DOE of residence time distribution experiment using pure water. *cont.*

Experiment	Rotational speed (rpm)	Flowrate (mL/min)
17	0	30
18	0	45
19	0	60
20	0	75

Effect of rotational speed

Generally, a narrower RTD curve implies the flow behavior inside the reactor is similar to the ideal plug flow; in contrast, a broader RTD curve represents the large deviation from plug flow which expresses the significance of dispersion phenomenon [76]. Figure C1 (a) – (d) present the influence of rotational speed on RTD based on (a) 30 mL/min, (b) 45 mL/min, (c) 60 mL/min and (d) 75 mL/min in RTR. The results showed that the disturbance of fluid flow by increasing the rotational speed revealed more turbulence which is the reason for the high magnitude of RTD curve. The sharper and narrower RTD curve referred to the dispersion in the direction of flow is negligible and fluid flow behavior within the RTR approached the ideal plug flow [116] which conformed to the output concentration profile as shown in the Figure 5.10 The relation between output concentration profile of tracer and average flow velocity profile. Moreover, the Ta values increased from 942 to 3,769 when increasing the rotational speed from 300 to 1,200 rpm which indicated that the intensity of mixing and turbulence were also grown. However, a presence of long tail at 30 mL/min and 1,200 rpm (in Figure B1(a)) referred to the stagnation zone where fluid flows very slowly or motionlessly [74, 163, 164] resulting in long residence time.
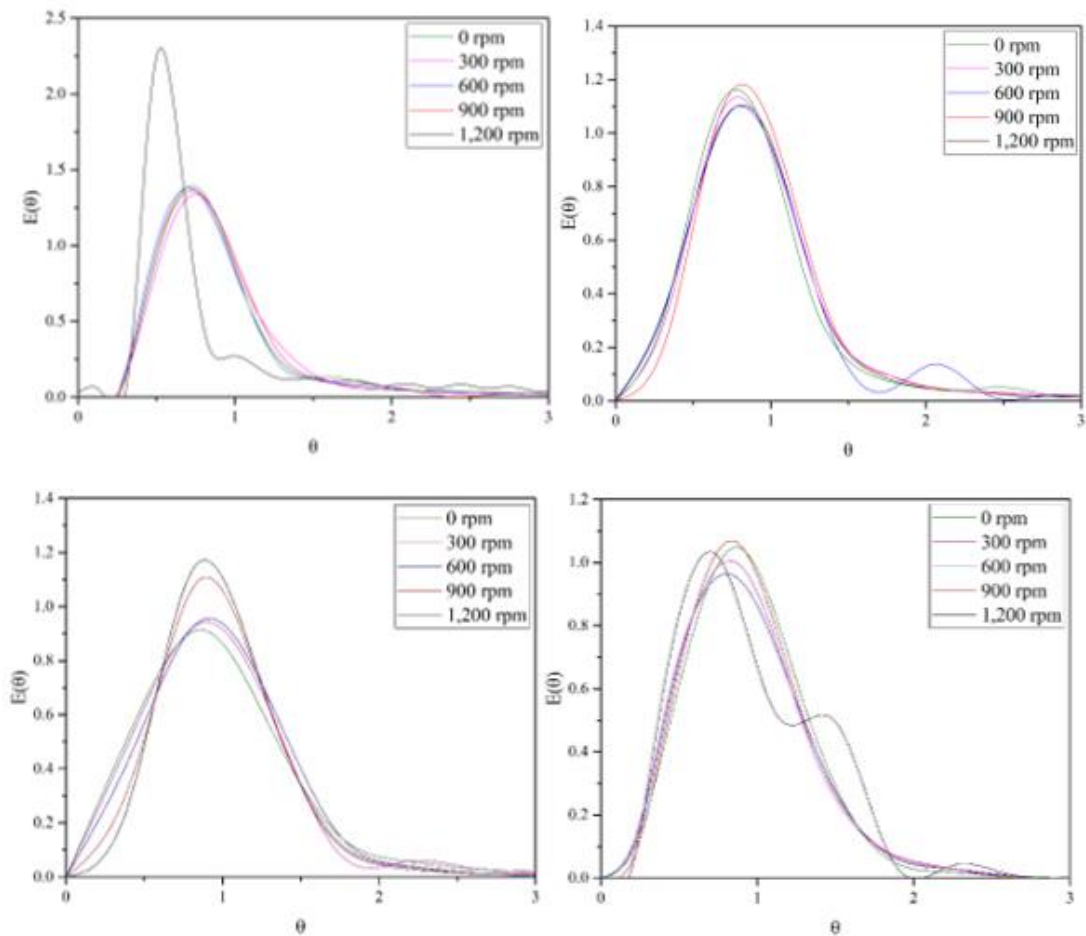
Figure C1 Influence of rotational speed on RTD based on (a) 30 mL/min,
(b) 45 mL/min, (c) 60 mL/min and (d) 75 mL/min in RTR based on pure water.

Effect of total flowrate

The total flowrate is an essential factor for RTD because the difference of total flowrate directly affects the residence time and axial velocity of fluid flow which influences the flow regime. Figure C2(a) – (d) present the influence of total flowrate on RTD based on (a) 300 rpm, (b) 600 rpm, (c) 900 rpm and (d) 1,200 rpm in RTR. The outlet tracer of the higher flowrate appeared earlier than others which indicated that these conditions had short residence time; in contrast, the tracer of lower flowrate spent more time in the reactor which related to the generation of vortices and backmixing [165].

The cellular structure of the Taylor-Couette flow can be classified into 2 types: local dispersion and global dispersion. The local dispersion mentions the appearance of all intra-vortex mixing in the reactor while the global dispersion refers to the overall axial dispersion effect. The axial dispersion can be neglected for the low fluid flowrate; therefore, the local dispersion which represents the flow behavior as same the conventional CSTRs behavior is the major effect for determining the hydrodynamic regime[166, 167]. At a lower flowrate, the information of RTD curve interpreted as the flow behavior is similar to the ideal plug flow. When increasing the total flowrate, the RTD curve had the broader peak (as shown in C2) which implied the films surfaces were unstable resulting in the generation of ripples, induction of the turbulence and generation of eddies motion, respectively.
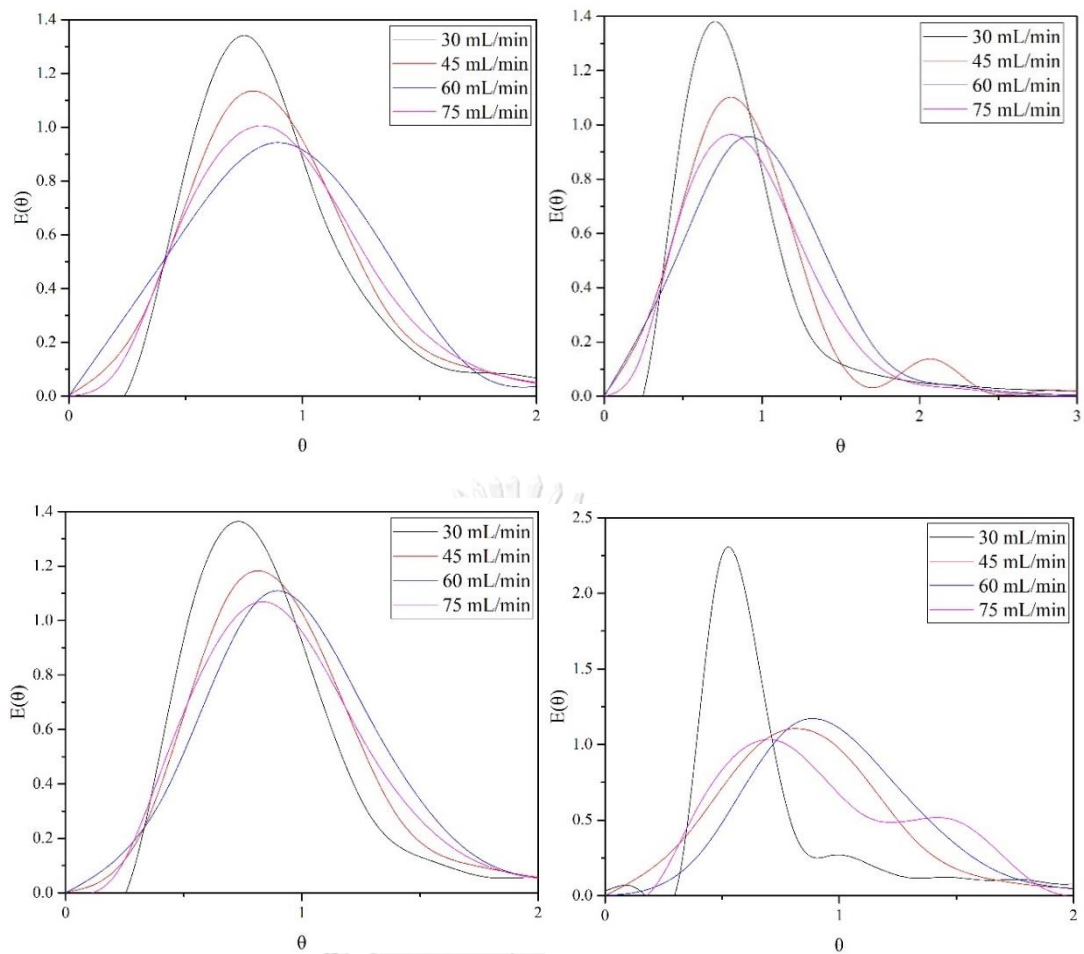
Figure C2 Influence of total flowrate on RTD based on (a) 300 rpm, (b) 600 rpm,
(c) 900 rpm and (d) 1,200 rpm in RTR based on pure water.

Table C2 Operating mean residence time (τ), the normalized variance (σ_θ^2) and dispersion number (D/uL) corresponding to the RTD measurement using pure water.

Rotational speed (rpm)	τ	σ_θ^2	D/uL
Flowrate 30 mL/min			
0	3.85	0.494	0.383
300	3.79	0.453	0.331
600	4.00	0.577	0.518
900	3.89	0.584	0.530
1,200	6.16	0.799	1.397
Flowrate 45 mL/min			
0	3.18	0.503	0.372
300	2.94	0.439	0.314
600	2.91	0.492	0.379
900	2.89	0.362	0.211
1,200	3.01	0.498	0.389
Flowrate 60 mL/min			
0	2.31	0.252	0.148
300	2.29	0.256	0.151
600	2.31	0.186	0.104
900	2.34	0.169	0.093
1,200	2.45	0.149	0.081
Flowrate 75 mL/min			
0	2.30	0.366	0.240
300	2.24	0.461	0.340
600	2.27	0.478	0.361
900	2.36	0.363	0.237
1,200	2.68	0.348	0.223

VITA

NAME	Narita Chanthon
DATE OF BIRTH	22 Aug 1993
PLACE OF BIRTH	Pathumthani
INSTITUTIONS ATTENDED	Chulalongkorn University
HOME ADDRESS	38/9 Phaholyothin Rd., Khlong Nueng, Khlong Luang, Pathumthani 12120